ACSNANO

www.acsnano.org

REVIEW

Polymer-Ligated Nanocrystals Enabled by Nonlinear Block Copolymer Nanoreactors: Synthesis, Properties, and Applications

Yijiang Liu,* Jialin Wang, Mingyue Zhang, Huaming Li, and Zhiqun Lin*

Cite This: *ACS Nano* 2020, 14, 12491−12521

Read Online

ACCESS | Metrics & More | Article Recommendations

ABSTRACT: The past several decades have witnessed substantial advances in synthesis and self-assembly of inorganic nanocrystals (NCs) due largely to their size- and shape-dependent properties for use in optics, optoelectronics, catalysis, energy conversion and storage, nanotechnology, and biomedical applications. Among various routes to NCs, the nonlinear block copolymer (BCP) nanoreactor technique has recently emerged as a general yet robust strategy for crafting a rich diversity of NCs of interest with precisely controlled dimensions, compositions, architectures, and surface chemistry. It is notable that nonlinear BCPs are unimolecular micelles, where each block copolymer arm of nonlinear BCP is covalently connected to a central core or polymer backbone. As such, their structures are static and stable, representing a class of functional polymers with complex architecture for directing the synthesis of NCs. In this review, recent progress in synthesizing NCs by capitalizing on two sets of nonlinear BCPs as nanoreactors are discussed. They are star-shaped BCPs for producing 0D spherical nanoparticles, including plain, hollow, and core−shell nanoparticles, and bottlebrush-like BCPs for creating 1D plain and core/shell nanorods (and nanowires) as well as nanotubes. As the surface of these NCs is intimately tethered with the outer blocks of nonlinear BCPs used, they can thus be regarded as polymer-ligated NCs (*i.e.*, hairy NCs). First, the rational design and synthesis of nonlinear BCPs *via* controlled/living radical polymerizations is introduced. Subsequently, their use as the NC-directing nanoreactors to yield monodisperse nanoparticles and nanorods with judiciously engineered dimensions, compositions, and surface chemistry is examined. Afterward, the intriguing properties of such polymer-ligated NCs, which are found to depend sensitively on their sizes, architectures, and functionalities of surface polymer hairs, are highlighted. Some practical applications of these polymer-ligated NCs for energy conversion and storage and drug delivery are then discussed. Finally, challenges and opportunities in this rapidly evolving field are presented.

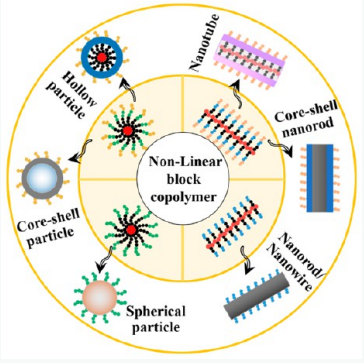

KEYWORDS: *controlled/living radical polymerization, nonlinear block copolymers, nanoreactors, polymer-ligated nanocrystals, controllable architectures, surface chemistry, dimension-dependent properties*

During the last several decades, significant development in synthesis approaches has provided access to a myriad of nanocrystals (NCs) with different dimensions, compositions, and surface functionalities of interest, offering great promise for fundamental study of their appealing size-dependent properties and as building blocks for various exciting applications across nearly every technology sector, including optics,[1] electronics,[2] catalysis,[3] bioimaging,[4] biosensors,[5] cancer therapy,[6] and so forth. It is notable that many conventional techniques (*e.g.*, hydrothermal reaction,[7] sol−gel process,[8] thermal decomposition,[9] linear block copolymer (BCP) micelle templating,[10] *etc.*) experience limited flexibility in synthesizing a large variety of NCs with good size, structural, and compositional control. By contrast, the unimolecular nonlinear BCP nanoreactor strategy has recently garnered much attention as it renders the crafting of a library of NCs with superior control over sizes, shapes, compositions, architectures, and surface functionalities.

With tremendous progress made in polymer synthesis *via* controlled/living radical polymerizations (*e.g.*, atom transfer radical polymerization (ATRP),[11,12] reversible addition−fragmentation chain transfer (RAFT) polymerization,[13,14]

Received: August 18, 2020
Accepted: September 16, 2020
Published: September 25, 2020

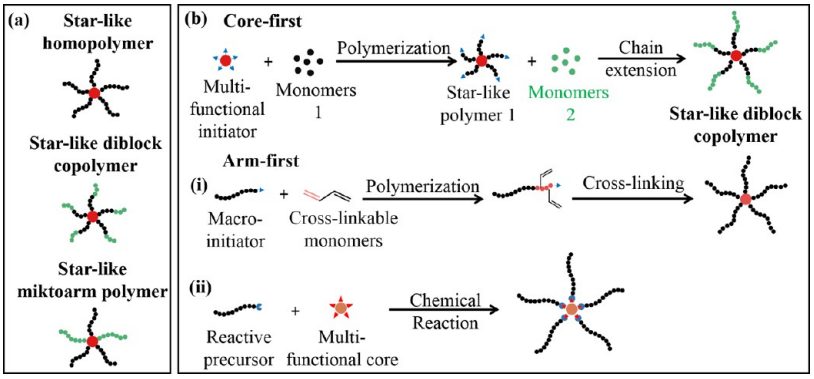

Figure 1. (a) Schematic illustration of the star-like homoarm (both homopolymer and diblock copolymer) and miktoarm polymers. (b) Core-first and arm-first strategies for the synthesis of star-like polymers.

and nitroxide-mediated radical polymerization (NMP)[15]) over the past several decades, a wide range of linear and nonlinear (*e.g.*, star-shaped, bottlebrush-like, hyperbranched, Janus, *etc.*) BCPs with well-defined molecular weights (MWs), narrow MW distribution of each block, desired compositions, and specifically tailored properties could be conveniently achieved. It is noteworthy that, despite the apparent analogies between linear and nonlinear BCPs for templated-growth of NCs, micelles formed *via* self-assembly of linear BCPs are dynamically stable. Thus, the variation in experimental conditions (*e.g.*, changes in pH, temperature, solvent polarity, *etc.*) could trigger the disassembly of micelles, thereby leading to NCs of irregular size and shape. For example, at pH >5, the self-assembly of linear poly(2-vinylpyridine)-*block*-poly(ethylene oxide) (P2VP-*b*-PEO) forms micelles composed of a poly(2-vinylpyridine) (P2VP) core and a poly(ethylene oxide) (PEO) corona; yet they are readily decomposed at low pH.[16] In stark contrast, due to the covalent linkage of each arm to a central core (*i.e.*, single junction) or each side chain/branch to polymer backbone (*i.e.*, numerous junctions), nonlinear BCPs are complex yet stable unimolecular superstructures. Such rationally designed and synthesized nonlinear BCPs can be exploited as unimolecular nanoreactors for precision synthesis of a large number of virtually unlimited NCs possessing the appealing attributes noted above. These NCs are highly stable and can be easily dispersed in solvents due to the intimate and permanent capping of the outer blocks of nonlinear BCP nanoreactors on the surface of NCs (*i.e.*, forming polymer-ligated hairy NCs).

In this context, this review centers primarily on the synthesis, properties, and applications of hairy NCs created using nonlinear BCPs and explicitly unimolecular star-like and bottlebrush-like BCPs as nanoreactors. First, the synthesis of nonlinear BCPs *via* controlled/living radical polymerization is reviewed by focusing on the synthetic methodologies for nonlinear BCPs with well-controlled architectures concerning MWs, polydispersity index (PDI), block sequence distribution, and functional groups. These nonlinear BCPs are characterized by the incorporation of heteroatoms (*i.e.*, N and O) in their side chains to provide reactive sites. Next, the crafting of polymer-ligated NCs with good dimensional, compositional, and architectural control by capitalizing on star-like and bottlebrush-like BCPs as nanoreactors is discussed. Particular attention is given to the parameters that affect the sizes, architectures, and compositions of NCs. Subsequently, the size-, architecture-, and surface-chemistry-dependent properties (*e.g.*, optical, magnetic, and ferroelectric characteristics) of a selected number of polymer-ligated NCs are elucidated. Examples of NCs for practical applications in solar cells, light-emitting diodes, catalysis, or nanocarriers for controlled release are then highlighted. Finally, the challenges and opportunities for understanding the growth of NCs, crafting NCs with more complex architectures and tailored surface responsivities, and developing self-assembled NC-based materials and devices with engineered structures and multifunctionalities are outlined.

SYNTHESIS OF NONLINEAR BLOCK COPOLYMERS

There have been tremendous advances in the synthesis of nonlinear polymers during the past decades. Star-like polymers, first synthesized by living anionic polymerization in the 1950s,[17] represent a class of widely studied nonlinear polymers consisting of many linear polymer arms with the chain end functionalities fused at a central core. On the basis of the chemical composition and sequence distribution of polymer arms, star-like polymers can be classified into a homoarm star-like polymer with identical arm types (top and middle panels, Figure 1a) and a miktoarm star-like polymer having dissimilar arms (bottom panel; Figure 1a).[18] There are two major synthetic strategies for star-like polymers: the core-first (top panel) and arm-first with (i) polymerizable and cross-linkable monomers and (ii) multifunctional core (Figure 1b). We make no attempt to highlight the synthesis of star-like homopolymers *via* the core-first strategy and star-like polymers *via* the arm-first strategy here but refer the reader to several comprehensive reviews.[19,20] In the following, our discussion will be concentrated on the core-first strategy for the synthesis of star-like BCPs as they could effectively template the growth of polymer-ligated NCs.

Synthesis of Star-Shaped Block Copolymers. As noted above, unimolecular star-like polymers have an architecture similar to that of self-assembled linear BCP micelles, yet with many arms tethered onto a central core and exhibiting markedly improved stability and robustness against the external stimuli such as pH, heat, solvent, salt, *etc.*[21] To date, various star-like BCPs with well-defined MWs, compositions, sequence structures, and functionalities have been synthesized by well-honed controlled/living radical polymerization techniques (*i.e.*, ATRP, RAFT, and NMP).[22,23] In addition, click chemistry is also a widely used method to produce star-like polymers that cannot be achieved otherwise by general controlled/living radical polymerization.[24]

https://dx.doi.org/10.1021/acsnano.0c06936
ACS Nano 2020, 14, 12491−12521

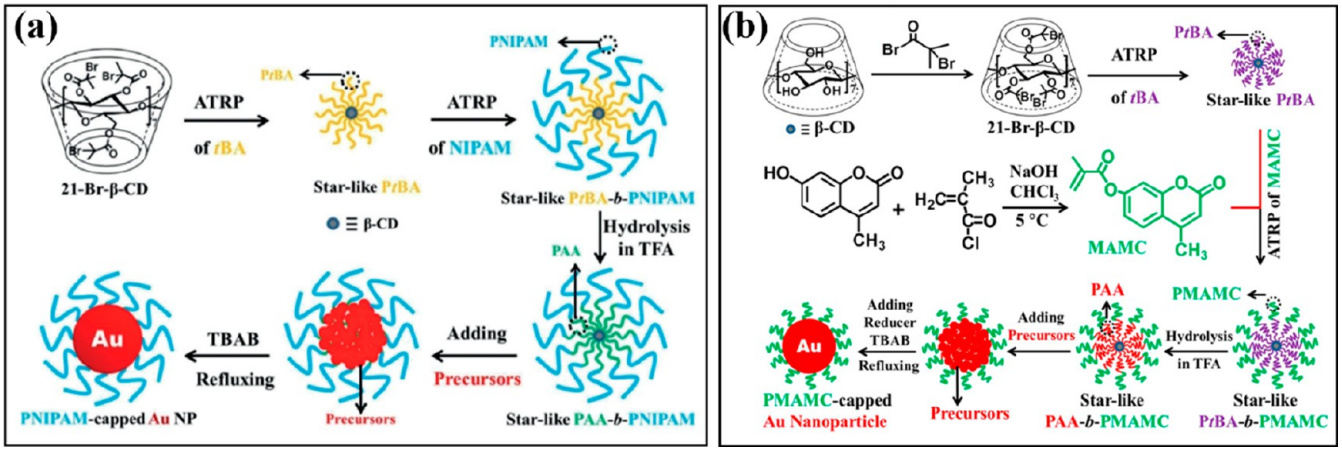

Figure 2. Synthetic routes to stimuli-responsive star-like diblock copolymers and polymer-ligated nanocrystals. (a) Synthesis of thermoresponsive star-like β-CD-*g*-[PAA-*b*-PNIPAM] and PNIPAM-capped AuNPs. Reproduced with permission from ref 41. Copyright 2019 Wiley-VCH. (b) Synthesis of photoresponsive star-like β-CD-*g*-[PAA-*b*-PMAMC] and PMAMC-capped AuNPs. Reproduced with permission from ref 42. Copyright 2018 National Academy of Sciences.

Particularly, in the core-first strategy, a multifunctional initiator is synthesized first, and polymer arms are then grafted sequentially *via* controlled/living radical polymerization to yield star-like polymers. It is notable that the synthesis of a multifunctional initiator represents the key step in the core-first strategy. The initiator is often a multifunctional molecule, such as cyclodextrins (CD),[25] calixarene,[26,27] polyhedral oligomeric silsequioxane (POSS),[28,29] and hyperbranched and/or dendritic polymers (*i.e.*, hyperbranched polyester,[30] hyperbranched polyglycerol,[31] and hyperbranched conjugated polymer[32]).

We choose β-CD as an example to demonstrate its use as a functional core in synthesizing a series of star-like BCPs. Starting from β-CD possessing 21 hydroxyl groups (−OH) for functionalization (*e.g.*, converting −OH into −Br functionality and thus forming a 21Br-β-CD macroinitiator[33−35]) and subsequent initiation, a star-like diblock copolymer of β-CD-*graft*-[polystyrene-*block*-poly(trimethoxysilyl)propyl methacrylate] (denoted β-CD-*g*-[PS-*b*-PTMSPMA]) was synthesized by sequential ATRP of styrene (St) and (trimethoxysilyl)-propyl methacrylate (TMSPMA).[36] Similarly, a star-like β-CD-*graft*-[poly(acrylic acid)-*block*-polystyrene] diblock copolymer (denoted β-CD-*g*-[PAA-*b*-PS]) was prepared by sequential ATRP of *tert*-butyl acrylate (*t*BA) and St, followed by the hydrolysis of poly(*tert*-butyl acrylate) (P*t*BA) block to PAA.[37−40] Recently, thermoresponsive star-like β-CD-grafted poly(acrylic acid)-*block*-poly(*N*-isopropylacrylamide) (denoted β-CD-*g*-[PAA-*b*-PNIPAM])[41] and photoresponsive star-like β-CD-grafted poly(acrylic acid)-*block*-poly(7-methylacryloyloxy-4-methylcoumarin) (β-CD-*g*-[PAA-*b*-PMAMC])[42] diblock copolymers were designed and synthesized by employing *N*-isopropylacrylamide (NIPAM) and 7-methylacryloyloxy-4-methylcoumarin (MAMC) as the second monomers, respectively (Figure 2). The MW of each block (*i.e.*, the arm length) can be readily tuned by varying the polymerization time. On the other hand, for β-CD-based star-like BCPs that cannot be prepared by controlled/living radical polymerization, such as β-CD-grafted poly(acrylic acid)-*block*-poly(3-hexylthiopene) (β-CD-*g*-[PAA-*b*-P3HT]),[43] poly(acrylic acid)-*block*-poly(ethylene oxide) (β-CD-*g*-[PAA-*b*-PEO]),[44] poly(acrylic acid)-*block*-poly(vinylidene fluoride) (β-CD-*g*-[PAA-*b*-PVDF]),[45] and poly(acrylic acid)-*block*-poly(3,4-ethylenedioxythiophene) (β-CD-*g*-[(PAA-*b*-PEDOT]),[46] a combination of ATRP and click reaction was then implemented. Star-like diblock copolymers composed of hydrophilic inner blocks (*e.g.*, PAA; *via* coordination interaction between carboxyl groups of PAA and metal moieties of precursors) are often used as nanoreactors for crafting plain polymer-ligated NCs.[37−43]

For preparation of polymer-ligated hollow and core/shell NCs, the use of star-like triblock copolymers is required, which can also be conveniently prepared by consecutive ATRP polymerization of three monomers. For example, similarly, by employing the 21Br-β-CD initiator, a series of star-like triblock polymers of poly(4-vinylpyridine)-*block*-poly(acrylic acid)-*block*-polystyrene (denoted β-CD-*g*-[P4VP-*b*-PAA-*b*-PS]),[33,34,47] poly(4-vinylpyridine)-*block*-poly(acrylic acid)-*block*-poly(ethylene oxide) (β-CD-*g*-[P4VP-*b*-PAA-*b*-PEO]),[48] polystyrene-*block*-poly(acrylic acid)-*block*-polystyrene (β-CD-*g*-[PS-*b*-PAA-*b*-PS]),[49] and polystyrene-*block*-poly(acrylic acid)-*block*-poly(ethylene oxide) (β-CD-*g*-[PS-*b*-PAA-*b*-PEO])[50] could be designed and synthesized by sequential ATRP of the corresponding monomers of interest. Likewise, the MW of each block can be facilely controlled by changing the polymerization time. As described above, the star-like triblock copolymers composed of an inner hydrophilic block (*i.e.*, P4VP) and intermediate hydrophilic block (*i.e.*, PAA) render the crafting of polymer-ligated core/shell NCs, where the outer block can be either hydrophobic (*e.g.*, PS as in β-CD-*g*-[P4VP-*b*-PAA-*b*-PS]) or hydrophilic (*e.g.*, PEO as in β-CD-*g*-[P4VP-*b*-PAA-*b*-PEO]) to impart the solubility of core/shell NCs in either nonpolar solvents or polar solvents (*e.g.*, H_2O), respectively. By contrast, the presence of a noncoordinating hydrophobic inner block yet coordinating hydrophilic intermediate block in star-like triblock copolymers enables the preparation of polymer-ligated hollow NCs with tunable surface solubility and wettability. For instance, nonpolar solvent-soluble PS-ligated and polar solvent-soluble PEO-ligated hollow NCs can be produced by exploiting β-CD-*g*-[PS-*b*-PAA-*b*-PS] and β-CD-*g*-[PS-*b*-PAA-*b*-PEO] as nanoreactors, respectively.

In addition, by coupling ATRP with click reaction, star-like triblock copolymers with functional outer block (*e.g.*, conjugated block) are also attainable. Recently, star-like triblock copolymers of β-CD-grafted polystyrene-*b*-poly(acrylic acid)-*block*-poly(3,4-ethylenedioxythiophene) (β-CD-*g*-[PS-*b*-

https://dx.doi.org/10.1021/acsnano.0c06936
ACS Nano 2020, 14, 12491−12521

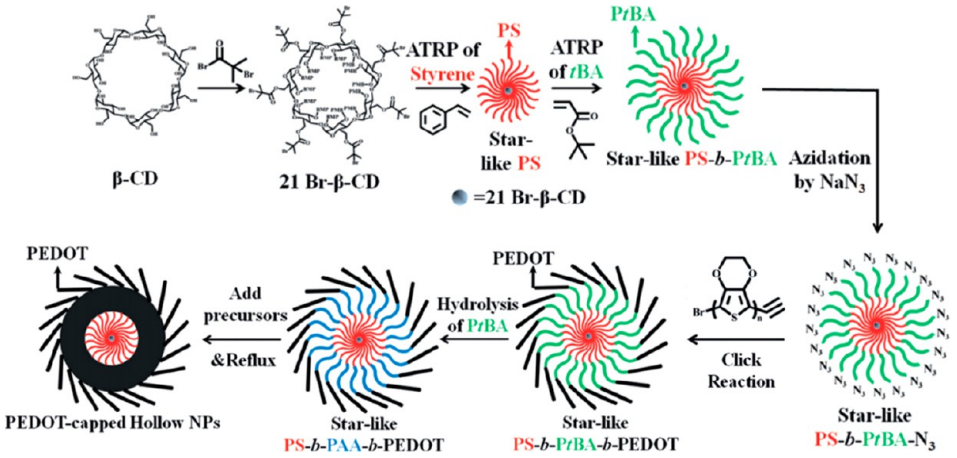

Figure 3. Stepwise representation of synthesis of star-like triblock copolymers of β-CD-*g*-[PS-*b*-PAA-*b*-PEDOT] and PEDOT-ligated hollow nanoparticles. Reproduced with permission from ref 35. Copyright 2017 Wiley-VCH.

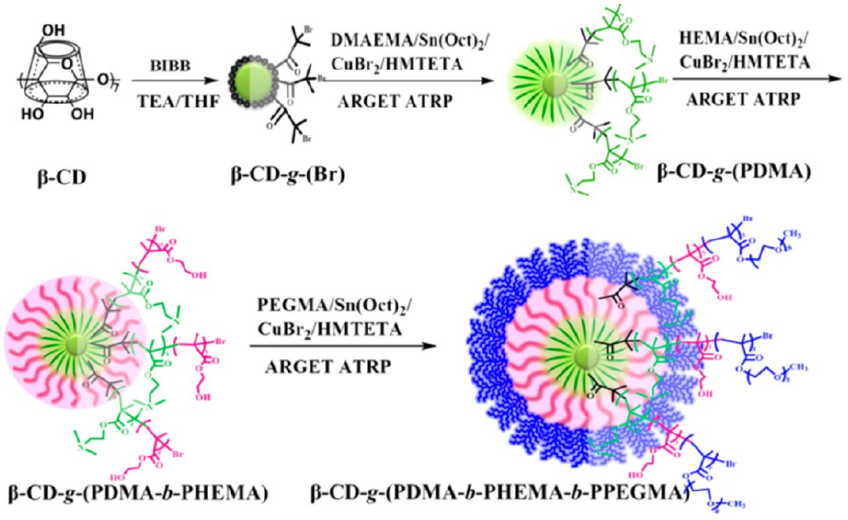

Figure 4. Schematic representation of the synthesis of β-CD-*g*-[PDMA-*b*-PHEMA-*b*-PPEGMA]. Reproduced with permission from ref 54. Copyright 2018 Elsevier.

PAA-*b*-PEDOT]) were synthesized.[35] First, the star-like PS-*b*-P*t*BA diblock copolymer was obtained by sequential ATRP of St and *t*BA, followed by the conversion of the terminal bromine functional groups at the P*t*BA blocks into azide functionalities. Afterward, the click reaction between azide-functionalized star-like PS-*b*-P*t*BA and ethynyl-terminated poly(3,4-ethylenedioxythiophene) (PEDOT) synthesized by the Grignard metathesis reaction yielded star-like *β*-CD-*g*-[PS-*b*-P*t*BA-*b*-PEDOT] containing the outer conductive PEDOT block (Figure 3).[35]

For biomedical application, the star-like triblock copolymer of *β*-CD-grafted {poly(lactide)-*block*-poly(2-(dimethylamino)-ethyl methacrylate)-*block*-poly[oligo(2-ethyl-2-oxazoline) methacrylate]} (*β*-CD-*g*-[PLA-*b*-PDMAEMA-*b*-PEtOxMA]) with a biodegradable inner PLA block was recently prepared *via* ring-opening polymerization (ROP) of lactide (LA) together with activators regenerated by electron transfer atom transfer radical polymerization (ARGET ATRP) of 2-(dimethylamino)ethyl methacrylate (DMAEMA) and oligo(2-ethyl-2-oxazoline)methacrylate (EtOxMA).[51,52] A similar synthetic approach was extended to synthesize a star-like triblock copolymer of *β*-CD-grafted {poly(*ε*-caprolactone)-*block*-poly(2-aminoethyl methacrylate)-*block*-poly[poly-(ethylene glycol)methyl ether methacrylate]} (*β*-CD-*g*-[PCL-*b*-PAEMA-*b*-PPEGMA] for tumor-targeted chemotherapy.[53] The inner biocompatible, hydrophobic PCL block was introduced to host the anticancer drug doxorubicin; the intermediate PAEMA block is pH-responsive and concurrently utilized to direct the formation of Au nanoparticles (NPs), and the outer PPEGMA block functions as a protective hydrophilic shell.[53] Moreover, by sequential ARGET ATRP of 2-(dimethylamino)ethyl methacrylate (DMA), 2-hydroxyethyl methacrylate (HEMA), and poly(ethylene glycol)methyl ether methacrylate (PEGMA) from the 21Br-*β*-CD initiator, a star-like triblock copolymer of *β*-CD-*g*-[PDMA-*b*-PHEMA-*b*-PPEGMA] was successfully synthesized (Figure 4), which was employed as an effective computed tomography (CT) imaging agent after *in situ* growth of AuNPs within the inner PDMA block.[54]

In addition to the widely used *β*-CD core that confers the growth of 21 polymer arms, star-like polymers with different numbers of arms can also be prepared from other functional cores, including resorcinarene (growth of four or eight arms),[55] calix[8]arene (eight arms),[26,27] POSS (eight arms),[28,29,56] stilbeneamine (three arms),[57] and 1,3,5-trivinylbenzene (three arms).[58] However, there have been no reports on controlled

https://dx.doi.org/10.1021/acsnano.0c06936
ACS Nano 2020, 14, 12491−12521

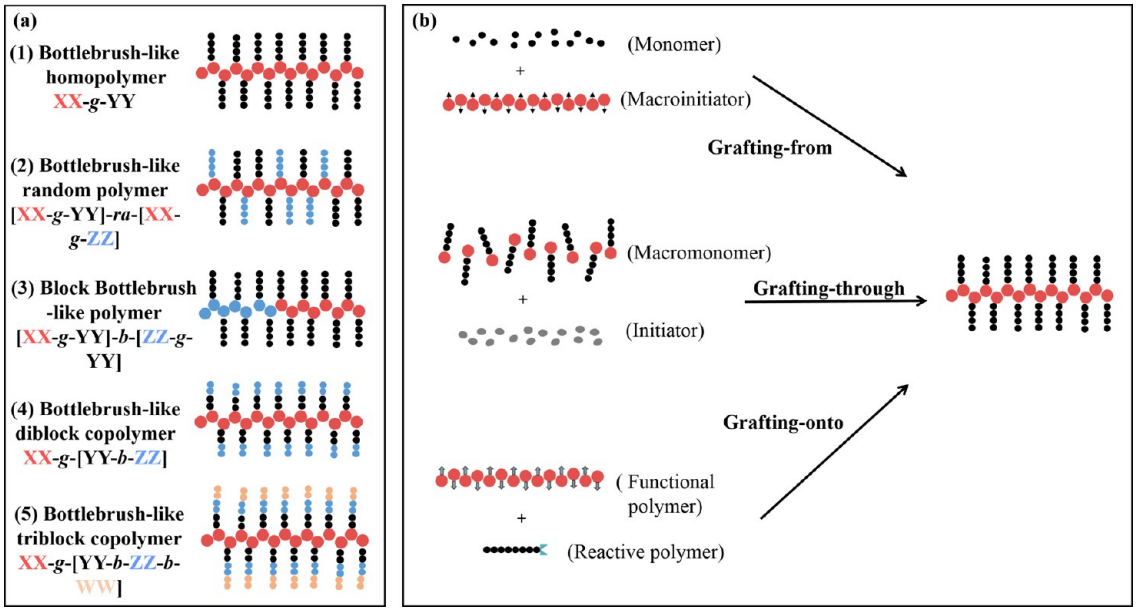

Figure 5. (a) Schematic illustration of a set of bottlebrush-like polymers with different compositions and architectures. (b) Three synthetic routes to bottlebrush-like polymers.

growth of NCs using these star-like BCPs, thus they will not be discussed further.

The *core-first* strategy carries several advantageous attributes: (i) the ability to precisely control the number of arms by judiciously choosing or selectively functionalizing the initiator core, (ii) the capability of facilely tailoring the chemical compositions of arms by identifying the monomer species of interest, and (iii) the easy purification of the crude product by precipitation. However, this approach also faces some challenges, including the difficulties in precise characterization of the arm structure (*i.e.*, MW, PDI) as well as synthesis of miktoarm star-like polymers. An alternative strategy to overcome these issues is to implement the *arm-first* strategy, where star-like polymers are yielded *via* the polymerization reaction between a macroinitiator (*i.e.*, premade polymer with reactive end groups) and a polymerizable monomer or coupling reaction between reactive linear polymer and multifunctional core.[59,60] For example, miktoarm star-like copolymers with various arm numbers and molar ratios by ATRP of two or more different species of premade linear macroinitiators in the presence of divinyl cross-linker (*e.g.*, divinylbenzene (DVB), ethylene glycol diacrylate (EGDA), *etc.*) were developed.[61−63] On the other hand, by coupling linear polymer arms with reactive end groups to a multifunctional coupling agent, star-like polymers can be derived.[64−71] For instance, the 3-arm star-like diblock polymer of (PS-*b*-PEO)$_3$ was synthesized by click reaction between azide-functionalized PS (PS-N$_3$) and alkyne-terminated PEO chains (PEO-≡), where PS-N$_3$ was first synthesized *via* ATRP of St, followed by converting the terminal Br functionalities into azido groups (−N$_3$) *via* the nucleophilic substitution with NaN$_3$.[72] Clearly, the integration of controlled/living radical polymerization with click reaction represents a robust strategy to develop star-like polymers with desired compositions and functions that cannot be accessed solely by controlled/living radical polymerization.[73,74] Nonetheless, the synthetic strategies briefly summarized here have their own advantages and limitations. As noted above, star-like BCPs produced by the core-first strategy stand out as favorable and reliable polymeric nanoreactors for directing the growth of NCs, which will be detailed later.

Synthesis of Bottlebrush-like Block Copolymers *via* a Grafting-from Strategy. Bottlebrush-like polymers, also known as "molecular bottlebrushes", can be regarded as a class of cylindrical unimolecular supermolecules consisting of a long polymer backbone with densely grafted shorter side chains.[75] Owing to the steric hindrance of heavily tethered side chains, the polymer backbone is forced to adopt a stretched, worm-like conformation. Interestingly, the extent of backbone stretching and the aspect ratio of the backbone/arm are dictated by the backbone length and grafting density of side chains. Such an architecture endows bottlebrush-like polymers a set of peculiar properties (*e.g.*, decreased chain entanglement, relatively rigid backbone, tailorable side chains functionalities, *etc.*) over their linear polymer counterparts.[75−77] For example, the greatly reduced chain entanglement of bottlebrush-like polymers can be used as building blocks to self-assemble into complex architecture with large domain size for use in photonic crystals,[78] lithographic patterning,[79] *etc.* According to the composition and distribution of side chains, they can be categorized into bottlebrush-like homopolymer, bottlebrush-like random polymer, block bottlebrush-like polymer, bottlebrush-like diblock copolymers, and bottlebrush-like triblock copolymers (Figure 5a).[80] Bottlebrush-like polymers with well-defined compositions and functionalities are generally synthesized by grafting-from, grafting-onto, and grafting-through strategies (Figure 5b).[77]

It is important to note that several excellent reviews in literature have summarized the synthesis, characterization, self-assembly, properties, and applications of bottlebrush-like polymers.[81−84] In this review, our focus is, however, set on the synthesis of bottlebrush-like polymers by the grafting-from strategy as the resulting unimolecular bottlebrushes function as the appropriate nanoreactors for precision synthesis of 1D nanorods (NRs) and nanowires (NWs).

In the grafting-from method, the shorter side chains are directly grown from the polymer backbone with predesigned and arranged initiator sites. Likewise, advanced polymerization

https://dx.doi.org/10.1021/acsnano.0c06936
ACS Nano 2020, 14, 12491−12521

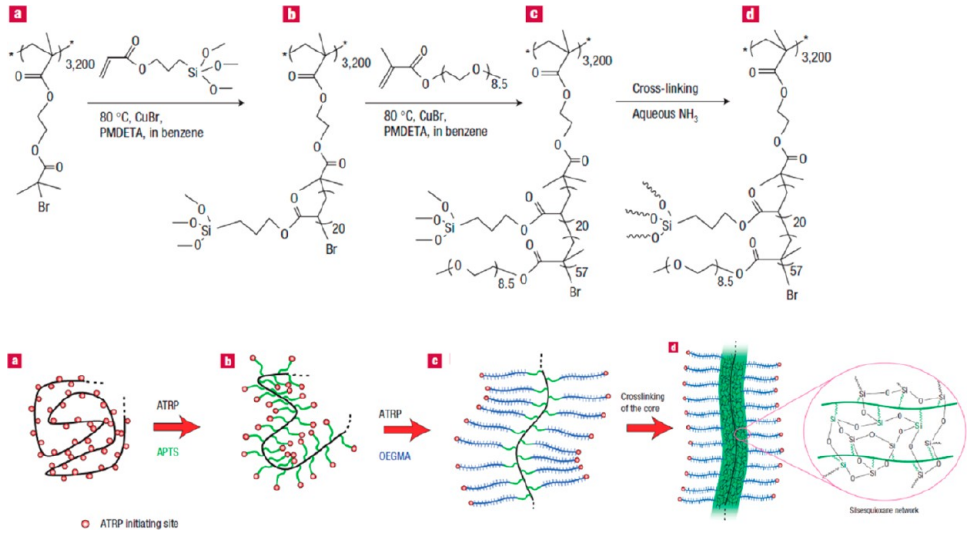

Figure 6. Top: (a–c) Synthetic route to bottlebrush-like diblock copolymer of PHEMA-*g*-[PAPTS-*b*-POEGMA] by ATRP and (d) formation of silica nanowires after hydrolysis and condensation of trimethoxysilyl groups in the PAPTS block. Bottom: Corresponding schematic illustration of the synthetic route. Reprinted with permission from ref 98. Copyright 2008 Springer Nature.

techniques, including living anionic polymerization, ring-opening metathesis polymerization (ROMP), ATRP, RAFT, and NMP have been employed to construct bottlebrush-like polymers with good control over chemical compositions, MWs, and PDIs for both backbone and side chains.[85,86] The synthesis of polymer backbone with multisites for initiation is crucial for the grafting-from strategy. The key feature of the polymer backbone lies in the presence of reactive groups along the backbone, which can be further converted into initiator sites. For example, poly(hydroxyethyl methacrylate) (PHEMA) with numerous reactive hydroxyl groups tethered to its main chain is a widely used backbone for constructing unimolecular bottlebrushes.[82] When hydroxyl groups of PHEMA are transformed into ATRP initiators after the esterification reaction with 2-bromoisobutyryl bromide (BIBB), a commonly used macroinitiator poly(2-(2-bromoisobutyryloxy)ethyl methacrylate) (PBIEM) is generated.[87] It is notable that various bottlebrush-like polymers have been synthesized *via* ATRP of different monomers based on the PHEMA backbone, including a bottlebrush-like homopolymer, diblock copolymers, and tribilock copolymers. For example, a bottlebrush-like homopolymer of PHEMA-*g*-PGMA was obtained by ATRP of glycidyl methacrylate (GMA) from the PHEMA backbone, which was further evolved into single-molecular hybrid nanocylinders after the reaction between a monothiol-functionalized polyhedral silsesquioxane (POSS-SH) and epoxy groups of PGMA.[88] Likewise, a bottlebrush-like homopolymer of PHEMA-*g*-qPDMAEMA was synthesized by ATRP of 2-(dimethylamino)-ethyl methacrylate (DMAEMA), followed by sequential quaternization with iodomethane. The positively charged qPDMAEMA brushes enabled the formation of palladium nanoparticles due to the electrostatic interaction; however, a Pd cluster was observed due to the absence of polymer ligands.[89]

In contrast to bottlebrush-like homopolymers, bottlebrush-like diblock copolymers are attractive when exploited as nanoreactors for crafting 1D NRs and NWs. Recently, a variety of bottlebrush-like diblock copolymers were synthesized *via* the sequential ATRP of two different monomers grafted from PHEMA backbone. For instance, PHEMA was first synthesized by anionic polymerization of 2-(trimethysilyloxy)ethyl methacrylate (TMS-HEMA) and then converted into PBIEM by cleavage of trimethysilyl groups and esterification with BIBB. Polymer side chains of P*t*BA-*b*-P*n*BA were anchored along the PHEMA backbone through sequential ATRP of *t*BA and *n*BA.[90−92] Similarly, consecutively grafting the monomer pairs of *tert*-butyl methacrylate (*t*BMA) and oligo(ethylene glycol) methacrylate (OEGMA), *t*BA and DMAEMA, and HEMA and OEGMA by ATRP from the PHEMA backbone yielded bottlebrush-like diblock copolymers of PHEMA-*g*-[P*t*BMA-*b*-POEGMA],[93] PHEMA-*g*-[P*t*BA-*b*-PDMAEMA],[94] and PHEMA-*g*-[PHEMA-*b*-POEGMA],[95] respectively. Furthermore, a stimuli-responsive bottlebrush-like diblock copolymer of poly(hydroxyethyl methacrylate) grafted poly(3-acryloylpropyltrimethoxysilane)-*b*-poly(2-(dimethylamino)ethyl methacrylate) (denoted PHEMA-*g*-[PAPTS-*b*-PDMAEMA]) was synthesized by the similar method with a salt-sensitive outer block of PDMAEMA.[96] By combining ROP of ε-caprolactone (CL) and ATRP of DMAEMA, bottlebrush-like PHEMA-*g*-[PCL-*b*-PDMAEMA] diblock copolymers with degradable inner PCL block was attained.[97] Figure 6 depicts a representative strategy to construct an intriguing bottlebrush-like diblock copolymer. Specifically, the polyinitiator of PBIEM with 3200 initiating sites was first synthesized by ATRP and then employed to sequentially grow 3-acryloylpropyltrimethoxysilane (APTS) and oligo(ethylene glycol) methacrylate (OEGMA) catalyzed by CuBr. The resulting bottlebrush-like diblock copolymer of PHEMA-*g*-[PAPTS-*b*-POEGMA] was used to produce a water-soluble silica nanowire by the hydrolysis and condensation of the trimethoxysilyl groups in the inner PAPTS block.[98] It is interesting to note that, by changing the ATRP initiator from one-site to four-site during the synthesis of PHEMA backbone, a four-arm PHEMA backbone was derived, rendering the creation of a four-arm molecular bottlebrush with PAA-*b*-PS side chains.[99]

Furthermore, bottlebrush-like triblock copolymers based on the PHEMA backbone can also be synthesized by consecutive ATRP of three monomers. The following are two representative examples. PHEMA-grafted poly(*tert*-butyl acrylate)-*block*-poly(3-acryloylpropyltrimethoxysilane)-*block*-poly(oligo-

https://dx.doi.org/10.1021/acsnano.0c06936
ACS Nano 2020, 14, 12491−12521

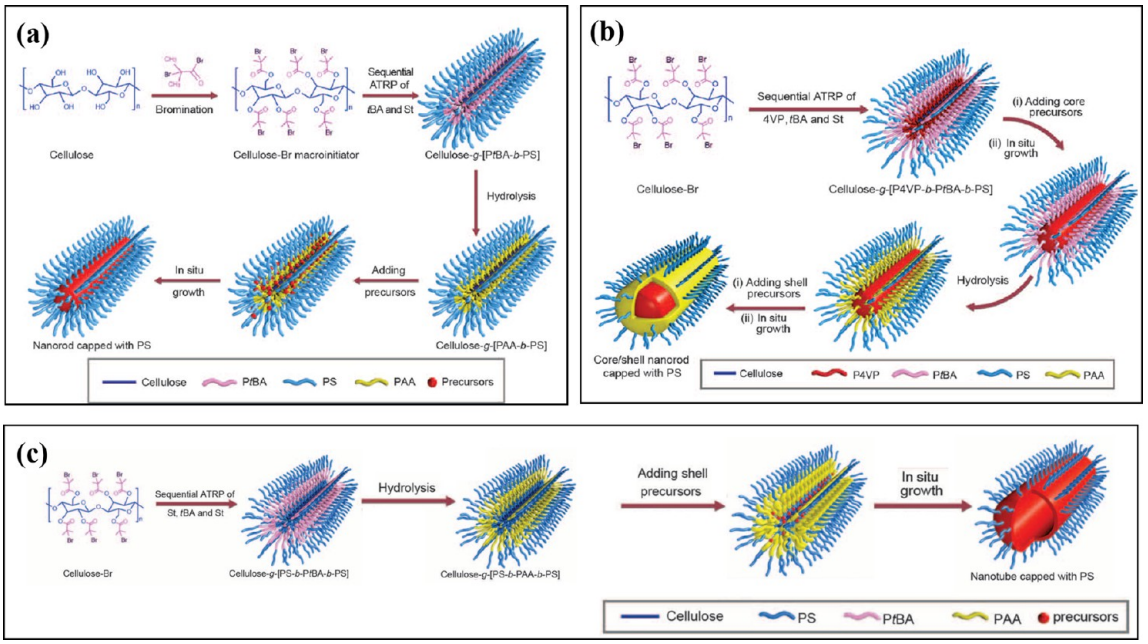

Figure 7. (a) Synthetic route to cellulose-*g*-[P*t*BA-*b*-PS] by sequential ATRP of *t*BA and St, followed by its use as a nanoreactor for crafting a PS-ligated nanorod. (b) Synthetic route to cellulose-*g*-[P4VP-*b*-P*t*BA-*b*-PS] by sequential ATRP of 4VP, *t*BA, and St, followed by its implementation as a nanoreactor to produce a PS-ligated core/shell nanorod. (c) Synthetic route to cellulose-*g*-[PS-*b*-P*t*BA-*b*-PS] by sequential ATRP of St, *t*BA, and St, followed by its utilization as a nanoreactor to yield PS-ligated nanotube. Reproduced with permission from ref 102. Copyright 2016 American Association for the Advancement of Science (AAAS).

(ethylene glycol)methacrylate) (denoted PHEMA-*g*-[P*t*BA-*b*-PAPTS-*b*-POEGMA]) was prepared by consecutive ATRP of *t*BA, APTS, and OEGMA.[100] The length of the outer POEGMA block is the key to successful synthesis of this bottlebrush triblock copolymer as the short POEGMA chain resulted in intermolecular coupling and large agglomerates. By integrating ROP with ATRP, bottlebrush-like triblock copolymers PHEMA-*g*-[PCL-*b*-PDMAEMA-*b*-POEGMA] consisting of the inner PCL block, intermediate polycationic PDMAEMA block, and outer solubilizing POEGMA block sequentially grafted from the PHEMA backbone were synthesized.[101]

As a polymer backbone, the three substitutable hydroxyl groups on each anhydroglucose unit (AGU) of cellulose render the grafting of dense polymer side chains from the cellulose backbone. As such, heavily grafted polymer brushes together with the inherent rigidity of the cellulose backbone force the formed bottlebrush polymers to adopt a well-defined, straight, cylindrical conformation.[102] Such architecture provides this type of bottlebrush polymers with some properties not accessible for flexible backbone analogues (*e.g.*, PHEMA as discussed above). Recently, brushes of PDMAEMA and PAA were grown from the cellulose backbone *via* ATRP of DMAEMA and *t*BA, respectively (*i.e.*, bottlebrush-like homopolymers).[103,104] It is notable that a rich variety of bottlebrush-like diblock and triblock copolymers based on the cellulose backbone were recently rationally designed and synthesized.[102] The compositions and functionalities of the resulting cylindrical unimolecular bottlebrushes can be readily tuned by simply selecting the monomers of interest and varying the sequence of each block grown.[102] Specifically, cellulose-based macroinitiators (*i.e.*, cellulose-Br) of different lengths were first synthesized by a two-step esterification and purified by fractional precipitation.[102] Subsequently, different polymer side chains (*i.e.*, brushes) including diblocks of P*t*BA-*b*-PS and P*t*BA-*b*-PEG, triblocks of P4VP-*b*-P*t*BA-*b*-PS, P4VP-*b*-P*t*BA-*b*-PEG, PS-*b*-P*t*BA-*b*-PS, and PS-*b*-P*t*BA-*b*-PEG were then grafted from the cellulose backbone *via* sequential ATRP of respective monomers. Finally, after hydrolysis of the P*t*BA into PAA blocks, amphiphilic cellulose-*g*-[PAA-*b*-PS], cellulose-*g*-[P4VP-*b*-PAA-*b*-PS], cellulose-*g*-[PS-*b*-PAA-*b*-PS], and cellulose-*g*-[PS-*b*-PAA-*b*-PEG] were derived, and double-hydrophilic cellulose-*g*-[PAA-*b*-PEG] and triple-hydrophilic cellulose-*g*-[P4VP-*b*-PAA-*b*-PEG] can also be obtained. These unimolecular bottlebrush-like micelles can be employed as nanoreactors for crafting 1D NRs of different architectures (plain, core/shell, and hollow), as depicted in Figure 7.[102]

In addition to flexible PHEMA and rigid cellulose backbones, amino-containing chitosan and epoxy-containing PGMA were also exploited as backbones to graft dibolck copolymer side chains.[105,106] Although an organic hollow tube was achieved using the PGMA backbone grafted with photo-cross-linkable poly[styrene-*rac*-(7-(2-methacryloyloxyethoxy)-4-methylcoumarin)], its utilization for the growth of inorganic NCs was not explored.[106]

We note that similar to star-like polymers, the MWs and compositions of polymer side chains in bottlebrush-like BCPs can be readily controlled by varying the polymerization time and use of disparate monomers of interest.

As discussed above, controlled/living radical polymerizations and/or ROP are frequently used in the grafting-from strategy, enabling the control over chemical compositions, MWs, PDI, and functionalities of grown side chains. Nevertheless, owing to the steric hindrance of massively grafted side chains along the backbone, the density of the initiator sites to be grafted is low. In contrast, in the grafting-onto approach, various efficient coupling reactions (*e.g.*, esterification reactions,[107] thiol−epoxy coupling,[108] and copper-catalyzed azide−alkyne cycloaddition reaction (CuAAC)[109−112]) are utilized to anchor presynthe-

https://dx.doi.org/10.1021/acsnano.0c06936
ACS Nano 2020, 14, 12491−12521

Table 1. Nonlinear Block Copolymers Used as Nanoreactors for Directing the Controlled Growth of Inorganic NCs

No.	Full Names	Abbreviations	Chemical Structures of Arms or Side Chains	Inorganic NCs	Refs.
1	β-CD-grafted polystyrene-*b*-poly(trimethoxysilyl)-propylmethacrylate	β-CD-*g*-[PS-*b*-PTMSPMA]	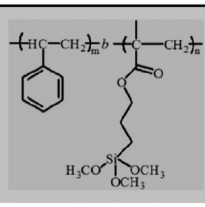	SiO_2 NPs	36
2	β-CD-grafted polystyrene-*b*-poly(acrylic acid)	β-CD-*g*-[PAA-*b*-PS]	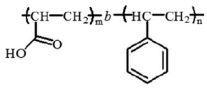	Au/$CsPbBr_3$ /$BaTiO_3$ NPs, *etc.*	37-40
3	β-CD-grafted poly(acrylic acid)-*b*-poly(N-isopropylacrylamide)	β-CD-*g*-[PAA-*b*-PNIPAM]	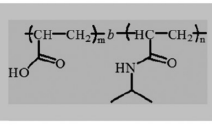	Au NPs	41
4	β-CD-grafted poly(acrylic acid)-*b*-poly(7-methylacryloyloxy-4-methylcoumarin)	β-CD-*g*-[PAA-*b*-PMAMC]	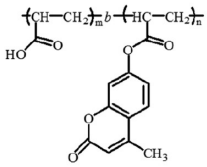	Au NPs	42
5	β-CD-grafted poly(acrylic acid)-*b*-poly(3-hexylthiopene)	β-CD-*g*-[PAA-*b*-P3HT]	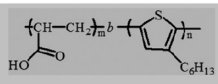	No mentioned	43
6	β-CD-grafted poly(acrylic acid)-*b*-poly(ethylene oxide)	β-CD-*g*-[PAA-*b*-PEO]	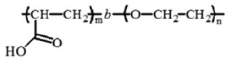	UCNPs	44
7	β-CD-grafted poly(acrylic acid)-*b*-poly(vinylidene fluoride)	β-CD-*g*-[PAA-*b*-PVDF]	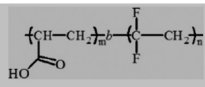	$BaTiO_3$ NPs	45
8	β-CD-grafted poly(acrylic acid)-*b*-poly(3,4-ethylenedioxythiophene)	β-CD-*g*-[PAA-*b*-PEDOT]	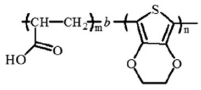	PbTe NPs	46
9	β-CD-grafted poly(4-vinylpyridine)-*b*-poly(acrylic acid)-*b*-polystyrene	β-CD-*g*-[P4VP-*b*-PAA-*b*-PS]	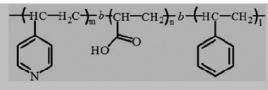	core-shell Fe_3O_4-$PbTiO_3$/Fe_3O_4 -Au/Au-CdSe, NPs	33,34 47, 49
10	β-CD-grafted polystyrene -*b*-poly(acrylic acid)-*b*-polystyrene	β-CD-*g*-[PS-*b*-PAA-*b*-PS]	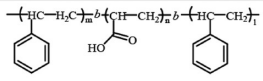	Hollow Au/PbTe NPs	34, 35
11	β-CD-grafted polystyrene -*b*-poly(acrylic acid)-*b*-poly (ethylene oxide)	β-CD-*g*-[PS-*b*-PAA-*b*-PEO]	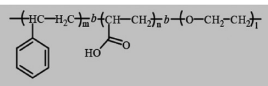	Hollow Au NPs	33

https://dx.doi.org/10.1021/acsnano.0c06936
ACS Nano 2020, 14, 12491−12521

Table 1. continued

No.	Full Names	Abbreviations	Chemical Structures of Arms or Side Chains	Inorganic NCs	Refs.
12	β-CD-grafted poly(4-vinylpyridine)-*b*-poly(acrylic acid)-*b*-poly (ethylene oxide)	β-CD-*g*-[P4VP-*b*-PAA-*b*-PEO]	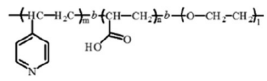	core-shell, Fe_3O_4-Au/$MAPbBr_3$-SiO_2	33, 48-50
13	β-CD-grafted polystyrene-*b*-poly(acrylic acid)-*b*-poly(3,4-ethylenedioxythiophene)	β-CD-*g*-[PS-b-PAA-b-PEDOT]	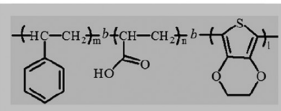	PbTe, PbS hollow	35
14	β-CD-grafted {poly(lactide)-poly(2-(dimethylamino)ethyl methacrylate)-poly[oligo(2-ethyl-2-oxazoline)methacrylate]}$_{21}$	β-CD-[PLA-*b*-PDMAEMA-*b*-PEtOxMA]$_{21}$	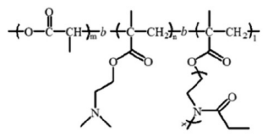	Au NPs	51,52
15	β-CD-grafted {poly(ε-caprolactone)-poly(2-aminoethyl methacrylate)-poly[poly (ethylene glycol) methyl ether methacrylate]}	β-CD-*g*-[PCL-*b*-PAEMA-*b*-PPEGMA]$_{21}$	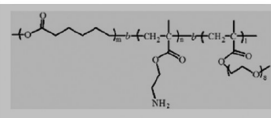	Hollow Au NPs	53
16	β-CD-grafted {poly(2-(dimethylamino) ethylmethacrylate)-*b*-poly(2-hydroxyethylmethacrylate)-*b*-poly(poly(ethylene glycol) methyl ether methacrylate)}	β-CD-*g*-[PDMA-*b*-PHEMA-*b*-PPEGMA]	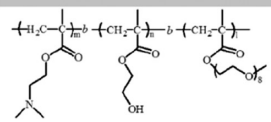	Au NPs	54
17	β-CD-grafted [poly(ethylene oxide) grafted poly(acrylic acid)]-*b*-poly (ethylene oxide)	β-CD-*g*-[(PEO-*g*-PAA)-*b*-PEO]$_{18}$	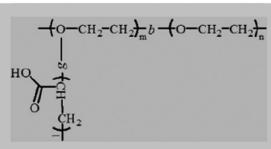	Fe_3O_4 NPs	153
18	Polydivinylbenzene-*g*-poly(*tert*-butyl acrylate)-*b*- poly(styrene-co-acrylonitrile)	PDVB-*g*-[P*t*BA-*b*-PSAN]	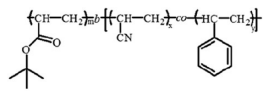	ZnO NPs	127
19	poly-(hydroxyethyl methacrylate)-grafted poly(*tert*-butyl acrylate)-*b*-poly(*n*-acrylate)	PHEMA-*g*-[P*t*BA-*b*-P*n*BA]	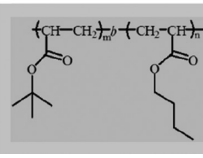	CdS, CdSe nanowires	90-92

https://dx.doi.org/10.1021/acsnano.0c06936
ACS Nano 2020, 14, 12491−12521

Table 1. continued

No.	Full Names	Abbreviations	Chemical Structures of Arms or Side Chains	Inorganic NCs	Refs.
20	poly-(hydroxyethyl methacrylate)-grafted poly (*tert*-butyl methacrylate)-*b*-poly(oligo(ethylene glycol) methacrylate)	PHEMA-*g*-[P*t*BMA-*b*-POEGMA]	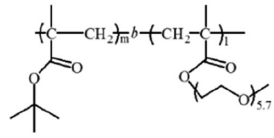	Fe_3O_4 nanowires	93
21	poly-(hydroxyethyl methacrylate)-grafted poly(*tert*-butyl acrylate)-*b*-poly(2-(dimethylamino)ethyl methacrylate)	PHEMA-*g*-[P*t*BA-*b*-PDMAEMA]	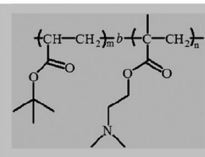	SiO_2 nanowires	94
22	poly-(hydroxyethyl methacrylate)-grafted poly-(hydroxyethyl methacrylate)-*b*-poly(2-(dimethylamino)ethyl methacrylate)	PHEMA-*g*-[PHEMA-*b*-POEGMA]	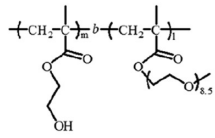	TiO_2 nanowires	95
23	poly-(hydroxyethyl methacrylate)-grafted poly(3-acryloylpropyltri methoxysilane)-*b*-poly(2-(dimethylamino)ethyl methacrylate)	PHEMA-*g*-[PAPTS-*b*-PDMAEMA]	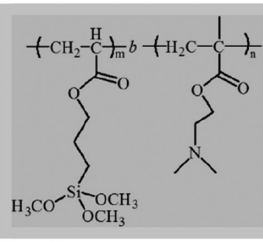	hybrid SiO_2 nanowires	96
24	Poly-(hydroxyethyl methacrylate)-grafted poly(ε-caprolactone)-*b*-poly(2-(dimethylamino)ethyl methacrylate)	PHEMA-*g*-[PCL-*b*-PDMAEMA]	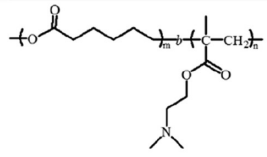	hybrid SiO_2 nanowires	97
25	poly-(hydroxyethyl methacrylate)-grafted poly(3-acryloylpropyl trimethoxysilane)-*b*-poly(oligo (ethylene glycol) methacrylate)	PHEMA-*g*-[PAPTS-*b*-POEGMA]	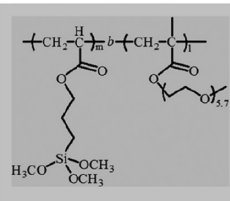	SiO_2 nanowires	98
26	poly-(hydroxyethyl methacrylate)-grafted poly(acrylic acid)-*b* -polystyrene	PHEMA-*g*-[PAA-*b*-PS]	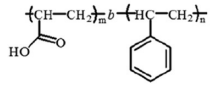	TiO_2 nanowires	99, 127

https://dx.doi.org/10.1021/acsnano.0c06936
ACS Nano 2020, 14, 12491−12521

Table 1. continued

No.	Full Names	Abbreviations	Chemical Structures of Arms or Side Chains	Inorganic NCs	Refs.
27	poly-(hydroxyethyl methacrylate)-grafted poly(*tert*-butyl acrylate) -*b*-poly(3-acryloylpropyl trimethoxysilane)-*b*-poly(oligo(ethylene glycol) methacrylate)	PHEMA-*g*-[P*t*BA-*b*-PAPTS-*b*-POEGMA]	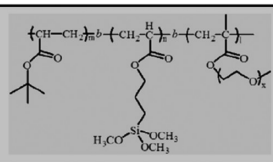	hybrid SiO_2 nanowires	100
28	poly-(hydroxyethyl methacrylate)-grafted poly(ε-caprolactone)-*b*-poly(2-(dimethylamino)ethyl methacrylate)-*b*-poly(oligo(ethylene glycol) methacrylate)	PHEMA-*g*-[PCL-*b*-PDMAEMA-*b*-POEGMA]	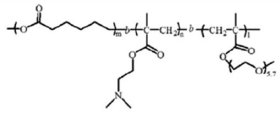	TiO_2 nanotube	101
29	Hydroxypropyl cellulose-graft-poly (acrylic acid)	HPC-*g*-PAA	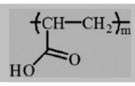	SnO_2	103
30	Cellulose-grafted poly(*tert*-butyl acrylate)-*b*-polystyrene	Cellulose-*g*-[P*t*BA-*b*-PS]	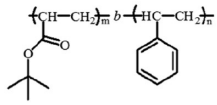	Au/Pt/Fe_3O_4/CdSe/PbTe nanorods	102
31	Cellulose-grafted poly(*tert*-butyl acrylate)-*b*-poly(ethylene glycol)	Cellulose-*g*-[P*t*BA-*b*-PEG]	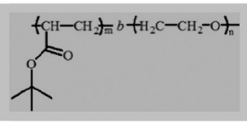	Au/ Fe_3O_4 nanorods	102
32	Cellulose-grafted poly(4-vinylpyridine)-*b*-poly(*tert*-butyl acrylate) -*b*-polystyrene	Cellulose-*g*-[P4VP-*b*-P*t*BA-*b*-PS]	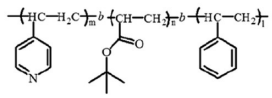	Au-TiO_2/UCNPs core-shell	102
33	Cellulose-grafted poly(4-vinylpyridine)-*b*-poly(*tert*-butyl acrylate) -*b*-poly(ethylene glycol)	Cellulose-*g*-[P4VP-*b*-P*t*BA-*b*-PEG]	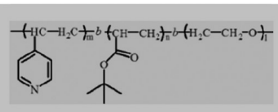	Au-TiO_2/UCNPs core-shell	102
34	Cellulose-grafted polystyrene -*b*-poly (*tert*-butyl acrylate)-*b*-polystyrene	Cellulose-*g*-[PS-*b*-P*t*BA-*b*-PS]	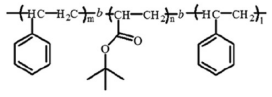	Au/TiO_2 /UCNPs nanotube	102
35	Cellulose-grafted polystyrene-*b*-poly(*tert*-butyl acrylate)-*b*-poly(ethylene glycol)	Cellulose-*g*-[PS-*b*-P*t*BA-*b*-PEG]	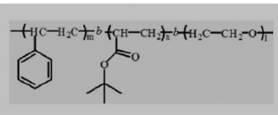	Au/TiO_2 /UCNPs nanotube	102

sized side chains onto the backbone with higher grafting density. Notable, it is also convenient to graft functional side chains (*e.g.*, conjugated polymers; PEDOT and P3HT) onto the backbone *via* CuAAC.[113,114] Finally, for the grafting-through method, bottlebrush-like BCPs with different blocks in the backbone and compartmentalized brushes attached to the same backbone can be attained by ROMP, controlled/living radical polymerization (*i.e.*, ATRP), and ROP of the

https://dx.doi.org/10.1021/acsnano.0c06936
ACS Nano 2020, 14, 12491−12521

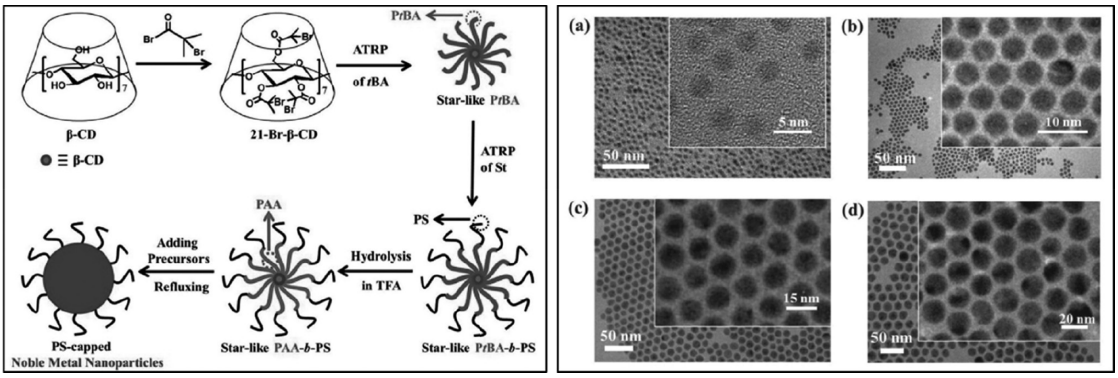

Figure 8. (Left) Synthesis of a PS-ligated AuNP using amphiphilic star-like diblock copolymer of *β*-CD-*g*-[PAA-*b*-PS] as a nanoreactor. (Right) TEM images of different sizes of AuNPs permanently ligated with PS hairs: (a) 3.2 ± 0.1 nm, (b) 5.1 ± 0.2 nm, (c) 12.2 ± 0.5 nm, and (d) 18.3 ± 0.4 nm. Reproduced with permission from ref 39. Copyright 2016 Wiley-VCH.

corresponding macromonomers.[115−126] It is also feasible to tune the length of side chains and the grafting density by regulating the respective MWs of side chains and backbone, respectively. As bottlebrush-like BCPs synthesized by grafting-onto and grafting-through strategies are rarely implemented in controlled growth of NCs, the examples of these polymers are thus not presented.

Table 1 summarizes all nonlinear BCPs discussed in this section including their full names, abbreviations, chemical structures of arms (as in star-like BCPs) or side chains (as in bottlebrush-like BCPs), and the corresponding template-grown NCs.

CRAFTING OF MONODISPERSE POLYMER-LIGATED NANOCRYSTALS *VIA* CAPITALIZING ON NONLINEAR BLOCK COPOLYMERS AS NANOREACTORS

0D Nanoparticles Templated by Star-like BCP Nanoreactors. As discussed above, star-like polymers, in essence, are stable unimolecular micelles with linear arms covalently fused at a central core, affording significant structural stability against various environmental perturbations. Exercising star-like BCPs as nanoreactors to direct the synthesis of polymer-ligated NCs has garnered considerable interest due to the following appealing features. First, it renders delicate control over the sizes and architectures of NPs as star-like BCP nanoreactors synthesized by controlled/living radical polymerizations possess well-defined MWs and low PDI. As such, plain, hollow, and core/shell NPs with precisely tailored dimensions (*i.e.*, diameter of plain NPs, diameter of hollow interior and shell thickness of hollow NPs, and core diameter and shell thickness of core/shell NPs) can be created. Second, chemical compositions of NPs can be readily altered by simply selecting proper inorganic precursors. Third, surface chemistry (*i.e.*, the outer blocks of star-like BCP function as surface ligands) can be easily tuned to yield polymer-ligated NPs with intriguing polarity, conductivity, stimuli responsivity, dielectric property, *etc.*, endowed by the functional outer blocks. Fourth, the outer blocks act as polymeric hairs that are intimately and permanently capped on the surface of NPs as these polymer chains are originally covalently connected to the inner and intermediate blocks of star-like BCP, thereby effectively preventing the aggregation of NPs and facilitating their dispersion in both solvents (liquid state) and polymer nanocomposites (solid state). Finally, a variety of virtually unlimited core/shell NPs of interest with large lattice mismatch between core and shell materials can be accessed by capitalizing on a star-like triblock copolymer nanoreactor strategy, which are otherwise challenging to be achieved by conventional methods.

Hairy Plain NPs. Star-like diblock copolymers with a CD core are regarded as a typical kind of nanoreactors for crafting uniform NPs. These NPs are *in situ* grown in the compartment occupied by hydrophilic inner blocks of star-like diblock copolymer due to the coordination interaction between the metal moieties of precursors and functional groups of the inner blocks, whereas the outer blocks that directly tethered on the surface of NPs (*i.e.*, forming polymer-ligated NPs) act as a layer of protective hairs to prohibit the aggregation of NPs and render them with different surface functionality as noted above. The size of these polymer-ligated NPs is dictated by the length of the inner hydrophilic block which can be conveniently regulated by controlling the polymerization time of this block. Moreover, the synthetic conditions, including the solvent polarity and the ratio of precursors to functional groups of the inner blocks, also affect the uniformity of the formed NPs.[52]

We first discuss the ability of a star-like diblock copolymer nanoreactor to enable the precise synthesis of polymer-ligated NPs by taking the crafting of AuNPs as example. Recently, the Au precursors ($HAuCl_4 \cdot 3H_2O$) was introduced into the star-like *β*-CD-*g*-[PAA-*b*-PS] (Table 1; No. 2 nanoreactor) solution containing 90% *N*,*N*-dimethylformamide (DMF) and 10% benzyl alcohol (BA) (by volume), within which the precursors are selectively loaded inside the PAA block compartment owing to coordination interaction between carboxyl groups (−COOH) of PAA blocks and metal moieties of precursors, leading to nucleation and growth into AuNPs permanently ligated with PS hairs upon addition of the reductant of *tert*-butylamine borane (Figure 8, left).[39] As described above, the diameter of AuNPs was largely determined by the length of inner PAA. As the MW of PAA block increased from 3300 to 19100 g/mol, the calculated hydrodynamic diameter of PAA extended from 3.2 ± 0.2 to 18.7 ± 1.0 nm. Consequently, uniform AuNPs with increasing average diameters (*i.e.*, from 3.2 ± 0.1 to 18.3 ± 0.4 nm) were crafted (Figure 8, right).[39]

It was found that the outer polymer chains also play a crucial role in controlling the monodispersity of AuNPs.[42] For example, when star-like diblock copolymers of *β*-CD-*g*-[PAA-*b*-PMAMC] (Table 1; No. 4 nanoreactor) with different lengths of PMAMC were utilized as nanoreactors to prepare PMAMC-ligated AuNPs, uniform AuNPs were only obtained with an intermediate length of PMAMC (MW = 13800 g/

https://dx.doi.org/10.1021/acsnano.0c06936
ACS Nano 2020, 14, 12491−12521

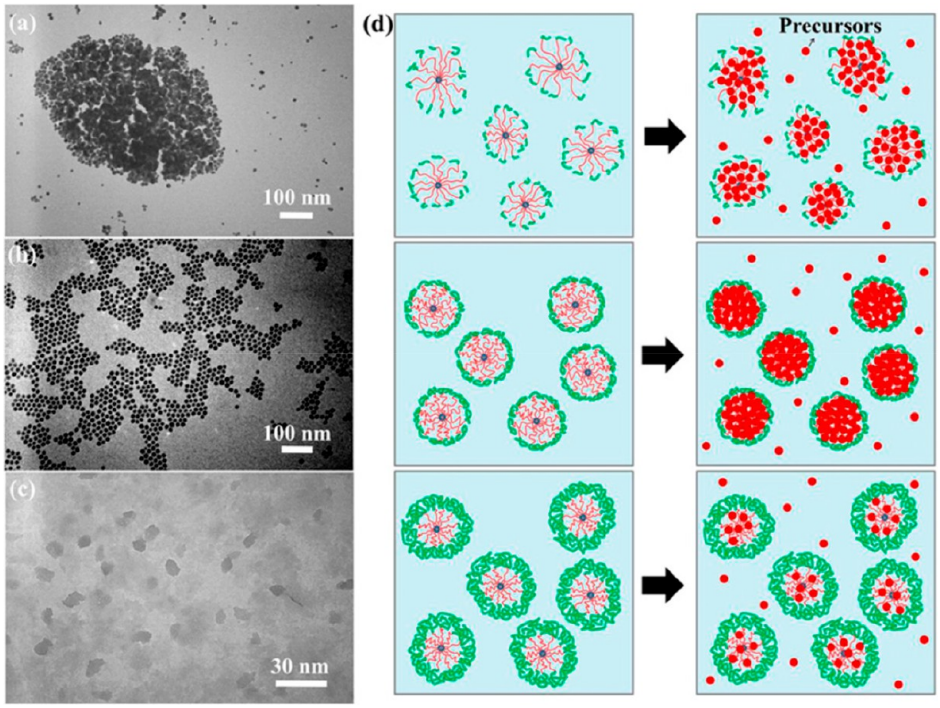

Figure 9. Effect of molecular weight of PMAMC chains on the morphology of *in situ* formed AuNPs synthesized by capitalizing on *β*-CD-*g*-[PAA-*b*-PMAMC] as a nanoreactor. TEM images of PMAMC-ligated AuNPs with the MWs of PMAMC: (a) 2700 g/mol, (b) 13800 g/mol, and (c) 35100 g/mol. (d) Mechanism of formation of AuNPs with different MWs of PMAMC. Reproduced with permission from ref 42. Copyright 2018 PNAS.

mol). The irregular AuNPs were otherwise formed with short (MW = 2700 g/mol) and long PMAMC chains (MW = 35100 g/mol) (Figure 9).[42] This observation was closely related to the solubility of star-like PAA-*b*-PMAMC in the mixed solvents of DMF/BA. DMF is a good solvent for both PAA and PMAMC blocks, and BA is a good solvent for PAA yet a poor solvent for PMAMC. At a DMF/BA = 7/3 ratio, the outer PMAMC chains are collapsed whereas the inner PAA chains adopt the expanded conformation, leading to the formation of a more compact and structurally stable spherical macromolecule as a nanoreactor[33] and thus AuNPs with excellent uniformity. By contrast, the short PMAMC chains could not effectively encapsulate the entire inner PAA regime, producing irregular AuNPs.[42] On the other hand, the long PMAMC chains densely covered the PAA regime, limiting the diffusion of Au precursors, thus yielding cluster-like AuNCs.

The solvents for precursor loading and NP growth are also key parameters for controlling the uniformity of as-synthesized NPs. For example, nearly monodisperse $BaTiO_3$ NPs were achieved in the mixed solvents containing 90% DMF and 10% BA (by volume) when star-like diblock copolymers of *β*-CD-*g*-[PAA-*b*-PS] were utilized as nanoreactors.[33] Irregular $BaTiO_3$ NPs were obtained without BA or at DMF/BA = 1/1. This phenomenon can also be rationalized by considering the solubility of PAA-*b*-PS. Similar to the case of star-like PAA-*b*-PMAMC, both PAA and PS are soluble in DMF. However, PAA is soluble in BA, yet PS is not. In pure DMF, both PAA and PS blocks are fully dissolved and extended. With the addition of BA, a progressively compact and stable spherical unimolecular micelle with the outer PS blocks collapsed on the coil-like inner PAA blocks is formed. When more BA is added, it results in heavily collapsed PS and thus prevents the diffusion of precursors into the inner PAA compartment, thereby leading to irregular NPs.[33] It is important to note that the optimum ratio of the mixed solvents for yielding well-structured polymer-ligated NPs depends heavily on the compositions of nanoreactors. For example, monodisperse PMAMC-ligated AuNPs were found to form at a DMF/BA ratio of 7/3,[42] as discussed above. In contrast, uniform PVDF-ligated $BaTiO_3$ NPs were derived in a mixed solvent containing 50% DMF and 50% BA using the *β*-CD-*g*-[PAA-*b*-PVDF] nanoreactor.[45]

In addition to noble metal (Au) and ferroelectric ($BaTiO_3$) NPs, star-like diblock copolymer nanoreactors enable the crafting of a rich diversity of NPs, including other metal NPs (Ag, Pt, *etc.*), semiconducting NPs (*n*-type ZnO and TiO_2 and *p*-type Cu_2O),[33,127] hard and soft magnetic NPs (Fe_3O_4, *etc.*),[33] luminescent II−IV NPs (visible-emitting CdSe, IR-emitting PbTe, *etc.*),[33,35] upconversion NPs of different emission colors (blue-emitting $NaYF_4$:Yb/Tm, green-emitting $NaYF_4$:Yb/Er, *etc.*),[44] and halide perovskite NPs ($MAPbI_3$, $CsPbBr_3$, *etc.*).[40,49,128] In the following, we will discuss the synthesis of several functional NPs listed above. For example, star-like diblock copolymers of PDVB-*g*-[P*t*BA-*b*-PSAN] (Table 1; No. 18 nanoreactor) were synthesized using a poly(styrene-*co*-acrylonitrile)-Br (PSAN-Br) as a macroinitiator to chain-expand with *t*BA to yield PSAN-*b*-P*t*BA-Br, where the PDVB core was concurrently formed by chain extension and cross-linking with DVB.[127] Subsequently, the precursors of zinc(2-ethylhexanoate) ($Zn(EH)_2$) were partitioned with PDVB-*g*-[PAA-*b*-PSAN] *via* a strong coordination between Zn^{2+} and −COOH groups of PAA blocks produced from the hydrolysis of P*t*BA. Finally, PSAN-ligated ZnO NPs were derived after thorough hydrolysis of $Zn(EH)_2$ in DMF under refluxing at 180 °C.[127] Recently, PEDOT-ligated PbTe NPs with a diameter approximately of 10.8 ± 0.5 nm were crafted

https://dx.doi.org/10.1021/acsnano.0c06936
ACS Nano 2020, 14, 12491−12521

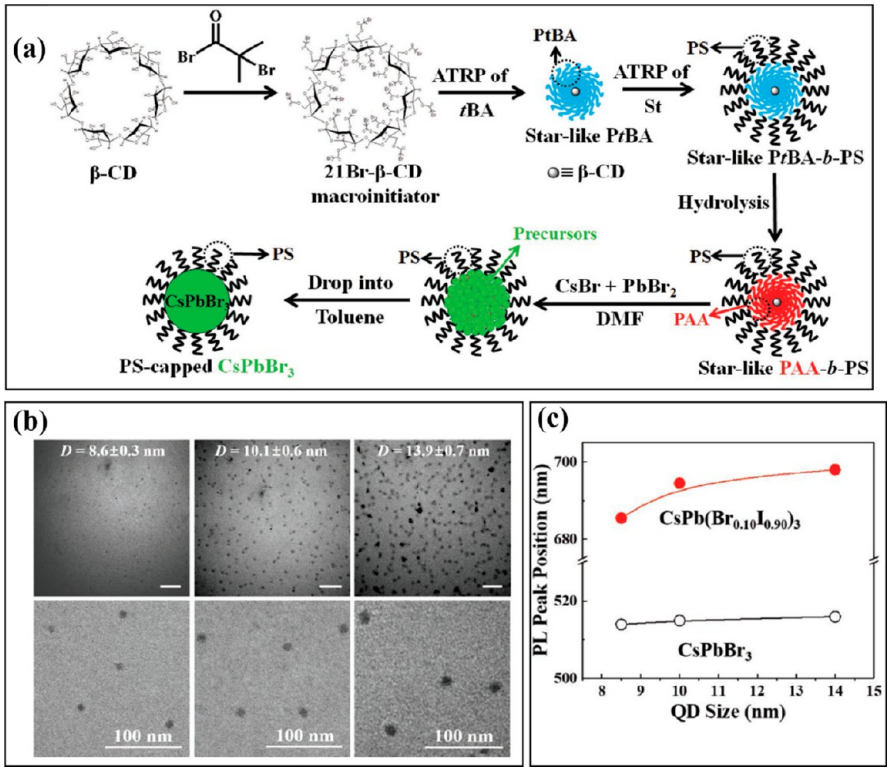

Figure 10. (a) Schematic illustration of crafting PS-ligated $CsPbBr_3$ NPs by capitalizing on an amphiphilic star-like β-CD-*g*-[PAA-*b*-PS] diblock copolymer as a nanoreactor. (b) TEM images of different-sized PS-ligated $CsPbBr_3$ NPs. (c) PL peak position as a function of NP size. Reproduced with permission from ref 40. Copyright 2019 Wiley-VCH.

by employing star-like β-CD-*g*-[PAA-*b*-PEDOT] as the nanoreactor, which was synthesized by ATRP and azide−alkyne cycloaddition between azide-functionalized P*t*BA and ethynyl-terminated PEDOT.[46] More interestingly, PS-ligated perovskite $CsPbBr_3$ NPs were recently *in situ* grown using a star-like β-CD-*g*-[PAA-*b*-PS] nanoreactor due to strong coordination interaction between −COOH of PAA blocks and metal ions (Cs^+ and Pb^{2+}) of precursors (Figure 10a).[40] The diameter of $CsPbBr_3$ NPs can be tailored by controlling the length (*i.e.*, MW) of the PAA block during ATRP, thereby leading to size-dependent emission when iodine ions were introduced to the NP (Figure 10b,c). Strikingly, these PS-ligated $CsPbBr_3$ NPs manifested a 20-fold improvement of stability against water owing to hydrophobic PS chains densely situated on the surface of $CsPbBr_3$ NPs.[40]

Additionally, a star-like triblock copolymer was also reported for the construction of polymer-ligated plain NPs. Recently, star-like β-CD-*g*-[PDMA-*b*-PHEMA-*b*-PPEGMA)] (Table 1; No. 16 nanoreactor) was used to template the formation of PHEMA-*b*-PPEGMA-ligated AuNPs *via* the coordination interaction between N of PDMA and Au precursors.[54] Clearly, the size of AuNPs was dependent on the length of PDMA block. Such PHEMA-*b*-PPEGMA-ligated AuNPs were employed for efficient CT imaging (Figure 4).[54] In addition to the creation plain NPs, star-like triblock copolymers have also been widely used for preparing more interesting hollow and core/shell NPs, as discussed below.

Hairy Hollow NPs. Hollow-structured nanomaterials have high surface area and low material density, showing potential applications in various areas such as drug delivery, photothermal therapy, bioimaging, and electrocatalysis.[129−131] It is important to note that a set of physical properties (*e.g.*, plasmonic, catalytic) of hollow nanomaterials depends sensitively on the diameter of the hollow interior and thickness of the shell.[34,48] Thus, the ability to precisely control these parameters enables one to systematically tailor the properties of hollow nanomaterials and compare them with those of solid nanomaterial counterparts. However, the commonly used methods such as sacrificial templates, Kirkendall effect, and Ostwald ripening experience issues in achieving hollow NPs with small size (<100 nm) and lack of good cavity size and shell thickness control.[132−134] In sharp contrast, star-like BCPs have recently emerged as a robust route to craft a large variety of small polymer-ligated hollow NPs with precisely tunable inner cavity, shell thickness, and surface functionality.

Two representative hollow NPs crafted using amphiphilic star-like triblock copolymers are discussed below. The first example is plasmonic hollow AuNPs and AgNPs templated by star-like β-CD-[PS-*b*-PAA-*b*-PS] triblock copolymer (Table 1; No. 10 nanoreactor) (Figure 11a).[34] Au (or Ag) precursors of $HAuCl_4$ (or $AgNO_3$) were selectively partitioned in the compartment occupied by the intermediate PAA blocks and ultimately reduced to hollow Au (or Ag) NPs ligated by hydrophobic PS chains situated on both inner and outer surfaces of Au (or Ag).[34] The cavity diameter and shell thickness of hollow Au (or Ag) NPs can be conveniently controlled by regulating the length (*i.e.*, MW) of inner PS blocks and the intermediate PAA blocks, respectively, during their polymerizations (Figure 11b). It is interesting to note that the surface chemistry of hollow AuNPs is tunable. For instance, instead of PS-ligated hollow AuNPs, water-soluble PEO-ligated hollow AuNPs can be crafted by capitalizing on star-like β-CD-[PS-*b*-PAA-*b*-PEO] triblock copolymer nanoreactor (Table 1; No. 11 nanoreactor).[33]

https://dx.doi.org/10.1021/acsnano.0c06936
ACS Nano 2020, 14, 12491−12521

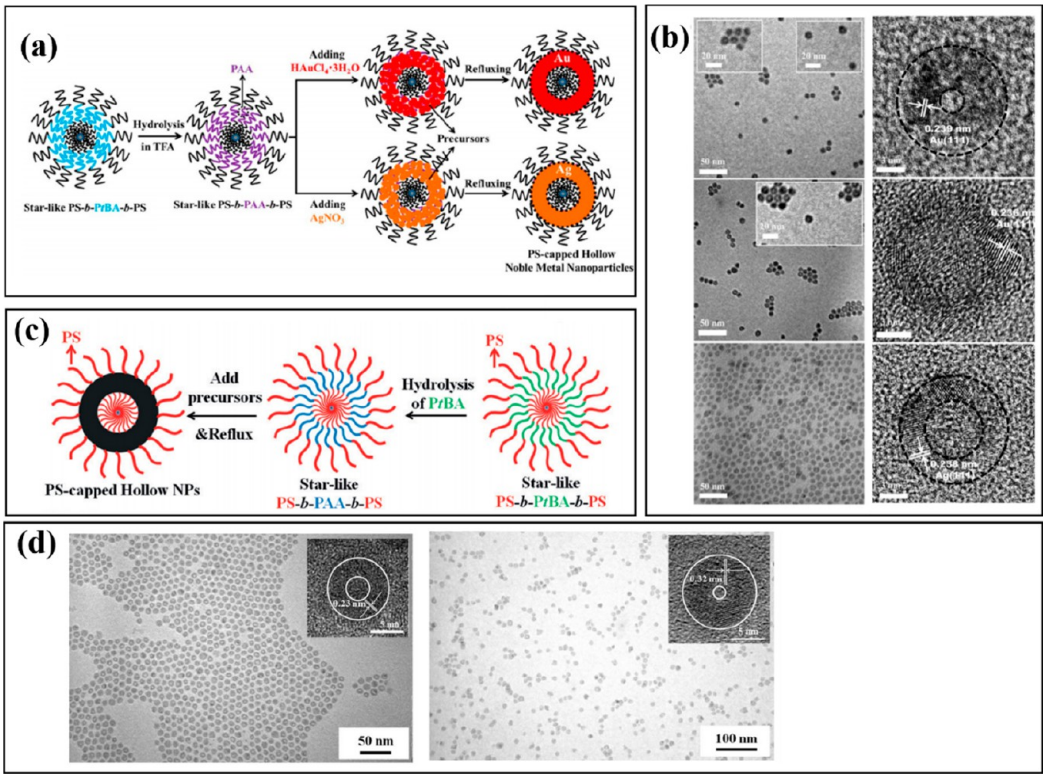

Figure 11. (a) Synthetic route to PS-ligated hollow metal NPs using star-like β-CD-*g*-[PS-*b*-PAA-*b*-PS] triblock copolymer as a nanoreactor. (b) TEM (left) and HRTEM (right) images of PS-ligated AuNPs of different sizes with the external diameter and shell thickness of 12 ± 0.4 nm and 4.7 ± 0.3 nm (top panels); 12 ± 0.5 nm and 2.7 ± 0.2 nm (middle panels); and 11.6 ± 0.4 nm and 2.7 ± 0.3 nm (bottom panels). Reproduced from ref 34. Copyright 2017 American Chemical Society. (c) Synthetic route to PS-ligated hollow PbTe NPs by employing star-like β-CD-*g*-[PS-*b*-PAA-*b*-PS] as a nanoreactor. (d) TEM images of PS-ligated hollow PbTe NPs with the hollow interior diameter D_{hollow} and shell thickness t_{shell} of D_{hollow} = 3.5 ± 0.2 nm and t_{shell} = 2.8 ± 0.2 nm (left) and D_{hollow} = 1.8 ± 0.2 nm and t_{shell} = 4.6 ± 0.4 nm (right) (inset: HRTEM of hollow PbTe NPs). Reproduced with permission from ref 35. Copyright 2017 Wiley-VCH.

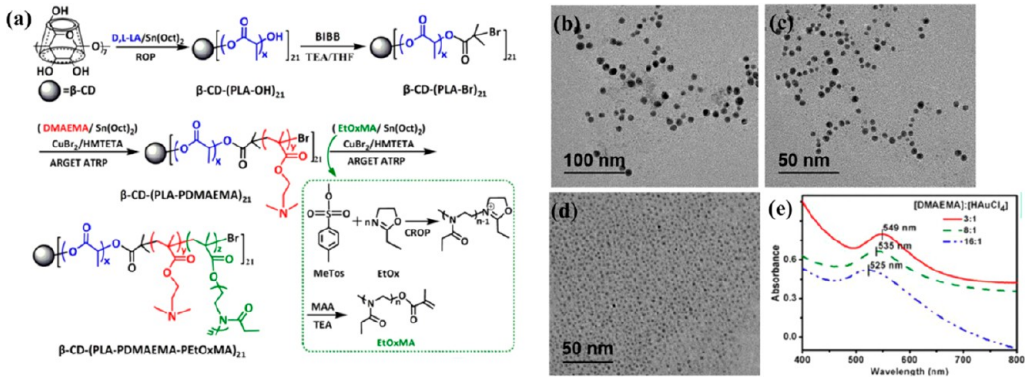

Figure 12. (a) Synthetic route to β-CD-[PLA-*b*-PDMAEMA-*b*-PEtOxMA]$_{21}$. Reproduced with permission from ref 51. Copyright 2016 Wiley-VCH. (b–d) TEM images of hollow AuNPs *in situ* crystallized in β-CD-[PLA-*b*-PDMAEMA-*b*-PEtOxMA]$_{21}$ with different molar ratios of DMAEMA to $HAuCl_4$ at (b) 16, (c) 8, and (d) 3. (e) UV–vis absorption spectra of hollow AuNPs synthesized using a β-CD-[PLA-*b*-PDMAEMA-*b*-PEtOxMA]$_{21}$ nanoreactor with different molar ratios of DMAEMA/$HAuCl_4$. We note that the hollow interior of AuNPs cannot be seen, which may be due likely to the low-magnification TEM imaging. Reproduced with permission from ref 52. Copyright 2017 Elsevier.

The second example involves the synthesis of semiconducting hollow PbTe NPs (Figure 11c).[35] Specifically, PbTe precursors ($Pb(NO_3)_2$ and Te power) were introduced into a DMF/BA (9/1, by volume) solution containing β-CD-*g*-[PS-*b*-PAA-*b*-PS] (Table 1; No. 10 nanoreactor)[35] and selectively loaded within the hydrophilic PAA compartment. The strong coordination interaction between −COOH groups of PAA blocks and PbTe precursors yielded hollow PbTe NPs with PS chains tethered on its inner and outer surfaces. Hollow PbTe NPs with different diameters of hollow interior (D_{hollow} = 3.5 ± 0.2 and 1.8 ± 0.2 nm) and shell thicknesses (t_{shell} = 2.8 ± 0.2 and 4.6 ± 0.4 nm) were attained using β-CD-*g*-[PS-*b*-PAA-*b*-PS] nanoreactors with different MWs of inner PS and intermediate PAA blocks (Figure 11d). The same nanoreactor was found to be applicable to craft hollow PbS NPs using $Pb(NO_3)_2$ and hexamethyldisilathiane as precursors.[35] Fur-

https://dx.doi.org/10.1021/acsnano.0c06936
ACS Nano 2020, 14, 12491–12521

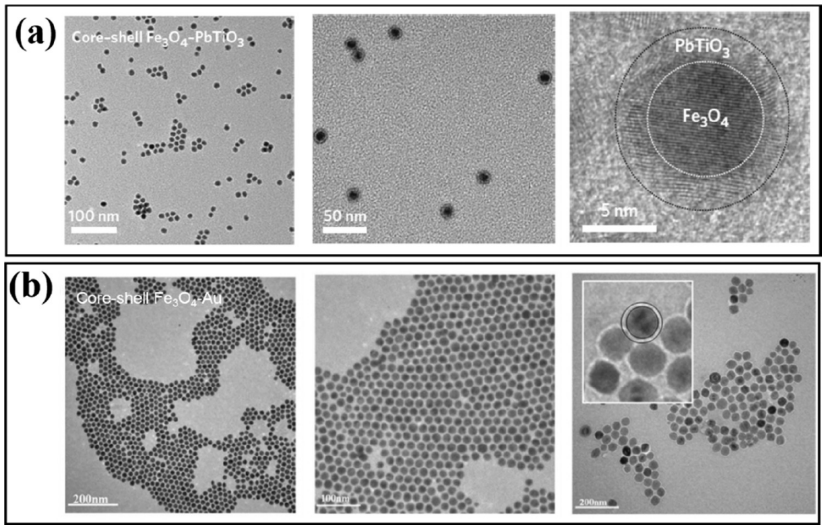

Figure 13. (a) TEM images of Fe_3O_4/$PbTiO_3$ core/shell NPs crafted using a β-CD-*g*-[P4VP-*b*-PAA-*b*-PS] nanoreactor. Reproduced with permission from ref 33. Copyright 2013 Springer Nature. (b) TEM images of Fe_3O_4/Au core/shell NPs prepared by employing a β-CD-*g*-[P4VP-*b*-PAA-*b*-PEO] nanoreactor. From left to right, the diameters of the Fe_3O_4 core are 6, 10, and 20 nm at the fixed Au shell thickness of 5 nm. Reproduced with permission from ref 50. Copyright 2015 Wiley-VCH.

thermore, conjugated polymer PEDOT-ligated hollow PbTe NPs were also prepared by utilizing β-CD-*g*-[PS-*b*-PAA-*b*-PEDOT] as a nanoreactor (Table 1; No. 13 nanoreactor).[35] Clearly, by rationally designing the outer polymer chains, a set of functional hollow NPs with tailorable surface functionalities can be readily crafted.

Recently, an intriguing star-like triblock copolymer of β-CD-*g*-[PCL-*b*-PAEMA-*b*-PPEGMA$_{21}$] (Table 1; No. 15 nanoreactor) grown from 21Br-β-CD initiator by the core-first strategy was exploited as a nanoreactor for crafting uniform hollow AuNPs formed within the intermediate PAEMA compartment as a result of complexation between Au precursors and N of PAEMA blocks. Doxorubicin (DOX) was further encapsulated within the inner PCL regime. The resulting DOX-loaded, PPEGMA-ligated hollow AuNPs were used for tumor-targeted chemotherapy and computed tomography imaging.[53] Similarly, in another example, star-like β-CD-[PLA-*b*-PDMAEMA-*b*-PEtOxMA$_{21}$] triblock copolymer (Table 1; No. 14 nanoreactor) was employed as a nanoreactor to create PEtOxMA-ligated hollow AuNPs *via* the complexation between Au precursors ($HAuCl_4$) and N of PDMAEMA, and the reduction of the Au precursor to AuNPs was catalyzed by PDMAEMA.[51,52] The size of AuNPs can be adjusted by changing the molar ratio of DMAEMA to $HAuCl_4$.[52] When the molar ratio of DMAEMA to $HAuCl_4$ increased from 3 to 8 and 16, the average external diameter of hollow AuNPs decreased from 16.2 to 5.2 and 2.1 nm, and accordingly, the characteristic plasmonic absorption peak shifted from 549 to 535 and 525 nm (Figure 12). This observation could be attributed to the thermodynamic balance between steric stabilization of AuNPs by unimolecular template and intrinsic aggregation of small AuNPs.[51,52] With decreasing concentration of Au precursors, the amount of AuNPs was low and the presence of polymer ligands was enough to prevent the AuNPs from aggregating. In stark contrast, the steric stabilization of a unimolecular nanoreactor decreased when more AuNPs formed in the solution. The insufficiently protected AuNPs were intercollided, resulting in large-sized AuNPs.

Hairy Core/Shell NPs. Core/shell NPs that integrate two dissimilar materials into one object with a distinct interface represent an important class of multifunctional nanomaterials as they facilitate the synergistic coupling of two constituents to yield different properties. It is important to note that in order to prepare high-quality core/shell NPs, a moderate lattice mismatch (<2%) between two disparate materials is required for the epitaxial growth of shell material over the highly curved surface of a spherical core. Such a prerequisite largely limits the attainable core/shell NPs of interest.[135] In this context, the use of star-like triblock copolymers as a nanoreactor offers a non-epitaxial growth strategy to produce a myriad of core/shell NPs with precisely controlled core diameter and shell thickness, dispensing with the need for lattice match as noted above. This is because the core and shell materials are independently template-grown within the inner and intermediate hydrophilic blocks of star-like triblock copolymer, respectively.

As an interesting example, magnetic Fe_3O_4/ferroelectric $PbTiO_3$ core/shell NPs with a large lattice mismatch (>40%) were successfully crafted using a star-like β-CD-*g*-[P4VP-*b*-P*t*BA-*b*-PS] triblock copolymer as a nanoreactor (Table 1; No. 9 nanoreactor).[33] First, the preferential partition of Fe_3O_4 precursors (*i.e.*, $FeCl_2{\cdot}4H_2O$/$FeCl_3{\cdot}6H_2O$) within the space occupied by the inner hydrophilic P4VP blocks and the coordination interaction between the metal moieties of precursors and pyridal groups of P4VP blocks yielded a P*t*BA-*b*-PS-ligated Fe_3O_4 core. Sequentially, P*t*BA blocks were hydrolyzed into PAA, which further directed the formation of the $PbTiO_3$ shell *via* coordination interaction between $PbTiO_3$ (*i.e.*, $PbTi[OCH(CH_3)_2]_6$) and −COOH groups of PAA blocks, thereby resulting in PS-ligated Fe_3O_4/$PbTiO_3$ core/shell NPs (Figure 13a). The outer PS hairs rendered good usability of Fe_3O_4/$PbTiO_3$ NPs in nonpolar solvents. In addition to nonpolar solvent-soluble core/shell NPs, polar-solvent-soluble core/shell NPs were also engineered using the similar strategy. For example, an array of uniform magnetic Fe_3O_4/plasmonic Au core/shell NPs with precisely controlled Fe_3O_4 core diameters and Au shell thicknesses were crafted using a series of star-like triblock copolymers of β-CD-*g*-

https://dx.doi.org/10.1021/acsnano.0c06936
ACS Nano 2020, 14, 12491−12521

[P4VP-*b*-P*t*BA-*b*-PEO] with varied MWs of P4VP and PAA as nanoreactors (Table 1; No. 12 nanoreactor).[50] In the mixed solvents containing DMF and diphenyl ether (DPE) (DMF/DPE = 9/1; by volume), a tight and spherical unimolecular micelle with coil-like inner P4VP blocks and collapsed P*t*BA-*b*-PEO outer blocks was formed due to their different solubilities in the mixed solvents. The precursors of $FeCl_2{\cdot}4H_2O$ and $FeCl_3{\cdot}6H_2O$ were preferentially entered into the P4VP regime and reduced into Fe_3O_4 NPs upon the addition of ammonium hydroxide, forming P*t*BA-*b*-PEO-ligated Fe_3O_4 NPs. Similar to the synthesis of $Fe_3O_4/PbTiO_3$ NPs discussed above, the P*t*BA blocks were then hydrolyzed into PAA blocks, followed by the loading and coordination reaction of $HAuCl_4$ precursors within the PAA regime, producing PEO-ligated Fe_3O_4/Au core/shell NPs. By varying the ATRP times of 4VP and *t*BA monomers, we achieved Fe_3O_4/AuNPs with different Fe_3O_4 core diameters at fixed Au shell thickness and *vice versa* (*i.e.*, at constant Fe_3O_4 core diameter and varied Au shell thicknesses) (Figure 13b). As such, their core-diameter- and shell-thickness-dependent optical properties can be scrutinized.[50]

Intriguingly, it is also feasible to transform the outer polymer hairs on the surface of core−shell NPs into functional materials such as a conductive carbon layer. For instance, uniform PS-ligated plasmonic Au/semiconducting TiO_2 core/shell NPs were created by capitalizing on the star-like β-CD-*g*-[P4VP-*b*-P*t*BA-*b*-PS] triblock copolymer as a nanoreactor (Table 1; No. 9 nanoreactor).[47] PS hairs on the surface of Au/TiO_2 NP can be calcined in an inert atmosphere to yield carbon-coated Au/TiO_2 NPs for use in dye-sensitized solar cells.[47] Recently, organolead halide perovskite/silica (*i.e.*, $MAPbBr_3/SiO_2$) core/shell NPs were produced using β-CD-*g*-[P4VP-*b*-P*t*BA-*b*-PS] as a nanoreactor.[49] In this study, $PbBr_2$ was preferentially loaded within the P4VP regime, followed by the hydrolysis of P*t*BA and the addition of another precursor MABr, yielding PAA-*b*-PS-ligated $MAPbBr_3$. Finally, PS-ligated $MAPbBr_3/SiO_2$ core/shell NPs were created *via* hydrolysis of tetramethyl orthosilicate (TMOS) within the space occupied by PAA chains. Likewise, PEO-ligated $MAPbBr_3/SiO_2$ NPs can also be prepared using β-CD-*g*-[P4VP-*b*-P*t*BA-*b*-PEO] as a nanoreactor (Table 1; No. 12 nanoreactor).[49] It is worth noting that such dual-shelled perovskite $MAPbBr_3$ NPs (*i.e.*, inorganic SiO_2 as an inner shell and polymer hairs (PS and PEO) as an outer shell) carry a stellar set of largely improved stabilities (*i.e.*, colloidal stability, chemical composition stability, water stability, photostability) as well as appealing solution processability.[49]

Based on the few representative examples discussed above, it is clear that the core and shell materials are template-grown independently within the inner and intermediate compartment of star-like triblock copolymers. Moreover, the surface chemistry of polymer-ligated core/shell NPs could be judiciously designed and enabled by advanced synthetic techniques, thereby offering this class of nanomaterials with additional engineered functionality for many applications.

1D Nanorods, Nanowires, and Nanotubes Directed by Bottlebrush-like Polymer Nanoreactors. As discussed above, the cylindrical architecture of bottlebrush-like polymers gives them unusual properties and promising applications in photonic crystals,[79,136] biomedicine,[137,138] hybrid nanostructures,[139,140] and self-assembled superstructures.[141,142] It is important to note that bottlebrush-like polymers are stable unimolecular cylindrical micelles against external stimuli. This contrasts sharply with cylindrical micellar analogues formed *via* self-assembly of linear BCPs, which are dynamically stable. Thus, in what follows, we review the implementation of unimolecular bottlebrush-like diblock and triblock copolymers to construct polymer-ligated 1D nanorods, nanowires, and nanotubes (NTs).

Hairy Plain Nanorods and Nanowires. We note that the length and diameter of polymer-ligated plain NRs and NWs can be readily controlled by adjusting the lengths of the polymer backbone and inner block of diblock side chains (brushes), respectively. By coordinating different kinds of precursors of interest, the composition of 1D NRs and NWs can also be easily tuned.

To date, a collection of 1D NWs have been reported using bottlebrush-like diblock copolymers as nanoreactors, including metal NWs, metal oxide NWs, nonmetal oxide NWs, and semiconducting NWs. For example, using a polymerizable silane (*e.g.*, 3-acryloylpropyltrimethoxysilane (3-APTS)) as monomer, the bottlebrush-like PHEMA-*g*-[PAPTS-*b*-PDMAEMA] diblock copolymer (Table 1; No. 23 nanoreactor) was synthesized.[96] Then, SiO_2 NWs were *in situ* grown through an alkali-catalyzed condensation reaction of the inner PAPTS blocks. PDMAEMA-ligated SiO_2 can be further functionalized by PtNPs as a result of coordination reaction between the quaternized PDMAEMA shell and Pt precursors.[96] Similarly, a soluble organo-silica NW was formed using the bottlebrush-like PHEMA-*g*-[PAPTS-*b*-POEGMA] diblock copolymer (Table 1; No. 25 nanoreactor) to enable *in situ* formation of SiO_2 within the inner PAPTS blocks.[98] Recently, rare-earth metal cation (Ln^{3+})-decorated hybrid SiO_2 NWs possessing photoluminescence and paramagnetic properties were produced using bottlebrush-like PHEMA-*g*-[PAA-*b*-PDMAEMA] diblock copolymers (Table 1; No. 21 nanoreactor).[94] Moreover, bottlebrush-like diblock copolymer nanoreactors can also be exploited to synthesize TiO_2 and ZnO NWs during which titanium(IV) 2-ethylhexanoate ($Ti(EH)_4$) and Zn precursors were selectively loaded, respectively, in the inner PAA blocks of PHEMA-*g*-[PAA-*b*-PS] (Table 1; No. 26 nanoreactor).[99,127] The length and diameter of the resulting hybrid NWs were controlled by the MWs of PHEMA backbone and PAA block, respectively.[99,127] Likewise, the use of a PHEMA-*g*-[PHEMA-*b*-POEGMA] nanoreactor (Table 1; No. 22 nanoreactor) enabled the synthesis of TiO_2 NWs using $Ti(OC_4H_9)_4$ as the TiO_2 precursor, and $Ti(OC_4H_9)_4$ was mainly positioned in the brush core (*i.e.*, PHEMA) *via* a transalcoholysis reaction.[95] It is interesting to note that the amphiphilic PHEMA-*g*-[PAA-*b*-P*n*BA] diblock copolymer (Table 1; No. 19 nanoreactor) directed the growth of cadmium sulfide (CdS) and cadmium selenide (CdSe) NWs *via* the absorption of Cd^{2+} by −COOH in the PAA block, followed by the introduction of H_2S and H_2Se, respectively.[91,92] Moreover, superparamagnetic hybrid nanocylinders were also prepared using the same PHEMA-*g*-[PAA-*b*-P*n*BA] nanoreactor.[90] To improve the magnetic response of the paramagnetic nanocylinders, presynthesized Fe_3O_4 NPs (∼10 nm in diameter) were incorporated into PHEMA-*g*-[PMAA-*b*-POEGMA] (Table 1; No. 20 nanoreactor) to yield excellent magnetic-responsive hybrid magnetic NWs.[93]

It is noteworthy that the use of PHEMA and other backbones cannot afford a high level of stiffness to yield rigid NRs or NWs. On many occasions, it is highly desirable to use the rigid backbone that enables the synthesis of high-quality NRs and NWs for exploring their aspect ratio-dependent physical properties. Recently, a general method-

https://dx.doi.org/10.1021/acsnano.0c06936
ACS Nano 2020, 14, 12491−12521

ology for the preparation of a rich variety of NRs including noble metallic (*e.g.*, Au, Pt), ferroelectric (*e.g.*, $BaTiO_3$), upconversion (*e.g.*, green-emitting $NaYF_4$:Yb/Er and blue-emitting $NaYF_4$:Yb/Tm), semiconducting (*e.g.*, CdSe), thermoelectric (*e.g.*, PbTe), and magnetic (*e.g.*, Fe_3O_4) have been crafted using bottlebrush-like cellulose-*g*-[PAA-*b*-PS] as a nanoreactor (Table 1; No. 30 nanoreactor) that contains a rigid cellulose backbone (Figure 14).[102] Likewise, owing to strong coordination interaction between −COOH groups of PAA blocks and metal moieties of precursors, these precursors were preferentially loaded in the cylinder-shaped PAA block compartment, leading to the nucleation and growth of inorganic NCs. The surface chemistry of NRs can be readily tuned. For example, water-soluble AuNRs ligated with hydrophilic poly(ethylene glycol) (PEG) hairs can be prepared by capitalizing on double-hydrophilic cellulose-*g*-[PAA-*b*-PEG] as a nanoreactor (Table 1; No. 31 nanoreactor), whereas organic solvent-soluble AuNRs ligated with hydrophobic PS can be synthesized using cellulose-*g*-[PAA-*b*-PS] as discussed above.[102] The length and diameter of NRs can be easily tailored by judiciously varying the length of the cellulose-Br macroinitiator and MW of inner PAA blocks, respectively.

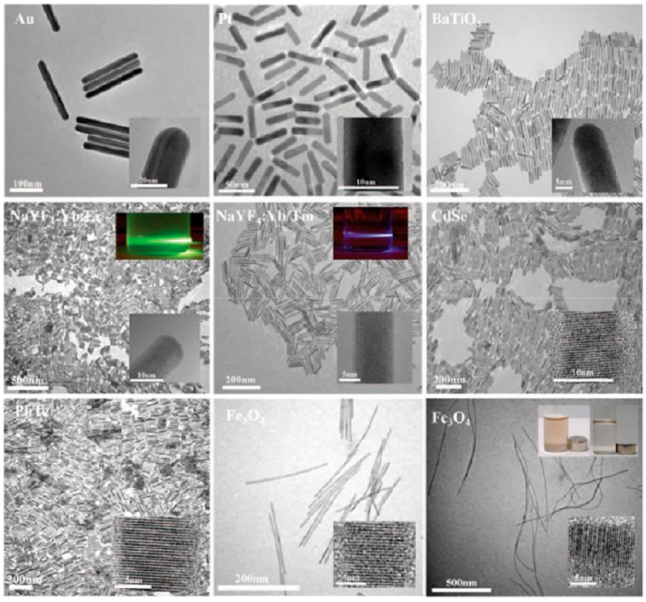

Figure 14. TEM and HRTEM images of various plain NRs synthesized using cellulose-*g*-[PAA-*b*-PS] as nanoreactor. Reproduced with permission from ref 102. Copyright 2016 American Association for the Advancement of Science (AAAS).

Hairy Nanotubes (i.e., Hollow Nanorods). It is also possible to create a polymer-ligated hollow 1D NR (*i.e.*, nanotube) by employing bottlebrush-like triblock copolymers as nanoreactors in which the intermediate hydrophilic blocks direct the synthesis of the NT. A pioneering work on the synthesis of hydrophilic organo-silica hybrid NTs involves the use of triblock polymer brushes consisting of a PHEMA backbone, a P*t*BA core, a PAPTS shell, and a POEGMA corona (*i.e.*, PHEMA-*g*-[P*t*BA-*b*-PAPTS-*b*-POEGMA]) (Table 1; No. 27 nanoreactor).[100] The SiO_2 shell was formed by the condensation of the trimethoxysilyl groups in PAPTS in aqueous solution. The length and thickness of the SiO_2 shell are tunable by varying the MW of PAPTS. Strictly speaking, these POEGMA-ligated SiO_2 NTs are not exactly hollow owing to the existence of inner P*t*BA blocks.[100] Likewise, by employing PHEMA-*g*-[PCL-*b*-PDMAEMA-*b*-POEGMA] as a nanoreator (Table 1; No. 28 nanoreactor),[101] anatase TiO_2 was formed in the PDMAEDA regime due to the interaction between the precursors (*i.e.*, titanium(IV) bis(ammonium lactate) dihydroxide; TALH) and PDMAEMA, yielding POEGMA-ligated TiO_2 NTs. The length and diameter of TiO_2 NTs can be adjusted by varying the lengths of PHEMA

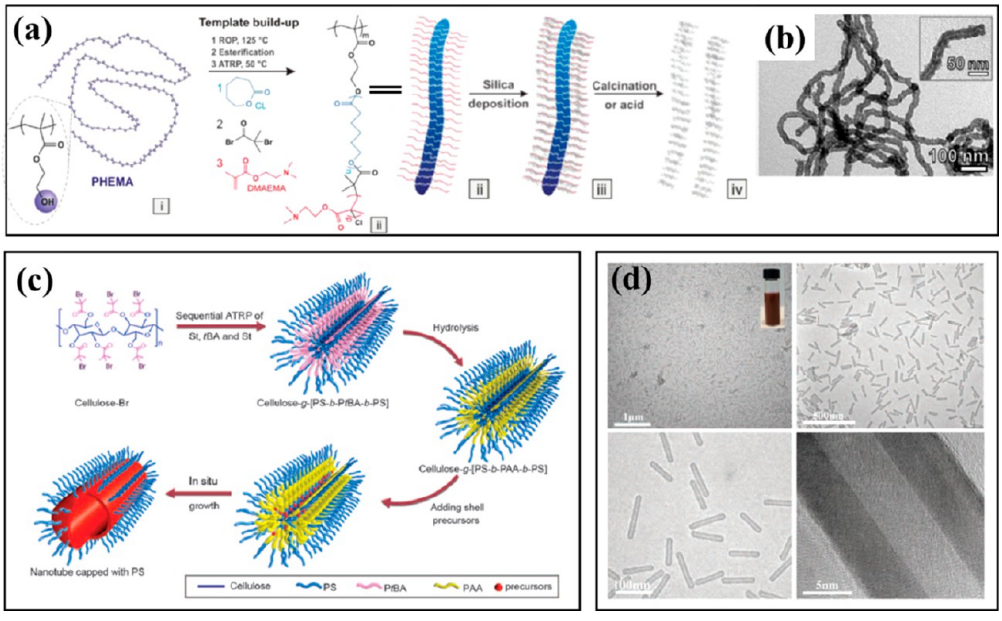

Figure 15. (a) Synthetic route to PHEMA-*g*-[PCL-*b*-PDAEMA] and subsequent SiO_2 NT formed using PHEMA-*g*-[PCL-*b*-PDAEMA] as a nanoreactor. (b) TEM image of a SiO_2 NT. Reproduced from ref 97. Copyright 2012 American Chemical Society. (c) Synthetic route to cellulose-*g*-[PS-*b*-PAA-*b*-PS] and their use as a nanoreactor for PS-ligated NTs. (d) TEM images of AuNTs templated by cellulose-*g*-[PS-*b*-PAA-*b*-PS]. Reproduced with permission from ref 102. Copyright 2016 American Association for the Advancement of Science (AAAS).

https://dx.doi.org/10.1021/acsnano.0c06936
ACS Nano 2020, 14, 12491−12521

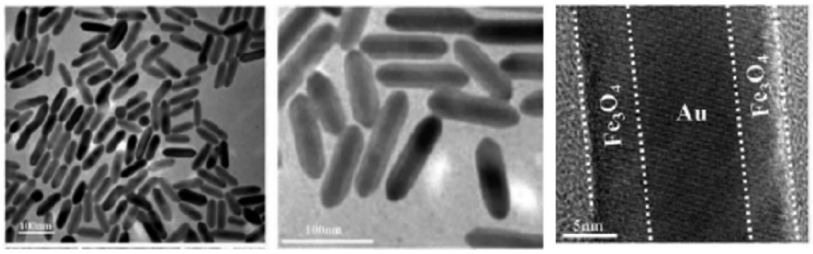

Figure 16. TEM and HRTEM images of Au/Fe_3O_4 core/shell NRs with a AuNR diameter of 10.5 ± 0.6 nm and a Fe_3O_4 shell thickness of 4.6 ± 0.4 nm, template-grown from the cellulose-*g*-[P4VP-*b*-P*t*BA-*b*-PS] nanoreactor. Reproduced with permission from ref 102. Copyright 2016 American Association for the Advancement of Science (AAAS).

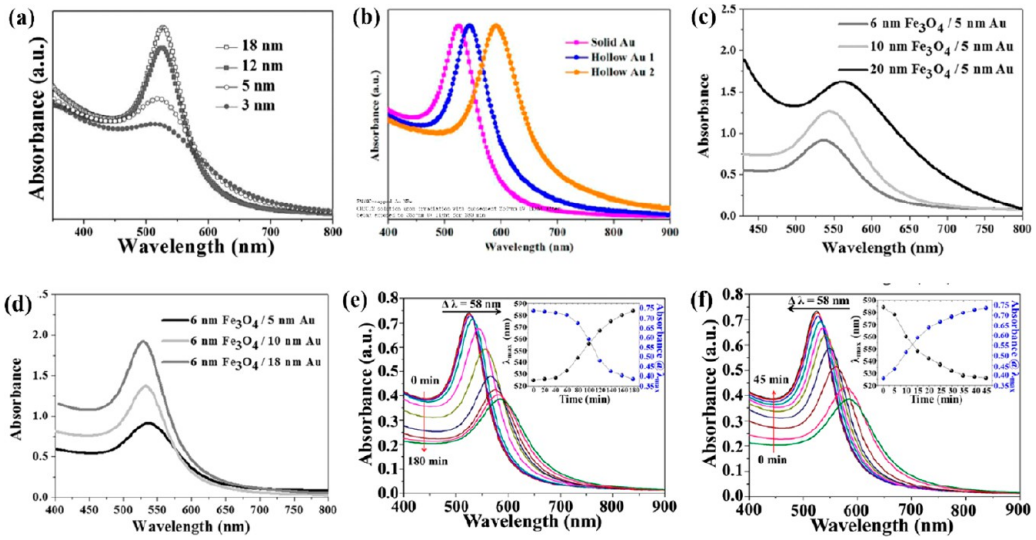

Figure 17. UV−vis spectra of (a) PS-ligated AuNPs of various sizes (prepared using *β*-CD-*g*-[P*t*BA-*b*-PS] as a nanoreactor). Reproduced with permission from ref 39. Copyright 2016 Wiley-CVH. (b) Solid AuNPs as well as hollow AuNPs 1 and 2 permanently ligated by PS (synthesized by employing *β*-CD-*g*-[PS-*b*-P*t*BA-*b*-PS] as a nanoreactor). Reproduced from ref 34. Copyright 2017 American Chemical Society. (c) Fe_3O_4/Au core/shell NPs with a Fe_3O_4 core of 6, 10, and 20 nm at a fixed Au shell of 5 nm (templated by *β*-CD-*g*-[PS-*b*-P*t*BA-*b*-PEO] as a nanoreactor). (d) Fe_3O_4/Au core/shell NPs with a Au shell thicknesses of 5, 10, and 18 nm at a constant Fe_3O_4 core of 6 nm. Reproduced with permission from ref 50. Copyright 2015 Wiley-CVH. (e) Photoresponsive PMAMC-ligated AuNPs when illuminated with a 365 nm UV lamp (crafted by utilizing *β*-CD-*g*-[P*t*BA-*b*-PMAMC] as a nanoreactor). (f) PMAMC-ligated AuNPs upon subsequent exposure to 254 nm UV lamp after irradiation by a 365 nm UV lamp for 3 h. Reproduced with permission from ref 42. Copyright, 2018 National Academy of Sciences.

and PDMAEMA blocks, respectively.[101] Moreover, using a bottlebrush-like diblock copolymer of PHEMA-*g*-[PCL-*b*-PDMAEMA] as a nanoreactor, a hollow SiO_2 NT was derived by depositing TMOS on quaternized PDMAEMA blocks, followed by sintering or reacting with an acid to remove the inner PCL core (Figure 15a,b).[97] We note the hollow SiO_2 NT formed in this study was not ligated by polymers.

As discussed above, it is not surprising that the SiO_2 NW can also be crafted using a bottlebrush-like PHEMA-*g*-[PCL-*b*-PDMAEMA] diblock copolymer with a long HEMA backbone as nanoreactor (*i.e.*, 1250 ± 200 nm, whereas 265 ± 20 nm for the NT).[97] Intriguingly, when Pt or AuNPs were first loaded in the PDMAEMA regime, followed by the formation of SiO_2 upon the addition of TMOS, the metal NP-containing hybrid SiO_2 NW can be obtained as a result of the coordination interactions between both metal precursors and TMOS with PDMAEMA.[97]

Quite interestingly, the implementation of cellulose-backbone-based bottlebrush-like triblock copolymers is also feasible for the construction of high-quality 1D NTs. Recently, by exploiting amphiphilic cellulose-*g*-[PS-*b*-PAA-*b*-PS] as a nanoreactor (Table 1; No. 34 nanoreactor), organic solvent-soluble PS-ligated AuNTs were synthesized as Au precursors were preferentially partitioned in the intermediate PAA blocks (Figure 15c,d).[102] The dimension of AuNTs including the diameter of the inner cavity and the thickness of the AuNT shell can be readily controlled by regulating ATRP reaction times of the inner PS blocks and the intermediate P*t*BA blocks (hydrolyzed into PAA blocks later), respectively. This strategy is greatly reliable to produce other PS-ligated NTs of different compositions and water-soluble PEG-ligated NTs by varying the precursors and employing the cellulose-*g*-[PS-*b*-PAA-*b*-PEG] nanoreactor.[102]

Hairy Core/Shell Nanorods. Recently, core/shell NRs with adjustable dimensions (core diameter, shell thickness, and length), chemical compositions, and solubility were achieved by exploiting amphiphilic bottlebrush-like cellulose-backbone-containing triblock copolymers as nanoreactors.[102] For example, PS-ligated plasmonic Au/magnetic Fe_3O_4 core/shell NRs were formed by employing cellulose-*g*-[P4VP-*b*-P*t*BA-*b*-PS] as a nanoreactor (Table 1; No. 32 nanoreactor), in which Au was first formed within the inner P4VP compartment, followed by the growth of the Fe_3O_4 shell templated by the PAA blocks obtained *via* hydrolyzing the intermediate P*t*BA

https://dx.doi.org/10.1021/acsnano.0c06936
ACS Nano 2020, 14, 12491−12521

blocks (Figure 16).[102] By combining ATRP with the click reaction, cellulose-*g*-[P4VP-*b*-P*t*BA-*b*-PEG] was synthesized, with which hydrophilic core/shell nanorods ligated with water-soluble PEG hairs can be crafted, such as plasmonic Au/semiconducting TiO_2 as well as plasmonic Au/upconversion $NaYF_4$:Yb/Er core/shell NRs.[102] It is notable that such an amphiphilic bottlebrush-like triblock copolymer strategy renders precise tailoring of the core diameter and shell thickness of NRs by varying the MWs of the inner P4VP blocks and intermediate P*t*BA blocks, respectively. By extension, polymer-ligated core/shell NWs may be achieved by extending the length of the cellulose backbone used in the synthesis of these bottlebrush-like triblock copolymers.

SIZE-, ARCHITECTURE-, AND SURFACE-CHEMISTRY-DEPENDENT PROPERTIES OF POLYMER-LIGATED NANOCRYSTALS

The physical properties of NCs depend heavily on their sizes and shapes (*e.g.*, core diameter and shell thickness as in core/shell NPs and diameter and length as in NRs), compositions, architecture (*e.g.*, plain, hollow, and core/shell), and surface chemistry. Thus, the ability to produce NCs with controlled structural characteristics noted above is the key to interrogate their fundamental structure−property relationship that occurs only at the nanoscale. It is notable that NCs prepared by conventional methods (*e.g.*, ligand-capped NCs) often possess limited long-term stability due to the dynamic association and dissociation of surface ligands.[143] In contrast, the unimolecular nonlinear block copolymer nanoreactor strategy described above imparts precise crafting of NCs that are intimately and stably tethered with polymers (*i.e.*, polymer-ligated NCs), thus facilitating investigation into the correlation of the properties with structures of this class of nanomaterials, as highlighted in several studies discussed below.

Modulating Optical Properties *via* Size, Architecture, and Surface Polymer Functionality Control. Precious metal NPs (*i.e.*, Ag and Au) exhibit appealing optical properties due to strong surface plasmon resonance (SPR) that originated from the interaction of an electromagnetic wave and the conduction electrons in metal nanostructures. Figure 17a shows the UV−vis absorption spectra of PS-ligated AuNPs with different diameters prepared using star-like diblock copolymers of β-CD-*g*-[PAA-*b*-PS] as a nanoreactor (Table 1; No. 2 nanoreactor).[39] Clearly, the characteristic SPR peak position was slightly red-shifted and accompanied by an obviously increased absorption intensity and decreased full width at half-maximum (fwhm) with increasing Au size, correlating well with the results in the literature.[144] The architecture of AuNPs (*i.e.*, hollow *versus* solid) was found to exert a significant effect on their SPR properties. As shown in Figure 17b, solid AuNPs with a diameter of 12.2 ± 0.5 nm demonstrated a SPR peak at 525 nm, whereas the characteristic SPR peak of hollow AuNPs 1 (*i.e.*, external diameter of 12 ± 0.4 nm and shell thickness of 4.7 ± 0.3 nm) with the same external diameter yet possessing an interior cavity was shifted to 545 nm. Moreover, a larger red shift (67 nm) was observed for hollow AuNPs 2 (*i.e.*, external diameter of 12 ± 0.5 nm and shell thickness of 2.7 ± 0.2 nm) with an increased cavity over that of AuNPs 1.[34]

In addition, polymer-ligated Au-containing core/shell NPs displayed a more intriguing SPR property. For example, the absorption peak of the PEO-ligated Fe_3O_4/Au core/shell NPs prepared by employing star-like β-CD-*g*-[P4VP-*b*-PAA-*b*-PEO] as a nanoreactor (Table 1; No. 12 nanoreactor) was red-shifted with increasing Fe_3O_4 core diameter at a fixed Au shell thickness (Figure 17c) due to the electron deficiency on Au caused by the electron trapping or charge compensation at the Fe_3O_4/Au interface.[50,145−147] In contrast, a blue shift was seen for PEO-ligated Fe_3O_4/AuNPs of increasing Au shell thickness at a fixed Fe_3O_4 core diameter (*i.e.*, 6 nm) (Figure 17d) as the increased Au content can decrease the effect of the Fe_3O_4 core diameter on the plasmonic absorption, thus blue-shifting toward the plasmonic absorption of pure AuNPs.[148] Similarly, PS-ligated Au/TiO_2 core/shell NPs with a fixed diameter of the Au core prepared by star-like β-CD-*g*-[P4VP-*b*-P*t*BA-*b*-PS][47] (Table 1; No. 9 nanoreactor) showed a red-shifted SPR band as the TiO_2 shell thickness increased owing to the change of local dielectric environment of Au as a result of the presence of a high dielectric TiO_2 shell.[144]

In addition to the architecture, the functionalities of surface polymers were also found to influence on the SPR property of AuNPs. Recently, thermoresponsive PNIPAM-ligated AuNPs prepared by employing star-like β-CD-*g*-[PAA-*b*-PNIPAM] as a nanoreactor (Table 1; No. 3 nanoreactor) experienced progressive red shifts and improved SPR peak intensities as the temperature increased from 10 to 50 °C.[41] Interestingly, the optical property of PNIPAM-ligated AuNPs can be tailored by manipulating the thermoresponsiveness of ligated PNIPAM hairs which experienced a transition from well-dispersed to collapsed chain conformation upon heating. Thus, the local refractive index of AuNPs was increased, leading to a red-shifted and enhanced SPR band.[149] In another study, the SPR peak position of light-responsive PMAMC-ligated AuNPs showed a 59 nm red shift in conjunction with reduced absorbance and increased fwhm after being irradiated with a 365 nm UV lamp (Figure 17e).[42] Quite intriguingly, such largely changed SPR properties can be fully recovered to their original state by subsequently exposing them to a 254 nm UV light (Figure 17f). This phenomenon can be rationalized by the photoinduced reversible self-assembly of PMAMC-capped AuNPs.[42]

Recently, uniform $CsPbX_3$ perovskite QDs were crafted by exploiting judiciously designed amphiphilic star-like β-CD-*g*-[PAA-*b*-PS] as a nanoreactor (Table 1; No. 2 nanoreactor).[40] Owing to the readily tunable MW of PAA and PS blocks by controlling their respective polymerization times, $CsPbX_3$ perovskite QDs with precisely size-tunable optical properties were rendered. As depicted in Figure 10c, PS-ligated $CsPbBr_3$ QDs with a diameter of 8.6 ± 0.3, 10.1 ± 0.6, and 13.9 ± 0.7 nm exhibited photoluminescence (PL) peaks at 514, 515, and 516 nm, respectively. In addition to the size-dependent optical properties, the composition of PS-capped $CsPbBr_3$ QDs can also be effectively altered to regulate their optical properties. For example, by employing $ZnCl_2$ and ZnI_2 as Cl^- and I^- sources, blue-emitting $CsPbCl_3$ and red-emitting $CsPbI_3$ QDs were formed *via* anion change with Br^- of PS-capped $CsPbBr_3$ QDs. Taken together, optical properties of PS-capped $CsPbX_3$ QDs can be conveniently and precisely tuned by varying their sizes and compositions.[40]

Tailoring Superparamagnetic Properties *via* Control over Size. When the size of magnetic nanostructures decreases to a critical radius r_c, where a single domain is formed instead of multiple domains, superparamagnetism appears.[150] The superparamagnetism refers to magnetic NPs that have a large and fixed magnetic moment, which display a rapid response to the external magnetic field without residual

https://dx.doi.org/10.1021/acsnano.0c06936
ACS Nano 2020, 14, 12491−12521

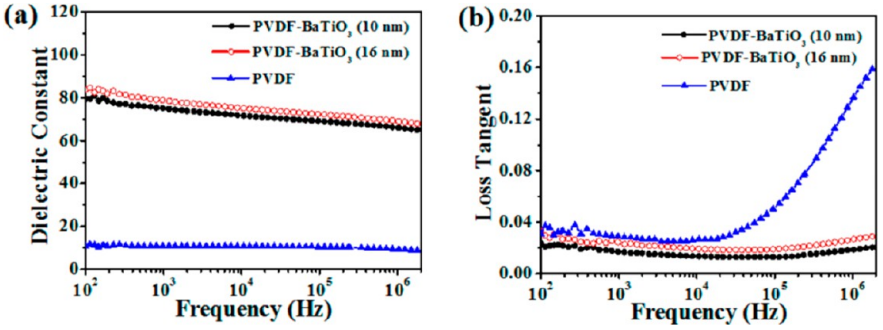

Figure 18. Dielectric constants and loss tangents of PVDF and PVDF-$BaTiO_3$ nanocomposites containing $BaTiO_3$ NPs (*i.e.*, PVDF-ligated $BaTiO_3$ NPs) with a diameter of 10.2 ± 0.6 and 16.1 ± 0.8 nm, respectively, prepared using star-like β-CD-*g*-[PAA-*b*-PVDF] as a nanoreactor. Reproduced from ref 45. Copyright 2015 American Chemical Society.

magnetism (M_r = 0) and coercivity.[151] The saturation magnetization of superparamagnetic NPs such as Fe_3O_4 is size-dependent. For example, different sizes of PS-ligated Fe_3O_4 NPs (6, 10, and 16 nm) prepared from the nanoreactor of β-CD-*g*-[(PAA-*b*-PS] were superparamagnetic at 300 K, and the saturation magnetization increased accordingly with increasing Fe_3O_4 NP size.[33] Starting from the bifunctional ligands with ATRP activity and iron precursors, PMMA-ligated Fe_3O_4 NPs were obtained by ATRP of MMA on the surface of Fe_3O_4 NPs.[152] There was no hysteresis loop for PMMA-ligated Fe_3O_4 NPs of different sizes, suggesting their superparamagnetic property. Accordingly, the saturation magnetization increased with increasing NP size.[153] A similar phenomenon was observed in Fe_3O_4 NCs created using star-like β-CD-*g*-$[(PEO\text{-}g\text{-}PAA)\text{-}b\text{-}PEO]_{18}$ as a nanoreactor (Table 1; No. 17 nanoreactor).[153] The diblock polymer arm of (PEO-*g*-PAA)-*b*-PEO was composed of PAA-grafted PEO as the first block and a pure PEO block as the second block. Likewise, Fe_3O_4 NCs were formed within the compartment occupied by PAA subunits due to coordination interaction between precursors and −COOH groups of PAA. The dimension of Fe_3O_4 NCs can be controlled by adjusting the length of the first PEO block as well as the grafting density of PAA subunits, thereby affording a changeable superparamagnetic behavior of Fe_3O_4 NCs. With increasing grafting density of PAA subunits, a larger saturation magnetization was seen, which can be attributed to the formation of larger-sized Fe_3O_4 as more precursors were loaded in the PAA compartment.[153]

Investigation into Size-Dependent Dielectric and Ferroelectric Properties. Ferroelectric materials manifest spontaneous electric polarization. Their polarization direction can be manipulated by the externally applied fields such as electric field, mechanical force, *etc.*[154] $BaTiO_3$ NPs represent one of the most widely studied ferroelectric nanomaterials because of their high dielectric constant and ferroelectric properties.[155,156] The ferroelectric properties of $BaTiO_3$ are closely related to its crystal phase, particle size, and surface chemistry.[157] The size-dependent dielectric and ferroelectric properties of $BaTiO_3$ are particularly interesting for applications in miniaturized electronic devices.[158] Therefore, it is highly desirable to synthesize $BaTiO_3$ NPs of controllable sizes with better ferroelectricity, higher permittivity, and lower dielectric loss.

As poly(vinylidene fluoride) (PVDF) is a promising polymer for dielectric nanocomposites, PVDF-ligated $BaTiO_3$ NPs were crafted using star-like β-CD-*g*-[PAA-*b*-PVDF] as a nanoreactor (Table 1; No. 7 nanoreactor).[45] The dielectric properties of PVDF-ligated $BaTiO_3$ NPs, referred to as PVDF-$BaTiO_3$ nanocomposites in this study,[45] were calculated by examining the capacitance and dissipation factor of parallel-plate capacitors prepared by hot-pressing the nanocomposite powders. As shown in Figure 18, the dielectric constants of PVDF-$BaTiO_3$ nanocomposites are much higher than those of pure PVDF, and PVDF-$BaTiO_3$ nanocomposites containing larger-sized $BaTiO_3$ NPs (D = 16.1 ± 0.8 nm) possessed dielectric constants higher than those of smaller-sized ones (D = 10.2 ± 0.6 nm). On the other hand, the dissipation factor of PVDF-$BaTiO_3$ nanocomposites is much lower than that of pure PVDF, offering promising applications in various energy storage devices.[159] Moreover, the ferroelectric properties of these PVDF-$BaTiO_3$ nanocomposites were also scrutinized.[45]

We note that, in addition to optical, magnetic, dielectric, and ferroelectric properties, other physical properties of polymer-ligated uniform NCs, including catalytic (*e.g.*, Pt, TiO_2, and Cu_2O NPs;[33,127] both photocatalysis and electrocatalysis), luminescent (*e.g.*, II−IV QDs as well as organic−inorganic and all-inorganic perovskite QDs),[33] upconverting (*e.g.*, $NaYF_4$:Yb/Tm and $NaYF_4$:Yb/Er),[102] multiferroic (*e.g.*, $BiFeO_3$), thermoelectric (as in PbTe NPs),[46] and magnetoelectric coupling (*e.g.*, $MFe_2O_4/BaTiO_3$), can also be explored to provide insight into their strong dependence to size, shape, and architecture of NPs.

APPLICATION OF POLYMER-LIGATED NANOCRYSTALS

Crafting a large variety of uniform NCs by capitalizing on judiciously designed nonlinear BCPs with well-defined MW and narrow MW distribution as nanoreactors represents a versatile strategy that offers a high level of tailorability in dimension, composition, architecture, surface chemistry, and stability of NCs with engineered functionalities for use in energy conversion and storage, electronics, photonics, optoelectronics, catalysis, nanotechnology, biotechnology, *etc.* In this section, we will exemplify several promising applications of polymer-ligated NCs.

Solar Energy Conversion. The implementation of upconversion NPs (UCNPs) in perovskite solar cells (PSCs) to capture near-infrared (NIR) solar photons for increased photocurrent may stand out as an appealing strategy to improve the power conversion efficiency (PCE) of PSCs. Recently, NIR organolead halide PSCs enabled by monodisperse dual-functional $NaYF_4$:Yb/Er UCNPs were reported.[44] The $NaYF_4$:Yb/Er UCNPs were synthesized by employing the double-hydrophilic star-like diblock copolymer

https://dx.doi.org/10.1021/acsnano.0c06936
ACS Nano 2020, 14, 12491−12521

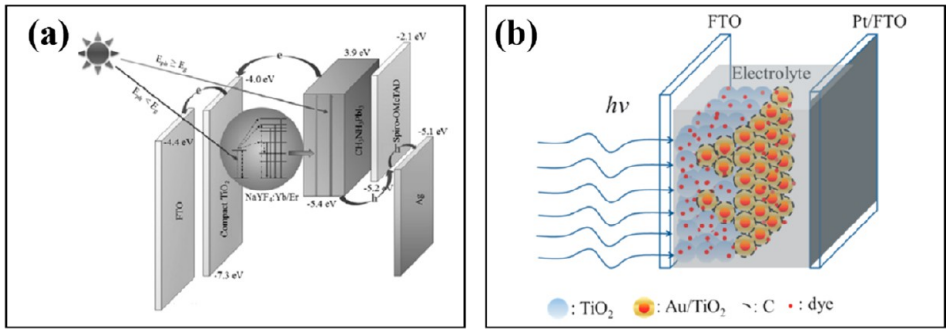

Figure 19. (a) Energy level diagram of $CH_3NH_3PbI_3$ solar cell containing the $NaYF_4$:Yb/Er mesoporous electrode. Reproduced with permission from ref 44. Copyright 2016 Wiley-VCH. (b) Scheme of DSSC where a TiO_2 photoanode is deposited with carbon-coated Au/TiO_2 core/shell NPs. Reproduced from ref 47. Copyright 2015 American Chemical Society.

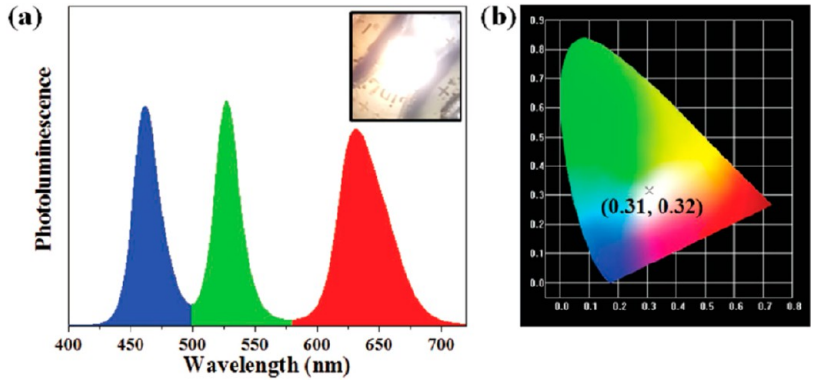

Figure 20. (a) Photoluminescence spectra of PS-ligated $CsPbBr_3$ QD-based white-light-emitting diode. Inset: Digital image of as-prepared WLED device. (b) CIE color diagram of the WLED device. Reprinted with permission from ref 40. Copyright 2019 Wiley-VCH.

of β-CD-*g*-[PAA-*b*-PEO] as a nanoreactor.[44] The exterior PEO chains not only offer the solubility and high stability of as-prepared $NaYF_4$:Yb/Er UCNPs in aqueous solution but also have the capability of regulating porosity of the electrode by adding a PEO homopolymer. A high PCE of 17.8% was obtained in $CH_3NH_3PbI_3$ PSC with a $NaYF_4$:Yb/Er UCNP-containing mesoporous electrode sandwiched between the compact TiO_2 film and $CH_3NH_3PbI_3$. The PCE was further increased to 18.1% under the irradiation of a 980 nm laser (Figure 19a).[44]

Recently, carbonized Au/TiO_2 core/shell NPs (*i.e.*, carbon-coated Au/TiO_2) were incorporated in dye-sensitized solar cells (DSSCs) by depositing a thin layer of PS-ligated Au/TiO_2 NPs on the top of P25 film (*i.e.*, TiO_2 as photoanode), followed by thermal annealing at 500 °C in argon to convert PS-ligated Au/TiO_2 NPs into carbon-coated Au/TiO_2 NPs (Figure 19b). The PS-ligated Au/TiO_2 NPs were prepared using star-like β-CD-*g*-[P4VP-P*t*BA-*b*-PS] as a nanoreactor. Owing to the synergetic effect of surface-plasmon-enabled light-harvesting enhancement of the Au core and fast electron transport promoted by the conductive carbon layer coating on Au/TiO_2 NPs, the short-circuit current density and PCE of the resulting DSSCs were increased by 18.4 and 13.6%, respectively, compared to a pure P25-based device.[47]

Light-Emitting Diodes. Recent impressive development in the synthesis of perovskite QDs (ABX_3; both organic–inorganic and all-inorganic) as building blocks for miniaturized materials and devices has emerged as an important research activity. They have found promising applications in photovoltaics, light-emitting dioxides (LEDs), scintillators, lasers, *etc.*[160] The practical applications of ABX_3 QDs have been primarily limited by the long-term stability due to their ionic crystal nature and tendency to decompose under external stimuli (*e.g.*, UV, water, oxygen, polar solvents, heat, *etc.*).[161] In this context, recently, uniform all-inorganic perovskite $CsPbBr_3$ QDs were prepared using a judiciously designed amphiphilic star-like diblock copolymer of β-CD-*g*-[PAA-*b*-PS] as a molecularly engineered nanoreactor.[40] The resulting $CsPbBr_3$ QDs were permanently ligated with hydrophobic PS chains, offering outstanding colloidal stability against water. Owing to their good optical properties, a white-light-emitting diode (WLED) device consisting of blue-emitting GaN blue chip, green-emitting PS-ligated $CsPbBr_3$ QDs, and red-emitting $CdSe/Cd_{1-x}Zn_xSe_{1-y}S_y/ZnS$ QDs was fabricated (Figure 20). The PS-capped $CsPbBr_3$ QD-based WLED had a color coordinate of (0.31, 0.32), very close to the white color coordinate of (0.33, 0.33), and a color gamut broader than that of NTSC and sRGB standards. Most importantly, the PS-ligated $CsPbBr_3$ QD-based WLED demonstrated excellent long-term stability under ambient conditions and high thermal cycling stability between 25 and 100 °C owing to the permanently ligated PS hairs.[40]

Catalysis. Nanosized catalytic materials have seen significant progress during the last few decades owing to their considerable increased surface area compared to that of their bulk counterpart. It is notable that catalytic NPs prepared by conventional methods often have the issue of the aggregation of NPs, thus leading to reduced catalytic activity. Polymer-ligated NPs template-grown from nonlinear BCPs possess robust polymer chains permanently tethered on the NP surface, providing them with good colloidal stability and dispersity during various catalytic reactions.

https://dx.doi.org/10.1021/acsnano.0c06936
ACS Nano 2020, 14, 12491–12521

Cylindrical diblock polymer brushes consisting of the inner silsesquioxane blocks (formed by the interaction between PAPTS and TMOS) and the outer PDMAEMA blocks along the PHEMA backbone were employed to template the growth of PtNPs *via* the coordination interaction between PDMAEMA and $H_2PtCl_6{\cdot}6H_2O$.[96] The resulting Pt-decorated hybrid NW displayed exceptional catalytic activity toward the reduction of 4-nitrophenol by $NaBH_4$, and the rate constant ($k_1 = 0.31\ s^{-1}m^{-2}\ L$) was larger than that of PtNPs stabilized in dendrimers ($k_1 = 0.16\ s^{-1}m^{-2}\ L$).[162] Similarly, using PHEMA-*g*-[PCL-*b*-PDMAEMA], a hybrid SiO_2 NW containing AuNPs (~3.5 nm) was obtained *via* sequential Au precursor loading, SiO_2 deposition, and metal ion reduction in the PDMAEMA regime.[97] The accessibility of AuNPs and their catalytic activity by converting 4-nitrophenol into 4-aminophenol were then elucidated. It is noteworthy that such *in situ* growth of catalytic noble metal NPs in the polymer template effectively avoids the aggregation of NPs owing to the dual protection of SiO_2 and polymer hairs.[97]

The ability to regulate the catalytic reaction of NCs in a controllable manner remains challenging, where tethering stimuli-responsive polymers on the catalytic NC surface may offer an appealing means of accomplishing it. Recently, thermoresponsive PNIPAM-ligated AuNPs with nonmonotonic or switchable on/off catalytic activities were crafted by utilizing star-like β-CD-*g*-[PAA-*b*-PNIPAM] as a nanoreactor.[41] By selecting the reduction of 4-nitrophenol as a model reaction, the catalytic activity of PNIPAM-ligated AuNPs was scrutinized. These NPs maintained good colloidal dispersity when the NP aqueous solution was heated over lower critical solution temperature (LCST) of thermoreposinve PNIPAM.[41] Accordingly, PNIPAM-capped AuNPs manifested a nonmonotonic (*i.e.*, non-Arrhenius) catalytic activity. Intriguingly, the addition of free linear PNIPAM chains into PNIPAM-capped AuNP aqueous solution led to the aggregation of AuNPs as temperature increased above the LCST. As a result, a switchable on/off catalytic reactivity of PNIPAM-ligated AuNPs was yielded (Figure 21). In sharp contrast to small-molecule-stabilized AuNPs, the size and shape of PNIPAM-ligated AuNPs were well retained after the catalytic reaction, signifying an improved stability of AuNPs due to permanent ligation with PNIPAM chains.[41]

Compared to the plain NPs described above, core/shell NPs may enable the further tailoring of catalytic property of NPs. To this end, recently a series of uniform Au/TiO_2 NPs with precisely controlled Au core diameter and TiO_2 shell thickness were crafted by exploiting the amphiphilic star-like triblock copolymer of β-CD-*g*-[P4VP-*b*-P*t*BA-*b*-PEO] as a nanoreactor.[48] The dimension-dependent photocatalytic activity of these Au/TiO_2 NPs was closely examined *via* the photodegradation of RhB under visible light irradiation. Compared with homemade TiO_2 NPs and P25, Au/TiO_2 core/shell NPs exhibited significantly enhanced degradation constants as a result of improved light harvesting enabled by localized surface plasmon resonance of the Au core and effective transfer of carriers at the Au/TiO_2 interface.[163] The influence of the Au core diameter and TiO_2 shell thickness on photocatalytic activity were also investigated. With a fixed Au core diameter of 15 nm, Au/TiO_2 NPs with a 5 nm TiO_2 shell thickness manifested the highest photocatalytic performance due to the delicate interplay of the surface area of TiO_2, the amount of TiO_2, and the extent of suppressed charge recombination.[164,165] Likewise, at a constant TiO_2 shell thickness of 5 nm, the photocatalytic performance of Au/TiO_2 NPs with a 10 nm Au core emerged as the best photocatalyst, which can be attributed largely to the appropriate amount of photoinduced electron−hole pairs and surface area. Clearly, the controlled synthesis of catalytic NPs by capitalizing on nonlinear BCPs as a nanoreactor offers a particularly promising approach to tailor the dimensions, compositions, and activities of nanocatalysts.

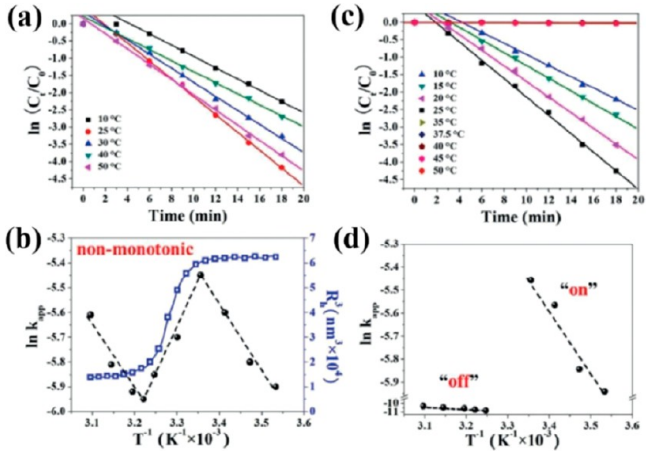

Figure 21. (a) Nonmonotonic catalytic activity and (b) corresponding Arrhenius plot of the apparent kinetic rate constant (k_{app}) in the reduction reaction of 4-nitrophenol catalyzed by PNIPAM-ligated AuNPs without the addition of free linear PNIPAM chains. (c) On/off catalytic activity and (d) corresponding Arrhenius plot of k_{app} for the catalytic reduction reaction of 4-nitrophenol by PNIPAM-ligated AuNPs with the addition of a large amount of linear PNIPAM chains (0.182 mM). Reproduced with permission from ref 41. Copyright 2019 Wiley-VCH.

Nanocarrier for Biomedicine. In recent years, self-assembled micelles and unimolecular micelles have attracted substantial attention as drug delivery vehicles in the biomedical fields. However, in this subsection, we concentrate on the biomedical applications of polymer-ligated NCs templated from nonlinear block polymers. Recently, a stable dual-functional nanovector was designed and prepared for tumor therapy and CT imaging, as depicted in Figure 22.[53] The star-like triblock copolymers of β-CD-*g*-[PCL-*b*-PAEMA-*b*-PPEGMA]$_{21}$ were exploited as the spherical nanocarrier for loading AuNPs and DOX. First, AuNPs were *in situ* grown in the intermediate PAEMA regime, and the anticancer drug DOX was then situated in the inner PCL compartment resulting from the hydrophobic interaction between DOX and PCL. The imaging capability of as-prepared β-CD-*g*-[PCL-*b*-PAEMA-*b*-PPEGMA]$_{21}$/AuNP/DOX composites was then investigated. The results revealed that AuNPs in the nanocarrier had an X-ray attenuation intensity higher than that of Omnipaque (*i.e.*, controlled sample) under the same conditions, demonstrating a higher CT contrast ability and a higher sensitive CT imaging. In addition, both *in vitro* and *in vivo* experiments suggested that the nanocarrier displayed an antitumor performance similar to that of free DOX. The integration of anticancer drug delivery with CT imaging represents a promising potential for future cancer theranostics. This synthetic approach for the preparation of AuNPs was further extended to β-CD-*g*-[PDMA-*b*-PHEMA-*b*-PPEGMA] that produced AuNPs without the addition of a reductant.[54] When incubated with HepG2 cells, β-CD-*g*-[PDMA-*b*-PHEMA-*b*-PPEGMA]/AuNPs showed highly intensive X-ray

https://dx.doi.org/10.1021/acsnano.0c06936
ACS Nano 2020, 14, 12491−12521

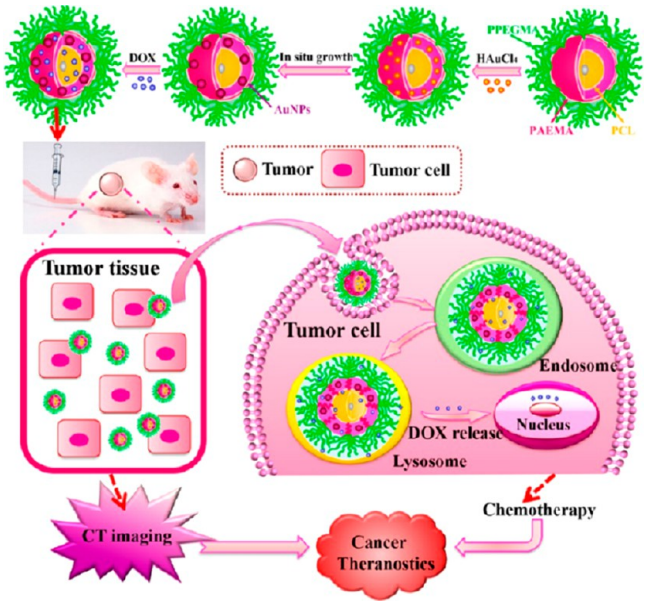

Figure 22. Schematic illustration of dual-functional β-CD-*g*-[PCL-*b*-PAEMA-*b*-PPEGMA]$_{21}$/AuNPs/DOX nanocarrier for cancer theranostics. Reprinted from ref 53. Copyright 2017 American Chemical Society.

attenuation property (>37%) compared with that of the controlled sample of Omnipaque, suggesting a useful method for increasing CT values of polymer carriers in cancer cells.[54]

GENERAL CONCLUSIONS AND FUTURE OUTLOOK

In summary, we reviewed recent progress in preparation of NCs templated by nonlinear BCP nanoreactors that afford access to a wide array of NPs and NRs with controlled size, shape, architectures, and surface characteristics. We first discussed the synthesis of nonlinear BCPs with well-defined MW of each block by controlled/living radical polymerization techniques in conjunction with the click reaction, where the core-first strategy for star-like BCPs and the grafting-from route to bottlebrush-like polymers were highlighted. Special attention was given to nonlinear BCPs with a β-CD core for star-like BCPs and a PHEMA backbone as well as a rigid cellulose backbone for bottlebrush-like BCPs. The MWs and PDI of nonlinear BCPs can be simply regulated by varying the polymerization time. The compositions and functionalities of nonlinear BCPs are dependent on the types of monomers used and their synthesis sequences.

As the universal and robust strategy, we detailed the precision and targeted synthesis of polymer-ligated NCs by exercising nonlinear BCPs as nanoreactors. Various architectures of NPs including plain, hollow, and core/shell nanostructures with tunable dimensions are formed using logically designed star-like BCP nanoreactors. The influence of polymer chemical compositions (*i.e.*, MW, monomer types, sequence of functional blocks, ratio of functional blocks to precursors, *etc.*) and solvents for precursor loading on the formation of NPs was discussed. With precise structural and compositional control of bottlebrush-like BCPs, 1D inorganic NRs, NWs, and NTs can be created. The length and diameter of these 1D NCs depend on the MWs of polymer backbone and brushes (*i.e.*, side chains), respectively. The NCs templated by nonlinear BCPs carry a number of advantages, including (a) precisely engineered dimensions and compositions of NCs, (b) excellent colloidal stability against various external perturbations due to intimately and permanently tethered polymer chains on the NC surface, (c) good dispersity and compatibility with a polymer matrix for preparation of functional nanocomposites, and (d) readily tunable solubility (*e.g.*, hydrophilic polymer ligating rendering water-soluble, and hydrophobic polymer ligating imparting organic-solvent-soluble) and surface functionality (*e.g.*, pH-, light-, and thermal-responsive, insulating, ferroelectric, conducting, *etc.*) by varying the outer polymer blocks.

Subsequently, some physical properties of polymer-ligated NCs were described, and their structure−property relationship was examined. Particularly, the size-dependent surface plasmon resonance of AuNPs, tunable emission of perovskite $CsPbBr_3$ QDs, superparamagnetic Fe_3O_4 NPs, and ferroelectric $BaTiO_3$ NPs were exemplified. Clearly, it is highly feasible to achieve targeted properties by adjusting the architectures of NCs through deliberately designing nonlinear BCP nanoreactors. Finally, the applications of polymer-ligated NCs in solar cells, WLEDs, catalysis, and CT imaging were outlined.

Despite recent advances in synthesis, properties, and applications of this class of NCs, questions and challenges remain to be addressed in order to realize the full potential of the nonlinear BCP nanoreactor strategy. The future opportunities in this extraordinarily rich field are also presented.

First, it is of key importance to controllably synthesize star-like block copolymers with a precise number of arms and uniform arm length, so the grafting density of polymer hairs on the surface of NPs can be tailored and the uniformity of NPs can be further strictly controlled. With the development in advanced polymerization techniques, it is feasible to synthesize star-like polymers with predetermined arm numbers and well-controlled MWs of each arm. Using the cyclodextrin initiator as an example, there are three commonly known CDs, namely, α-CD, β-CD, and γ-CD, containing 6, 7, and 8 glucose repeating units, respectively.[166] It is notable that there are 18, 21, and 24 hydroxyl groups (−OH) in α-CD, β-CD, and γ-CD, which can be converted into ATRP sites by reacting with BIBB, thus enabling the synthesis of star-like BCPs with 18, 21, and 24 BCP arms, respectively, that radiate from the CD core. Moreover, by replacing BIBB with 3-bromo-2-(bromomethyl)-propanoyl chloride during the esterification reaction, one hydroxyl can be transformed into two bromine groups (*i.e.*, two ATRP initiator sites) for growing two polymer chains. Thus, doubling or even tripling the number of ATRP initiator sites on the CD core can be easily achieved by rationally choosing reagents for bromination of hydroxyl groups, thereby resulting in polymer arms with multifold yet predictable numbers.

In addition, hydroxyl groups on these CDs can be categorized into primary hydroxyls and secondary hydroxyls and can thus be selectively modified. For instance, seven primary hydroxyls at position 6 of β-CD can be substituted by iodine (I_2) and then converted into an azide group ($-N_3$). On the other hand, 14 secondary hydroxyls may react with BIBB and further generate 14 arms of polymer side chains by ATRP.[167] Thus, by controlling the reaction condition of CDs, it is possible to accurately tune the arm numbers and arm composition of star-like BCPs. With the combination of click reaction and arm-first strategy, polymer arms with well-controlled MWs are accessible. Consequently, polymer-ligated NPs with a deliberate number of polymer hairs situated on the surface of NP can be crafted.

https://dx.doi.org/10.1021/acsnano.0c06936
ACS Nano 2020, 14, 12491−12521

Second, due to multistep synthesis and purification, it is challenging to obtain nonlinear BCPs with a scalable yield. The ability to scale up the synthesis of nonlinear BCPs will facilitate the large-scale production of NCs. To this end, a large-sized reaction vessel with a built-in heating and stirring system and with increased concentration of monomers and initiators may be used while maintaining the optimized reaction conditions derived from the small batch production.

Third, with regard to polymer-ligated NCs, the mechanism that underpins the nucleation and growth of NC within the compartment held by hydrophilic blocks of nonlinear BCPs has yet to be largely explored. This merits a detailed investigation. *In situ* TEM measurement may provide insight into the coordination reaction between precursors and functional hydrophilic blocks. Yet, due to significant electron density contrast of the polymer and NC in conjunction with the instability of polymers under high energy electron beam due to their organic nature, such *in situ* TEM study to elucidate the growth mechanism of NCs may be challenging. In addition to possible degradation of nonlinear BCPs, organic solvents used in the NC growth, directed by nonlinear BCP nanoreactor, may also be decomposed or carbonized under an electron beam, thus interfering with *in situ* imaging of the nucleation and growth process of NCs.

Nonetheless, computational modeling of NCs can also be performed, aiming at better understanding complex NC synthesis templated by nonlinear BCPs.[168] It is important to note that the loading of precursors and their coordination interaction with hydrophilic polymer blocks is a rather complicated phenomenon as it depends sensitively on a set of factors such as polymer architectures, precursor functional group interactions, and polymer chain length for precursors to diffuse to, access, and interact (*i.e.*, polymer chain spatial distribution which could restrict the mobility of precursors), *etc.*[168]

Fourth, related to the growth mechanism study discussed above, hydrophilic blocks of nonlinear BCPs that template the formation of NCs are believed to be encapsulated within the NC. As a result, as-prepared polymer-ligated NCs are not single crystals. Although polymer-ligated monodisperse NCs (*e.g.*, PS-ligated AuNPs) has been the focus of nanomaterials crafted from the BCP nanoreactors (*e.g.*, *β*-CD-*g*-[PAA-*b*-PS]), the ability to pinpoint the location and integrity of embedded hydrophilic polymers (*e.g.*, PAA chains) inside the NCs may provide fundamental and practical insights into the role that such polymer chains play in physical properties of NCs (*e.g.*, electrocatalysis) and materials and devices derived using these NCs as building blocks. In this context, high-resolution TEM on microtomed NCs before and after staining enclosed hydrophilic polymers can be conducted to scrutinize the position and unity of these polymers. Conversely, to substantiate the structural integrity of polymers (*e.g.*, PAA) confined within NCs, as-synthesized NCs can be selectively dissolved using acid or alkali of proper concentration or *via* metathesis reaction to release the NC confinement, thereby regenerating nonlinear BCPs. Subsequently, the recovered nonlinear BCPs can be applied for crafting NCs of different compositions. If successful, this would signify that the integrity of nonlinear BCPs restricted inside NCs is retained.

Fifth, the ability to expand the architectures and structural complexity of NCs will provide a platform for the exploration of emerging properties and construction of miniaturized materials and devices. The structures that have been attained by nonlinear BCP nanoreactor to date include plain, hollow, and core/shell NPs and NRs as well as nanonecklaces. The latter was composed of uniform inorganic nanodisks periodically assembled along a stretched flexible polymer chain templated by an amphiphilic worm-like diblock copolymer synthesized from a polyrotaxane-based macroinitiator.[169] Although rational design and synthesis of other complex nonlinear BCPs (*e.g.*, nanosheet-like BCPs, helical BCPs, *etc.*) will certainly render the creation of intriguing polymer-ligated nanomaterials (*e.g.*, 2D nanomaterials, inorganic helices, *etc.*), self-assembly of polymer-ligated NCs may represent another important endeavor toward constructing superstructures that may possess attractive and collective properties. The formation of superstructures *via* self-assembly of NCs capped by small molecules and noncovalently bonded polymer chains have been demonstrated.[170,171] However, the superstructures may, to some extent, aggregate due to unavoidable dissociation of surface ligands over a long period of time.[172] In contrast, as polymer hairs are permanently ligated on the NC surface, the superstructures assembled from polymer-ligated NCs will likely be stable, without the aggregation of adjacent NCs. Recent success in self-assembling of AuNPs covalently capped by polymer ligands suggests the feasibility of creating self-assembled superstructures using polymer-ligated NCs.[173]

With the appropriate conditions for self-assembly, polymer-ligated NCs may be directed into zero-, one-, two-, and three-dimensional superstructures. As a multitude of polymer-ligated NCs with well-controlled yet varied dimensions, compositions, architectures, and surface chemistry can be readily crafted using a nonlinear BCP nanoreactor strategy, an assortment of superstructures may be yielded from the self-assembly of polymer-ligated NC building blocks. For example, these superstructures may comprise NCs of the same size and composition yet different (or same) surface chemistry (*i.e.*, polymer hairs), NCs of same surface chemistry yet different compositions and different (or same) sizes, NCs of same (or different) composition and surface chemistry yet different shapes, *etc.* Clearly, physical properties of such superstructures rely heavily on not only the characteristics of NC constituents themselves as noted above but also the close proximity of adjacent NCs within the superstructure. This can be the subject of a future study.

Sixth, it is of great interest in synthesizing biodegradable and biocompatible nonlinear BCP nanoreactors for biomedical applications, for instance, the synthesis of nonlinear BCPs containing biodegradable PCL and PLA blocks. It is appealing to encapsulate enzymes within a special regime of BCP nanoreactors to yield well-maintained activity of enzymes in physiological conditions. Furthermore, responsive polymer nanoreactors with preloaded drugs in conjunction with CT imaging NCs are also enticing, which enables the controlled release of drugs at targeted sites *via* changing the external environment. To this end, a star-like triblock copolymer composed of hydrophobic poly(ethyl methacrylate-*co*-poly(methacrylic acid) (pH-responsive) as the inner block for both hydropobic drug loading and pH-responsive release, poly(2-(dimethylamino)ethyl methacrylate) (PDMAEMA) as the intermediate block for magnetic NP formation, and PPEGMA as the outer block for solubility and protective ligand may be rationally designed to render multifunctional properties, that is, as a drug carrier, pH-enabled drug release, and CT imaging.[174]

Finally, as discussed above, creating NCs with more complex morphology and architecture may facilitate investigation into

https://dx.doi.org/10.1021/acsnano.0c06936
ACS Nano 2020, 14, 12491−12521

their intriguing properties. In this regard, Janus NCs with good intimacy between two constituents (*e.g.*, metals, metal oxides (sulfides), metal carbides, metal nitrides (phosphides), *etc.*) have garnered considerable attention over the past several decades. The noncentrosymmetric architecture of Janus NCs gives them peculiar properties that are inaccessible to homogeneous counterparts. Similar to star-like and bottlebrush-like BCPs, the use of Janus BCPs as nanoreactors, synthesized *via* controlled/living radical polymerization techniques, will yield polymer-ligated Janus NCs. For example, by selectively modifying β-CD, the Janus β-CD is obtained.[167] Thus, Janus star-like BCPs could be synthesized and employed for directing the formation of Janus NPs. A similar strategy can be extended to bottlebrush-like BCPs by compartmentalizing the polymer backbone and brushes along the backbone, where it is conceivable to craft left−right-type Janus NRs and NTs along their long axis. These 0D and 1D Janus NCs carry advantages over conventional NCs by concurrently exposing the surface of two constituents and rendering the concerted effect between them for use in switchable display devices, smart nanomotors, (electro)catalysis, energy conversion, sensors, bioimaging, drug delivery, *etc.* This will be an active area of exploration.

AUTHOR INFORMATION

Corresponding Authors

Yijiang Liu − *College of Chemistry, Key Laboratory of Environmentally Friendly Chemistry and Application of Ministry of Education, Xiangtan University, Xiangtan 411105, Hunan Province, China*; Email: liuyijiang84@xtu.edu.cn

Zhiqun Lin − *School of Materials Science and Engineering, Georgia Institute of Technology, Atlanta, Georgia 30332, United States*; orcid.org/0000-0003-3158-9340; Email: zhiqun.lin@mse.gatech.edu

Authors

Jialin Wang − *College of Chemistry, Key Laboratory of Environmentally Friendly Chemistry and Application of Ministry of Education, Xiangtan University, Xiangtan 411105, Hunan Province, China*

Mingyue Zhang − *School of Materials Science and Engineering, Georgia Institute of Technology, Atlanta, Georgia 30332, United States*

Huaming Li − *College of Chemistry, Key Laboratory of Environmentally Friendly Chemistry and Application of Ministry of Education, Xiangtan University, Xiangtan 411105, Hunan Province, China*; orcid.org/0000-0003-4575-9945

Complete contact information is available at: https://pubs.acs.org/10.1021/acsnano.0c06936

Notes

The authors declare no competing financial interest.

ACKNOWLEDGMENTS

This work is supported by the AFOSR (FA9550-19-1-0317) and the NSF (CMMI 1914713 and DMR 1903990). Acknowledgment is also made to National Natural Science Foundation of China (NSFC 51603177) and Natural Science Foundation of Hunan Province (2020JJ5542).

VOCABULARY

Nanocrystals (NCs): crystals with dimensions at the nanometer scale, including nanoparticles (plain, hollow, core−shell), nanowires, nanorods and nanotubes

Star-like polymers: a class of nonlinear polymer with polymer arms radiating from a central core

bottlebrush-like polymers: a class of grafted polymers consisting of a long polymer backbone and polymer side chains densely tethered to the backbone

Nanoreactor: a nanoscopic reactor that is exploited to template the growth of NCs

Hairy NCs: nanocrystals with polymers covalently connected on the surface, also referred to as polymer-ligated NCs

Surface chemistry: different chemical compositions and properties of polymers on the surface of NCs

REFERENCES

(1) Xu, Y. H.; Wang, X. X.; Zhang, W. L.; Lv, F.; Guo, S. J. Recent Progress in Two-Dimensional Inorganic Quantum Dots. *Chem. Soc. Rev.* **2018**, *47*, 586−625.

(2) Zhang, H.; Cheng, H. M.; Ye, P. 2D Nanomaterials: Beyond Graphene and Transition Metal Dichalcogenides. *Chem. Soc. Rev.* **2018**, *47*, 6009−6012.

(3) Park, J.; Kwon, T.; Kim, J.; Jin, H.; Kim, H. Y.; Kim, B.; Joo, S. H.; Lee, K. Hollow Nanoparticles as Emerging Electrocatalysts for Renewable Energy Conversion Reactions. *Chem. Soc. Rev.* **2018**, *47*, 8173−8202.

(4) Zhao, M. Y.; Li, B. H.; Wang, P. Y.; Lu, L. F.; Zhang, Z. C.; Liu, L.; Wang, S. F.; Li, D. D.; Wang, R.; Zhang, F. Supramolecularly Engineered NIR-II and Upconversion Nanoparticles *In Vivo* Assembly and Disassembly to Improve Bioimaging. *Adv. Mater.* **2018**, *30*, 1804982−1804989.

(5) Cho, E. S.; Kim, J.; Tejerina, B.; Hermans, T. M.; Jiang, H.; Nakanishi, H.; Yu, M.; Patashinski, A. Z.; Glotzer, S. C.; Stellacci, F.; Grzybowski, B. A. Ultrasensitive Detection of Toxic Cations through Changes in the Tunnelling Current across Films of Striped Nanoparticles. *Nat. Mater.* **2012**, *11*, 978−985.

(6) Lim, E. K.; Kim, T.; Paik, S.; Haam, S.; Huh, Y. M.; Lee, K. Nanomaterials for Theranostics: Recent Advances and Future Challenges. *Chem. Rev.* **2015**, *115*, 327−394.

(7) Liang, Y.; Li, Y.; Wang, H.; Zhou, J.; Wang, J.; Regier, T.; Dai, H. Co_3O_4 Nanocrystals on Graphene as a Synergistic Catalyst for Oxygen Reduction Reaction. *Nat. Mater.* **2011**, *10*, 780−786.

(8) Wang, X.; Li, G.; Chen, T.; Yang, M.; Zhang, Z.; Wu, T.; Chen, H. Polymer-Encapsulated Gold-Nanoparticle Dimers: Facile Preparation and Catalytical Application in Guided Growth of Dimeric ZnO-Nanowires. *Nano Lett.* **2008**, *8*, 2643−2647.

(9) Murray, C.; Norris, D. J.; Bawendi, M. G. Synthesis and Characterization of Nearly Monodisperse CdE (E = Sulfur, Selenium, Tellurium) Semiconductor Nanocrystallites. *J. Am. Chem. Soc.* **1993**, *115*, 8706−8715.

(10) Bakshi, M. S. Colloidal Micelles of Block Copolymers as Nanoreactors, Templates for Gold Nanoparticles, and Vehicles for Biomedical Applications. *Adv. Colloid Interface Sci.* **2014**, *213*, 1−20.

(11) Matyjaszewski, K.; Xia, J. Atom Transfer Radical Polymerization. *Chem. Rev.* **2001**, *101*, 2921−2990.

(12) Wang, J. S.; Matyjaszewski, K. Controlled/ "Living" Radical Polymerization. Atom Transfer Radical Polymerization in the Presence of Transition-Metal Complexes. *J. Am. Chem. Soc.* **1995**, *117*, 5614−5615.

(13) Chiefari, J.; Chong, Y. K.; Ercole, F.; Krstina, J.; Jeffery, J.; Le, T. P. T.; Mayadunne, R. T. A.; Meijs, G. F.; Moad, C. L.; Moad, G.; Rizzardo, E.; Thang, S. H. Living Free-Radical Polymerization by Reversible Addition-Fragmentation Chain Transfer: The RAFT Process. *Macromolecules* **1998**, *31*, 5559−5562.

(14) Huang, K.; Rzayev, J. Well-Defined Organic Nanotubes from Multicomponent Bottlebrush Copolymers. *J. Am. Chem. Soc.* **2009**, *131*, 6880−6885.
(15) Cheng, C.; Qi, K.; Khoshdel, E.; Wooley, K. L. Tandem Synthesis of Core-Shell Brush Copolymers and Their Transformation to Peripherally Cross-Linked and Hollowed Nanostructures. *J. Am. Chem. Soc.* **2006**, *128*, 6808−6809.
(16) Bronstein, L. M.; Sidorov, S. N.; Valetsky, P. M.; Hartmann, J.; Colfen, H.; Antonietti, M. Induced Micellization by Interaction of Poly(2-Binylpyridine)-*Block*-Poly(ethylene Oxide) with Metal Compounds. Micelle Characteristics and Metal Nanoparticle Formation. *Langmuir* **1999**, *15*, 6256−6262.
(17) Wang, Y.; Grayson, S. M. Approaches for the Preparation of Non-Linear Amphiphilic Polymers and Their Applications to Drug Delivery. *Adv. Drug Delivery Rev.* **2012**, *64*, 852−865.
(18) Ren, J. M.; McKenzie, T. G.; Fu, Q.; Wong, E. H. H.; Xu, J. T.; An, Z. S.; Shanmugam, S.; Davis, T. P.; Boyer, C.; Qiao, G. G. Star Polymers. *Chem. Rev.* **2016**, *116*, 6743−6836.
(19) Higashihara, T.; Hayashi, M.; Hirao, A. Synthesis of Well-Defined Star-Branched Polymers by Stepwise Iterative Methodology Using Living Anionic Polymerization. *Prog. Polym. Sci.* **2011**, *36*, 323−375.
(20) Altintas, O.; Vogt, A. P.; Barner-Kowollik, C.; Tunca, U. Constructing Star Polymers *via* Modular Ligation Strategies. *Polym. Chem.* **2012**, *3*, 34−45.
(21) Li, X.; Iocozzia, J.; Chen, Y. H.; Zhao, S. Q.; Cui, X.; Wang, W.; Yu, H. F.; Lin, S. L.; Lin, Z. Q. From Precision Synthesis of Block Copolymers to Properties and Applications of Nanoparticles. *Angew. Chem., Int. Ed.* **2018**, *57*, 2046−2070.
(22) Michalski, A.; Brzezinski, M.; Lapienis, G.; Biela, T. Star-Shaped and Branched Polylactides: Synthesis, Characterization, and Properties. *Prog. Polym. Sci.* **2019**, *89*, 159−212.
(23) Altintas, O.; Vogt, A. P.; Barner-Kowollik, C.; Tunca, U. Constructing Star Polymers *via* Modular Ligation Strategies. *Polym. Chem.* **2012**, *3*, 34−45.
(24) Sharpless, K. B.; Kolb, H. C.; Finn, M. G. Click Chemistry: Diverse Chemical Function from a Few Good Reactions. *Angew. Chem., Int. Ed.* **2001**, *40*, 2004−2021.
(25) Seidi, F.; Shamsabadi, A. A.; Amini, M.; Shabanian, M.; Crespy, D. Functional Materials Generated by Allying Cyclodextrin-Based Supramolecular Chemistry with Living Polymerization. *Polym. Chem.* **2019**, *10*, 3674−3711.
(26) Nitta, N.; Takatsuka, M.; Kihara, S.; Sekiya, R.; Haino, T. Facile Synthesis of an Eight-Armed Star-Shaped Polymer *via* Coordination-Driven Self-Assembly of a Four-Armed Cavitand. *ACS Macro Lett.* **2018**, *7*, 1308−1311.
(27) Simonova, M. A.; Tarasova, E. V.; Dudkina, M. M.; Tenkovtsev, A. V.; Filippov, A. P. Synthesis and Hydrodynamic and Conformation Properties of Star-Shaped Polystyrene with Calix [8] Arene Core. *Int. J. Polym. Anal. Charact.* **2019**, *24*, 87−95.
(28) Fan, X. S.; Wang, Z.; He, C. B. Breathing" Unimolecular Micelles Based on a Novel Star-Like Amphiphilic Hybrid Copolymer. *J. Mater. Chem. B* **2015**, *3*, 4715−4722.
(29) Cao, P. F.; Wojnarowska, Z.; Hong, T.; Carroll, B.; Li, B. R.; Feng, H. B.; Parsons, L.; Wang, W. Y.; Lokitz, B. S.; Cheng, S. W.; Bocharova, V.; Sokolov, A. P.; Saito, T. A Star-Shaped Single Lithium-Ion Conducting Copolymer by Grafting a POSS Nanoparticle. *Polymer* **2017**, *124*, 117−127.
(30) Chen, G. J.; Wang, L. W.; Cordie, T.; Vokoun, C.; Eliceiri, K. W.; Gong, S. Q. Multi-Functional Self-Fluorescent Unimolecular Micelles for Tumor-Targeted Drug Delivery and Bioimaging. *Biomaterials* **2015**, *47*, 41−50.
(31) Iocozzia, J.; Lin, Z. Q. A Clean and Simple Route to Soft, Biocompatible Nanocapsules *via* UV-Cross-Linkable Azido-Hyperbranched Polyglycerol. *Macromolecules* **2017**, *50*, 4906−4912.
(32) Qiu, F.; Zhu, Q.; Tong, G. S.; Zhu, L. J.; Wang, D. L.; Yan, D. Y.; Zhu, X. Y. Highly Fluorescent Core-Shell Hybrid Nanoparticles Templated by a Unimolecular Star Conjugated Polymer for a Biological Tool. *Chem. Commun.* **2012**, *48*, 11954−11956.
(33) Pang, X. C.; Zhao, L.; Han, W.; Xin, X. K.; Lin, Z. Q. A General and Robust Strategy for the Synthesis of Nearly Monodisperse Colloidal Nanocrystals. *Nat. Nanotechnol.* **2013**, *8*, 426−431.
(34) Chen, Y. H.; Yang, D.; Yoon, Y. J.; Pang, X. C.; Wang, Z. W.; Jung, J.; He, Y. J.; Harn, Y. W.; He, M.; Zhang, S. G.; Zhang, G. Z.; Lin, Z. Q. Hairy Uniform Permanently Ligated Hollow Nanoparticles with Precise Dimension Control and Tunable Optical Properties. *J. Am. Chem. Soc.* **2017**, *139*, 12956−12967.
(35) He, Y. J.; Pang, X. C.; Jiang, B. B.; Feng, C. W.; Harn, Y. W.; Chen, Y. H.; Yoon, Y. J.; Pan, S.; Lu, C. H.; Chang, Y. J.; Zebarjadi, M.; Kang, Z. T.; Thadhani, N.; Peng, J.; Lin, Z. Q. Unconventional Route to Uniform Hollow Semiconducting Nanoparticles with Tailorable Dimensions, Compositions, Surface Chemistry, and Near-Infrared Absorption. *Angew. Chem., Int. Ed.* **2017**, *56*, 12946−12951.
(36) Feng, C. W.; Pang, X. C.; He, Y. J.; Chen, Y. H.; Zhang, G. Z.; Lin, Z. Q. A Versatile Strategy for Uniform Hybrid Nanoparticles and Nanocapsules. *Polym. Chem.* **2015**, *6*, 5190−5197.
(37) Pang, X. C.; Zhao, L.; Akinc, M.; Kim, J. K.; Lin, Z. Q. Novel Amphiphilic Multi-Arm, Star-Like Block Copolymers as Unimolecular Micelles. *Macromolecules* **2011**, *44*, 3746−3752.
(38) Pang, X. C.; He, Y. J.; Jiang, B. B.; Iocozzia, J.; Zhao, L.; Guo, H. Z.; Liu, J.; Akinc, M.; Bowler, N.; Tan, X. L.; Lin, Z. Q. Block Copolymer/Ferroelectric Nanoparticle Nanocomposites. *Nanoscale* **2013**, *5*, 8695−8702.
(39) Chen, Y. H.; Yoon, Y. J.; Pang, X. C.; He, Y. J.; Jung, J.; Feng, C. W.; Zhang, G. Z.; Lin, Z. Q. Precisely Size-Tunable Monodisperse Hairy Plasmonic Nanoparticles *via* Amphiphilic Star-Like Block Copolymers. *Small* **2016**, *12*, 6714−6723.
(40) Yoon, Y. J.; Chang, Y. J.; Zhang, S. G.; Zhang, M.; Pan, S.; He, Y. J.; Lin, C. H.; Yu, S. T.; Chen, Y. H.; Wang, Z. W.; Ding, Y.; Jung, J.; Thadhani, N.; Tsukruk, V. V.; Kang, Z. T.; Lin, Z. Q. Enabling Tailorable Optical Properties and Markedly Enhanced Stability of Perovskite Quantum Dots by Permanently Ligating with Polymer Hairs. *Adv. Mater.* **2019**, *31*, 1901602−1901610.
(41) Chen, Y. H.; Wang, Z. W.; Harn, Y. W.; Pan, S.; Li, Z. L.; Lin, S. L.; Peng, J.; Zhang, G. Z.; Lin, Z. Q. Resolving Optical and Catalytic Activities in Thermoresponsive Nanoparticles by Permanent Ligation with Temperature-Sensitive Polymers. *Angew. Chem., Int. Ed.* **2019**, *58*, 11910−11917.
(42) Chen, Y. H.; Wang, Z. W.; He, Y. J.; Yoon, Y. J.; Jung, J.; Zhang, G. Z.; Lin, Z. Q. Light-Enabled Reversible Self-Assembly and Tunable Optical Properties of Stable Hairy Nanoparticles. *Proc. Natl. Acad. Sci. U. S. A.* **2018**, *115*, E1391−E1400.
(43) Pang, X. C.; Zhao, L.; Feng, C. W.; Lin, Z. Q. Novel Amphiphilic Multiarm, Starlike Coil-Rod Diblock Copolymers *via* a Combination of Click Chemistry with Living Polymerization. *Macromolecules* **2011**, *44*, 7176−7183.
(44) He, M.; Pang, X. C.; Liu, X. Q.; Jiang, B. B.; He, Y. J.; Snaith, H.; Lin, Z. Q. Monodisperse Dual-Functional Upconversion Nanoparticles Enabled Near-Infrared Organolead Halide Perovskite Solar Cells. *Angew. Chem., Int. Ed.* **2016**, *55*, 4280−4284.
(45) Jiang, B. B.; Pang, X. C.; Li, B.; Lin, Z. Q. Organic-Inorganic Nanocomposites *via* Placing Monodisperse Ferroelectric Nanocrystals in Direct and Permanent Contact with Ferroelectric Polymers. *J. Am. Chem. Soc.* **2015**, *137*, 11760−11767.
(46) Xu, H.; Pang, X. C.; He, Y. J.; He, M.; Jung, J.; Xia, H. P.; Lin, Z. Q. An Unconventional Route to Monodisperse and Intimately Contacted Semiconducting Organic-Inorganic Nanocomposites. *Angew. Chem., Int. Ed.* **2015**, *54*, 4636−4640.
(47) Zheng, D. J.; Pang, X. C.; Wang, M.; He, Y. J.; Lin, C. J.; Lin, Z. Q. Unconventional Route to Hairy Plasmonic/Semiconductor Core/Shell Nanoparticles with Precisely Controlled Dimensions and Their Use in Solar Energy Conversion. *Chem. Mater.* **2015**, *27*, 5271−5278.
(48) Wang, M. Y.; Pang, X. C.; Zheng, D. J.; He, Y. J.; Sun, L.; Lin, C. J.; Lin, Z. Q. Nonepitaxial Growth of Uniform and Precisely Size-Tunable Core/Shell Nanoparticles and Their Enhanced Plasmon-Driven Photocatalysis. *J. Mater. Chem. A* **2016**, *4*, 7190−7199.

https://dx.doi.org/10.1021/acsnano.0c06936
ACS Nano 2020, 14, 12491−12521

(49) He, Y. J.; Yoon, Y. J.; Harn, Y. W.; Biesold-McGee, G. V.; Liang, S.; Lin, C. H.; Tsukruk, V. V.; Thadhani, N.; Kang, Z. T.; Lin, Z. Q. Unconventional Route to Dual-Shelled Organolead Halide Perovskite Nanocrystals with Controlled Dimensions, Surface Chemistry, and Stabilities. *Sci. Adv.* **2019**, *5*, eaax4424−4434.
(50) Yang, D.; Pang, X. C.; He, Y. J.; Wang, Y. Q.; Chen, G. X.; Wang, W. Z.; Lin, Z. Q. Precisely Size-Tunable Magnetic/Plasmonic Core/Shell Nanoparticles with Controlled Optical Properties. *Angew. Chem.* **2015**, *127*, 12259−12264.
(51) Yao, N.; Lin, W. J.; Zhang, X. F.; Gu, H. W.; Zhang, L. J. Amphiphilic *β*-Cyclodextrin-Based Star-Like Block Copolymer Unimolecular Micelles for Facile *In Situ* Preparation of Gold Nanoparticles. *J. Polym. Sci., Part A: Polym. Chem.* **2016**, *54*, 186−196.
(52) Lin, W. J.; Yao, N.; Qian, L.; Zhang, X. F.; Chen, Q.; Wang, J. F.; Zhang, L. J. pH-Responsive Unimolecular Micelle-Gold Nanoparticles-Drug Nanohybrid System for Cancer Theranostics. *Acta Biomater.* **2017**, *58*, 455−465.
(53) Lin, W. J.; Zhang, X. F.; Qian, L.; Yao, N.; Pan, Y.; Zhang, L. J. Doxorubicin-Loaded Unimolecular Micelle-Stabilized Gold Nanoparticles as a Theranostic Nanoplatform for Tumor-Targeted Chemotherapy and Computed Tomography Imaging. *Biomacromolecules* **2017**, *18*, 3869−3880.
(54) Lin, W. J.; Yang, C. F.; Xue, Z. L.; Huang, Y. W.; Luo, H. S.; Zu, X. H.; Zhang, L. J.; Yi, G. B. Controlled Construction of Gold Nanoparticles *In Situ* from *β*-Cyclodextrin Based Unimolecular Micelles for *In Vitro* Computed Tomography Imaging. *J. Colloid Interface Sci.* **2018**, *528*, 135−144.
(55) Nitta, N.; Takatsuka, M.; Kihara, S. I.; Sekiya, R.; Haino, T. Facile Synthesis of an Eight-Armed Star-Shaped Polymer *via* Coordination-Driven Self-Assembly of a Four-Armed Cavitand. *ACS Macro Lett.* **2018**, *7*, 1308−1311.
(56) Han, D.; Wen, T. J.; Han, G.; Deng, Y. Y.; Deng, Y.; Zhang, Q.; Fu, Q. Synthesis of Janus POSS Star Polymer and Exploring Its Compatibilization Behavior for PLLA/PCL Polymer Blends. *Polymer* **2018**, *136*, 84−91.
(57) Gopinath, A.; Sultan Nasar, A. Fluorescent Star ATRP Initiators and Fluorescent Star Poly(methyl Methacrylate)s: Synthesis and Photophysical Properties. *Polymer* **2018**, *153*, 139−149.
(58) Qiu, F.; Zhu, Q.; Tong, G. S.; Zhu, L. J.; Wang, D. L.; Yan, D. Y.; Zhu, X. Y. Highly Fluorescent Core-Shell Hybrid Nanoparticles Templated by a Unimolecular Star Conjugated Polymer for a Biological Tool. *Chem. Commun.* **2012**, *48*, 11954−11956.
(59) Chen, Q.; Cao, X.; Xu, Y.; An, Z. Emerging Synthetic Strategies for Core Cross-Linked Star (CCS) Polymers and Applications as Interfacial Stabilizers: Bridging Linear Polymers and Nanoparticles. *Macromol. Rapid Commun.* **2013**, *34*, 1507−1517.
(60) Durmaz, H.; Dag, A.; Erdogan, E.; Demirel, A. L.; Hizal, G.; Tunca, U. Multiarm Star Block and Multiarm Star Mixed-Block Copolymers *via* Azide-Alkyne Click Reaction. *J. Polym. Sci., Part A: Polym. Chem.* **2010**, *48*, 99−108.
(61) Gao, H. F.; Matyjaszewski, K. Arm-First Method as a Simple and General Method for Synthesis of Miktoarm Star Copolymers. *J. Am. Chem. Soc.* **2007**, *129*, 11828−11834.
(62) Li, W. W.; Matyjaszewski, K. Star Polymers *via* Cross-Linking Amphiphilic Macroinitiators by AGET ATRP in Aqueous Media. *J. Am. Chem. Soc.* **2009**, *131*, 10378−10379.
(63) Ding, H. J.; Park, S.; Zhong, M. J.; Pan, X. C.; Pietrasik, J.; Bettinger, C. J.; Matyjaszewski, K. Facile Arm-First Synthesis of Star Block Copolymers *via* ARGET ATRP with ppm Amounts of Catalyst. *Macromolecules* **2016**, *49*, 6752−6760.
(64) Shi, Y.; Cao, X. S.; Gao, H. F. The Use of Azide-Alkyne Click Chemistry in Recent Syntheses and Applications of Polytriazole-Based Nanostructured Polymers. *Nanoscale* **2016**, *8*, 4864−4881.
(65) Gao, H. F.; Matyjaszewski, K. Synthesis of Star Polymers by a Combination of ATRP and the "Click" Coupling Method. *Macromolecules* **2006**, *39*, 4960−4965.
(66) Chen, Y. G.; Xiao, N.; Fukuoka, M.; Yoshida, K.; Duan, Q.; Satoh, T.; Kakuchi, T. Synthesis and Thermoresponsive Property of Four-Arm Star-Shaped Poly(N-Isopropylacrylamide)s Bearing Covalent and Non-Covalent Cores. *Polym. Chem.* **2015**, *6*, 3608−3616.
(67) Hoogenboom, R.; Moore, B. C.; Schubert, U. S. Synthesis of Star-Shaped Poly(*ε*-Caprolactone) *via* 'Click' Chemistry and 'Supramolecular Click' Chemistry. *Chem. Commun.* **2006**, 4010−4012.
(68) Liang, J. H.; Liu, Y. Y.; Zhang, X. Y. Silver Metallic Cyclodextrin-Core Star Mpeg. *Macromol. Rapid Commun.* **2019**, *40*, 1800562−1800568.
(69) Zhang, C. H.; Shen, X. D.; Sakai, R.; Gottschaldt, M.; Schubert, U. S.; Hirohara, S.; Tanihara, M.; Yano, S.; Obata, M.; Xiao, N.; Satoh, T.; Kakuchi, T. Syntheses of 3-Arm and 4-Arm Star-Branched Polystyrene Ru(II) Complexes by the Click-To-Chelate Approach. *J. Polym. Sci., Part A: Polym. Chem.* **2011**, *49*, 746−753.
(70) Tinmaz, H. B.; Arslan, I.; Tasdelen, M. A. Star Polymers by Photoinduced Copper-Catalyzed Azide-Alkyne Cycloaddition Click Chemistry. *J. Polym. Sci., Part A: Polym. Chem.* **2015**, *53*, 1687−1695.
(71) Li, Y. J.; Zhang, B. Y.; Hoskins, J. N.; Grayson, S. M. Synthesis, Purification, and Characterization of "Perfect" Star Polymers *via* "Click" Coupling. *J. Polym. Sci., Part A: Polym. Chem.* **2012**, *50*, 1086−1101.
(72) Gao, H. F.; Min, K.; Matyjaszewski, K. Synthesis of 3-Arm Star Block Copolymers by Combination of "Core-First" and "Coupling-Onto" Methods Using ATRP and Click Reactions. *Macromol. Chem. Phys.* **2007**, *208*, 1370−1378.
(73) Iskin, B.; Yilmaz, G.; Yagci, Y. ABC Type Miktoarm Star Copolymers Through Combination of Controlled Polymerization Techniques with Thiol-Ene and Azide-Alkyne Click Reactions. *J. Polym. Sci., Part A: Polym. Chem.* **2011**, *49*, 2417−2422.
(74) Zhang, Y. F.; Liu, H.; Hu, J. M.; Li, C. H.; Liu, S. Y. Synthesis and Aggregation Behavior of Multi-Responsive Double Hydrophilic ABC Miktoarm Star Terpolymer. *Macromol. Rapid Commun.* **2009**, *30*, 941−947.
(75) Müllner, M.; Müller, A. H. E. Cylindrical Polymer Brushes-Anisotropic Building Blocks, Unimolecular Templates and Particulate Nanocarriers. *Polymer* **2016**, *98*, 389−401.
(76) Verduzco, R.; Li, X.; Pesek, S. L.; Stein, G. E. Structure, Function, Self-Assembly, and Applications of Bottlebrush Copolymers. *Chem. Soc. Rev.* **2015**, *44*, 2405−2420.
(77) Xie, G. J.; Martinez, M. R.; Olszewski, M.; Sheiko, S. S.; Matyjaszewski, K. Molecular Bottlebrushes as Novel Materials. *Biomacromolecules* **2019**, *20*, 27−54.
(78) Miyake, G. M.; Weitekamp, R. A.; Piunova, V. A.; Grubbs, R. H. Synthesis of Isocyanate-Based Brush Block Copolymers and Their Rapid Self-Assembly to Infrared-Reflecting Photonic Crystals. *J. Am. Chem. Soc.* **2012**, *134*, 14249−14254.
(79) Sun, G.; Cho, S.; Clark, C.; Verkhoturov, S. V.; Eller, M. J.; Li, A.; Pavía-Jiménez, A.; Schweikert, E. A.; Thackeray, J. W.; Trefonas, P.; Wooley, K. L. Nanoscopic Cylindrical Dual Concentric and Lengthwise Block Brush Terpolymers as Covalent Preassembled High-Resolution and High-Sensitivity Negative-Tone Photoresist Materials. *J. Am. Chem. Soc.* **2013**, *135*, 4203−4206.
(80) Tu, S. D.; Choudhury, C. K.; Luzinov, I.; Kuksenok, O. Recent Advances towards Applications of Molecular Bottlebrushes and Their Conjugates. *Curr. Opin. Solid State Mater. Sci.* **2019**, *23*, 50−61.
(81) Pelras, T.; Mahon, C. S.; Müllner, M. Synthesis and Applications of Compartmentalised Molecular Polymer Brushes. *Angew. Chem., Int. Ed.* **2018**, *57*, 6982−6994.
(82) Lee, H.; Pietrasik, J.; Sheiko, S. S.; Matyjaszewski, K. Stimuli-Responsive Molecular Brushes. *Prog. Polym. Sci.* **2010**, *35*, 24−44.
(83) Sheiko, S. S.; Sumerlin, B. S.; Matyjaszewski, K. Cylindrical Molecular Brushes: Synthesis, Characterization, and Properties. *Prog. Polym. Sci.* **2008**, *33*, 759−785.
(84) Rzayev, J. Molecular Bottlebrushes: New Opportunities in Nanomaterials Fabrication. *ACS Macro Lett.* **2012**, *1*, 1146−1149.
(85) Asman, S.; Mohamad, S.; Sarih, N. M. Study of the Morphology and the Adsorption Behavior of Molecularly Imprinted Polymers Prepared by Reversible Addition-Frag-Mentation Chain Transfer (RAFT) Polymerization Process Based on Two Functionalized *β*-Cyclodextrin as Monomers. *J. Mol. Liq.* **2016**, *214*, 59−69.

https://dx.doi.org/10.1021/acsnano.0c06936
ACS Nano 2020, 14, 12491−12521

(86) Palacios-Hernandez, T.; Luo, H. Y.; Garcia, E. A.; Pacheco, L. A.; Herrera-Alonso, M. Nanoparticles from Amphiphilic Heterografted Macromolecular Brushes with Short Backbones. *Macromolecules* **2018**, *51*, 2831−2837.
(87) Beers, K. L.; Gaynor, S. G.; Matyjaszewski, K.; Sheiko, S. S.; Moeller, M. The Synthesis of Densely Grafted Copolymers by Atom Transfer Radical Polymerization. *Macromolecules* **1998**, *31*, 9413−9415.
(88) Xu, Y. Y.; Yuan, J. Y.; Müller, A. H. E. Single-Molecular Hybrid Nano-Cylinders: Attaching Polyhedral Oligomeric Silsesquioxane Covalently to Poly(glycidyl Methacrylate) Cylindrical Brushes. *Polymer* **2009**, *50*, 5933−5939.
(89) Raguzin, I.; Stamm, M.; Ionov, L. Conductive Nanowires Templated by Molecular Brushes. *ACS Appl. Mater. Interfaces* **2015**, *7*, 23305−23309.
(90) Zhang, M. F.; Estournes, C.; Bietsch, W.; Müller, A. H. E. Superparamagnetic Hybrid Nanocylinders. *Adv. Funct. Mater.* **2004**, *14*, 871−882.
(91) Zhang, M. F.; Drechsler, M.; Müller, A. H. E. Template-Controlled Synthesis of Wire-Like Cadmium Sulfide Nanoparticle Assemblies within Core Shell Cylindrical Polymer Brushes. *Chem. Mater.* **2004**, *16*, 537−543.
(92) Yuan, J. Y.; Drechsler, M.; Xu, Y. Y.; Zhang, M. F.; Müller, A. H. E. Cadmium Selenide Nanowires within Core-Shell Cylindrical Polymerbrushes: Synthesis, Characterization and the Double-Loading Process. *Polymer* **2008**, *49*, 1547−1554.
(93) Xu, Y. Y.; Yuan, J. Y.; Fang, B.; Drechsler, M.; Müllner, M.; Bolisetty, S.; Ballauff, M.; Müller, A. H. E. Hybrids of Magnetic Nanoparticles with Double-Hydrophilic Core/Shell Cylindrical Polymer Brushes and Their Alignment in a Magnetic Field. *Adv. Funct. Mater.* **2010**, *20*, 4182−4189.
(94) Zheng, Z. C.; Daniel, A.; Yu, W.; Weber, B.; Ling, J.; Müller, A. H. E. Rare-Earth Metal Cations Incorporated Silica Hybrid Nanoparticles Templated by Cylindrical Polymer Brushes. *Chem. Mater.* **2013**, *25*, 4585−4594.
(95) Yuan, J. Y.; Lu, Y.; Schacher, F.; Lunkenbein, T.; Weiss, S.; Schmalz, H.; Müller, A. H. E. Template-Directed Synthesis of Hybrid Titania Nanowires within Core-Shell Bishydrophilic Cylindrical Polymer Brushes. *Chem. Mater.* **2009**, *21*, 4146−4154.
(96) Yuan, J. Y.; Schacher, F.; Drechsler, M.; Hanisch, A.; Lu, Y.; Ballauff, M.; Müller, A. H. E. Stimuli-Responsive Organosilica Hybrid Nanowires Decorated with Metal Nanoparticles. *Chem. Mater.* **2010**, *22*, 2626−2634.
(97) Mullner, M.; Lunkenbein, T.; Breu, J.; Caruso, F.; Müller, A. H. E. Template-Directed Synthesis of Silica Nanowires and Nanotubes from Cylindrical Core-Shell Polymer Brushes. *Chem. Mater.* **2012**, *24*, 1802−1810.
(98) Yuan, J. Y.; Xu, Y. Y.; Walther, A.; Bolisetty, S.; Schumacher, M.; Schmalz, H.; Ballauff, M.; Müller, A. H. E. Water-Soluble Organo-Silica Hybrid Nanowires. *Nat. Mater.* **2008**, *7*, 718−722.
(99) Xie, G. J.; Ding, H. J.; Daniel, W. F.M.; Wang, Z. Y.; Pietrasik, J.; Sheiko, S. S.; Matyjaszewski, K. Preparation of Titania Nanoparticles with Tunable Anisotropy and Branched Structures from Core-Shell Molecular Bottlebrushes. *Polymer* **2016**, *98*, 481−486.
(100) Mullner, M.; Yuan, J.; Weiss, S.; Walther, A.; Fortsch, M.; Drechsler, M.; Muller, A. H. E. Water-Soluble Organo Silica Hybrid Nanotubes Templated by Cylindrical Polymer Brushes. *J. Am. Chem. Soc.* **2010**, *132*, 16587−16592.
(101) Müllner, M.; Lunkenbein, T.; Schieder, M.; Groschel, A. H.; Miyajima, N.; Fortsch, M.; Breu, J.; Caruso, F.; Müller, A. H. E. Template-Directed Mild Synthesis of Anatase Hybrid Nanotubes within Cylindrical Core-Shell-Corona Polymer Brushes. *Macromolecules* **2012**, *45*, 6981−6988.
(102) Pang, X. C.; He, Y. J.; Jung, J.; Lin, Z. Q. 1D Nanocrystals with Precisely Controlled Dimensions, Compositions, and Architectures. *Science* **2016**, *353*, 1268−1272.
(103) Morits, M.; Hynninen, V.; Nonappa; Niederberger, A.; Ikkala, O.; Gröschel, A. H.; Müllner, M. Polymer Brush Guided Templating on Well-Defined Rod-Like Cellulose Nanocrystals. *Polym. Chem.* **2018**, *9*, 1650−1657.
(104) Jiang, B. B.; He, Y. J.; Li, B.; Zhao, S. Q.; Wang, S.; He, Y. B.; Lin, Z. Q. Polymer-Templated Formation of Polydopamine-Coated SnO_2 Nanocrystals: Anodes for Cyclable Lithium-Ionbatteries. *Angew. Chem., Int. Ed.* **2017**, *56*, 1869−1872.
(105) Hall-Edgefield, D. L.; Shi, T.; Nguyen, K.; Sidorenko, A. Hybrid Molecular Brushes with Chitosan Backbone: Facile Synthesis and Surface Grafting. *ACS Appl. Mater. Interfaces* **2014**, *6*, 22026−22033.
(106) Onbulak, S.; Rzayev, J. Cylindrical Nanocapsules from Photo-Cross-Linkable Core-Shell Bottlebrush Copolymers. *Polym. Chem.* **2015**, *6*, 764−771.
(107) Huang, Y. J.; Yuan, R.; Xu, F. G.; Mai, Y. Y.; Feng, X. L.; Yan, D. Y. Ultra-Large Sheet Formation by 1D to 2D Hierarchical Self-Assembly of a "Rod-Coil" Graft Copolymer with a Polyphenylene Backbone. *Polym. Chem.* **2016**, *7*, 1234−1238.
(108) Gadwal, I.; Rao, J. Y.; Baettig, J.; Khan, A. Functionalized Molecular Bottlebrushes. *Macromolecules* **2014**, *47*, 35−40.
(109) Iha, R. K.; Wooley, K. L.; Nystrom, A. M.; Burke, D. J.; Kade, M. J.; Hawker, C. J. Applications of Orthogonal "Click" Chemistries in the Synthesis of Functional Soft Materials. *Chem. Rev.* **2009**, *109*, 5620−5686.
(110) Gao, H. F.; Matyjaszewski, K. Synthesis of Molecular Brushes by "Grafting Onto" Method: Combination of ATRP and Click Reactions. *J. Am. Chem. Soc.* **2007**, *129*, 6633−6639.
(111) Engler, A. C.; Lee, H. I.; Hammond, P. T. Highly Efficient "Grafting Onto" a Polypeptide Backbone Using Click Chemistry. *Angew. Chem., Int. Ed.* **2009**, *48*, 9334−9338.
(112) Tang, H. Y.; Li, Y. C.; Lahasky, S. H.; Sheiko, S. S.; Zhang, D. H. Core-Shell Molecular Bottlebrushes with Helical Polypeptide Backbone: Synthesis, Characterization, and Solution Conformations. *Macromolecules* **2011**, *44*, 1491−1499.
(113) Heinrich, C. D.; Thelakkat, M. Poly-(3-Hexylthiophene) Bottlebrush Copolymers with Tailored Side-Chain Lengths and High Charge Carrier Mobilities. *J. Mater. Chem. C* **2016**, *4*, 5370−5378.
(114) Pang, X. C.; Zhao, L.; Feng, C. W.; Wu, R. F.; Ma, H. H.; Lin, Z. Q. Functional Copolymer Brushes Composed of a Hydrophobic Backbone and Densely Grafted Conjugated Side Chains *via* a Combination of Living Polymerization with Click Chemistry. *Polym. Chem.* **2013**, *4*, 2025−2032.
(115) Fenyves, R.; Schmutz, M.; Horner, I. J.; Bright, F. V.; Rzayev, J. Aqueous Self-Assembly of Giant Bottlebrush Block Copolymer Surfactants as Shape-Tunable Building Blocks. *J. Am. Chem. Soc.* **2014**, *136*, 7762−7770.
(116) Feng, C.; Li, Y. G.; Yang, D.; Hu, J. H.; Zhang, X. H.; Huang, X. Y. Well-Defined Graft Copolymers: From Controlled Synthesis to Multipurpose Applications. *Chem. Soc. Rev.* **2011**, *40*, 1282−1295.
(117) Wang, Q.; Xiao, A. Q.; Shen, Z. H.; Fan, X. H. Janus Particles with Tunable Shapes Prepared by Asymmetric Bottlebrush Block Copolymers. *Polym. Chem.* **2019**, *10*, 372−378.
(118) Sveinbjörnsson, B. R.; Weitekamp, R. A.; Miyake, G. M.; Xia, Y.; Atwater, H. A.; Grubbs, R. H. Rapid Self-Assembly of Brush Block Copolymers to Photonic Crystals. *Proc. Natl. Acad. Sci. U. S. A.* **2012**, *109*, 14332−14336.
(119) Gu, W. Y.; Huh, J.; Hong, S. W.; Sveinbjornsson, B. R.; Park, C.; Grubbs, R. H.; Russell, T. P. Self-Assembly of Symmetric Brush Diblock Copolymers. *ACS Nano* **2013**, *7*, 2551−2558.
(120) Xia, Y.; Olsen, B. D.; Kornfield, J. A.; Grubbs, R. H. Efficient Synthesis of Narrowly Dispersed Brush Copolymers and Study of Their Assemblies: The Importance of Side Chain Arrangement. *J. Am. Chem. Soc.* **2009**, *131*, 18525−18532.
(121) Song, D. P.; Li, C.; Colella, N. S.; Xie, W. T.; Li, S. K.; Lu, X. M.; Gido, S.; Lee, J. H.; Watkins, J. J. Large-Volume Self-Organization of Polymer Nanoparticle Hybrids with Millimeter-Scale Grain Sizes Using Brush Block Copolymers. *J. Am. Chem. Soc.* **2015**, *137*, 12510−12513.
(122) Li, Z.; Ma, J.; Cheng, C.; Zhang, K.; Wooley, K. L. Synthesis of Hetero-Grafted Amphiphilic Diblock Molecular Brushes and Their

https://dx.doi.org/10.1021/acsnano.0c06936
ACS Nano 2020, 14, 12491−12521

Self-Assembly in Aqueous Medium. *Macromolecules* **2010**, *43*, 1182−1184.
(123) Chang, A. B.; Bates, C. M.; Lee, B.; Garland, C. M.; Jones, S. C.; Spencer, R. K. W.; Matsen, M. W.; Grubbs, R. H. Manipulating the ABCs of Self-Assembly *via* Low-χ Block Polymer Design. *Proc. Natl. Acad. Sci. U. S. A.* **2017**, *114*, 6462−6467.
(124) Li, Y. K.; Themistou, E.; Zou, J.; Das, B. P.; Tsianou, M.; Cheng, C. Facile Synthesis and Visualization of Janus Double-Brush Copolymers. *ACS Macro Lett.* **2012**, *1*, 52−56.
(125) Kawamoto, K.; Zhong, M. J.; Gadelrab, K. R.; Cheng, L. C.; Ross, C. A.; Alexander-Katz, A.; Johnson, J. A. Graft-Through Synthesis and Assembly of Janus Bottlebrush Polymers from A-Branch-B Diblock Macromonomers. *J. Am. Chem. Soc.* **2016**, *138*, 11501−11504.
(126) Li, Z.; Ma, J.; Lee, N. S.; Wooley, K. L. Dynamic Cylindrical Assembly of Triblock Copolymers by a Hierarchical Process of Covalent and Supramolecular Interactions. *J. Am. Chem. Soc.* **2011**, *133*, 1228−1231.
(127) Ding, H. J.; Yan, J. J.; Wang, Z. Y.; Xie, G. J.; Mahoney, C.; Ferebee, R.; Zhong, M. J.; Daniel, W. F. M.; Pietrasik, J.; Sheiko, S. S.; Bettinger, C. J.; Bockstaller, M. R.; Matyjaszewski, K. Preparation of ZnO Hybrid Nanoparticles by ATRP. *Polymer* **2016**, *107*, 492−502.
(128) Liu, Y. J.; Wang, Z. W.; Liang, S.; Li, Z. L.; Zhang, M. Y.; Li, H. M.; Lin, Z. Q. Polar Organic Solvent-Tolerant Perovskite Nanocrystals Permanently Ligated with Polymer Hairs *via* Star-Like Molecular Bottlebrush Trilobe Nanoreactors. *Nano Lett.* **2019**, *19*, 9019−9028.
(129) Wang, X. J.; Feng, J.; Bai, Y. C.; Zhang, Q.; Yin, Y. D. Synthesis, Properties, and Applications of Hollow Micro-/Nanostructures. *Chem. Rev.* **2016**, *116*, 10983−11060.
(130) Park, J.; Kwon, T.; Kim, J.; Jin, H.; Kim, H. Y.; Kim, B.; Joo, S. H.; Lee, K. Hollow Nanoparticles as Emerging Electrocatalysts for Renewable Energy Conversion Reactions. *Chem. Soc. Rev.* **2018**, *47*, 8173−8202.
(131) Wang, J. P.; Li, N. Functional Hollow Nanostructures for Imaging and Phototherapy of Tumors. *J. Mater. Chem. B* **2017**, *5*, 8430−8445.
(132) Yin, Y. D.; Rioux, R. M.; Erdonmez, C. K.; Hughes, S.; Somorjai, G. A.; Alivisatos, A. P. Formation of Hollow Nanocrystals through the Nanoscale Kirkendall Effect. *Science* **2004**, *304*, 711−714.
(133) Kim, D.; Park, J.; An, K.; Yang, N. K.; Park, J. G.; Hyeon, T. Synthesis of Hollow Iron Nanoframes. *J. Am. Chem. Soc.* **2007**, *129*, 5812−5813.
(134) Zeng, H. C. Synthetic Architecture of Interior Space for Inorganic Nanostructures. *J. Mater. Chem.* **2006**, *16*, 649−662.
(135) Zhang, J.; Tang, Y.; Lee, K.; Ouyang, M. Nonepitaxial Growth of Hybrid Core-Shell Nanostructures with Large Lattice Mismatches. *Science* **2010**, *327*, 1634−1638.
(136) Macfarlane, R. J.; Kim, B.; Lee, B.; Weitekamp, R. A.; Bates, C. M.; Lee, S. F.; Chang, A. B.; Delaney, K. T.; Fredrickson, G. H.; Atwater, H. A.; Grubbs, R. H. Improving Brush Polymer Infrared One-Dimensional Photonic Crystals *via* Linear Polymer Additives. *J. Am. Chem. Soc.* **2014**, *136*, 17374−17377.
(137) Johnson, J. A.; Lu, Y. Y.; Burts, A. O.; Lim, Y. H.; Finn, M. G.; Koberstein, J. T.; Turro, N. J.; Tirrell, D. A.; Grubbs, R. H. Core-Clickable PEG-Branch-Azide Bivalent-Bottle-Brush Polymers by ROMP: Grafting-Through and Clicking-To. *J. Am. Chem. Soc.* **2011**, *133*, 559−566.
(138) Sowers, M. A.; McCombs, J. R.; Wang, Y.; Paletta, J. T.; Morton, S. W.; Dreaden, E. C.; Boska, M. D.; Ottaviani, M. F.; Hammond, P. T.; Rajca, A.; Johnson, J. A. Redox-Responsive Branched-Bottlebrush Polymers for *In Vivo* MRI and Fluorescence Imaging. *Nat. Commun.* **2014**, *5*, 5460−5468.
(139) Hu, J. M.; Wu, T.; Zhang, G. T.; Liu, S. Y. Efficient Synthesis of Single Gold Nanoparticle Hybrid Amphiphilic Triblock Copolymers and Their Controlled Self-Assembly. *J. Am. Chem. Soc.* **2012**, *134*, 7624−7627.
(140) Nandan, B.; Horechyy, A. Hairy Core-Shell Polymer Nano-Objects from Self-Assembled Block Copolymer Structures. *ACS Appl. Mater. Interfaces* **2015**, *7*, 12539−12558.
(141) Song, D. P.; Lin, Y.; Gai, Y.; Colella, N. S.; Li, C.; Liu, X. H.; Gido, S.; Watkins, J. J. Controlled Supramolecular Self-Assembly of Large Nanoparticles in Amphiphilic Brush Block Copolymers. *J. Am. Chem. Soc.* **2015**, *137*, 3771−3774.
(142) Runge, M. B.; Bowden, N. B. Synthesis of High Molecular Weight Comb Block Copolymers and Their Assembly into Ordered Morphologies in the Solid State. *J. Am. Chem. Soc.* **2007**, *129*, 10551−10560.
(143) Zhao, B.; Brittain, W. J. Polymer Brushes: Surface-Immobilized Macromolecules. *Prog. Polym. Sci.* **2000**, *25*, 677−710.
(144) Willets, K. A.; Van Duyne, R. P. Localized Surface Plasmon Resonance Spectroscopy and Sensing. *Annu. Rev. Phys. Chem.* **2007**, *58*, 267−297.
(145) Daniel, M. C.; Astruc, D. Gold Nanoparticles: Assembly, Supramolecular Chemistry, Quantum-Size-Related Properties, and Applications toward Biology, Catalysis, and Nanotechnology. *Chem. Rev.* **2004**, *104*, 293−346.
(146) Sheng, Y.; Xue, J. Synthesis and Properties of Au−Fe_3O_4 Heterostructured Nanoparticles. *J. Colloid Interface Sci.* **2012**, *374*, 96−101.
(147) Yu, H.; Chen, M.; Rice, P. M.; Wang, S. X.; White, R. L.; Sun, S. Dumbbell-Like Bifunctional Au−Fe_3O_4 Nanoparticles. *Nano Lett.* **2005**, *5*, 379−382.
(148) Jain, P. K.; El-Sayed, M. A. Universal Scaling of Plasmon Coupling in Metal Nanostructures: Extension from Particle Pairs to Nanoshells. *Nano Lett.* **2007**, *7*, 2854−2858.
(149) Contreras-Cáceres, R.; Sánchez-Iglesias, A.; Karg, M.; Pastoriza-Santos, I.; Pérez-Juste, J.; Pacifico, J.; Hellweg, T.; Fernández-Barbero, A.; Liz-Marzán, L. M. Encapsulation and Growth of Gold Nanoparticles in Thermoresponsive Microgels. *Adv. Mater.* **2008**, *20*, 1666−1670.
(150) Xuan, S. H.; Wang, Y. X. J.; Yu, J. C.; Cham-Fai Leung, K. Tuning the Grain Size and Particle Size of Superparamagnetic Fe_3O_4 Microparticles. *Chem. Mater.* **2009**, *21*, 5079−5087.
(151) Jeong, U.; Teng, X. W.; Wang, Y.; Yang, H.; Xia, Y. N. Superparamagnetic Colloids: Controlled Synthesis and Niche Applications. *Adv. Mater.* **2007**, *19*, 33−60.
(152) Wang, X. B.; You, N.; Lan, F. Q.; Fu, P.; Cui, Z.; Pang, X. C.; Liu, M. Y.; Zhao, Q. X. Facile Synthesis of Size-Tunable Superparamagnetic/Polymeric Core/Shell Nanoparticles by Metal-Free Atom Transfer Radical Polymerization at Ambient Temperature. *RSC Adv.* **2017**, *7*, 7789−7792.
(153) Bai, J.; Wang, X.; Fu, P.; Cui, Z.; Zhao, Q.; Pang, X.; Liu, M. Highly Water-Dispersed Superparamagnetic Magnetite Colloidal Nanocrystal Clusters from Multifunctional Polymeric Nanoreactors: Synthesis and Properties. *RSC Adv.* **2016**, *6*, 9429−9435.
(154) Wang, M. Y.; Wang, B.; Huang, F.; Lin, Z. Q. Enabling PIEZO Potential in PIEZO Electric Semiconductors for Enhanced Catalytic Activities. *Angew. Chem., Int. Ed.* **2019**, *58*, 7526−7536.
(155) Tsuyumoto, I.; Kobayashi, M.; Are, T.; Yamazaki, N. Nanosized Tetragonal $BaTiO_3$ Powders Synthesized by a New Peroxo-Precursor Decomposition Method. *Chem. Mater.* **2010**, *22*, 3015−3020.
(156) Smith, M. B.; Page, K.; Siegrist, T.; Redmond, P. L.; Walter, E. C.; Seshadri, R.; Brus, L. E.; Steigerwald, M. L. Crystal Structure and the Paraelectric-To-Ferroelectric Phase Transition of Nanoscale $BaTiO_3$. *J. Am. Chem. Soc.* **2008**, *130*, 6955−6963.
(157) Jiang, B. B.; Iocozzia, J.; Zhao, L.; Zhang, H. F.; Harn, Y. W.; Chen, Y. H.; Lin, Z. Q. Barium Titanate at the Nanoscale: Controlled Synthesis and Dielectric and Ferroelectric Properties. *Chem. Soc. Rev.* **2019**, *48*, 1194−1228.
(158) Guo, H. Z.; Mudryk, Y.; Ahmad, M. I.; Pang, X. C.; Zhao, L.; Akinc, M.; Pecharsky, V. K.; Bowler, N.; Lin, Z. Q.; Tan, X. Structure Evolution and Dielectric Behavior of Polystyrene-Capped Barium Titanate Nanoparticles. *J. Mater. Chem.* **2012**, *22*, 23944−23951.

https://dx.doi.org/10.1021/acsnano.0c06936
ACS Nano 2020, 14, 12491−12521

(159) Ghayour, H.; Abdellahi, M. A Brief Review of the Effect of Grain Size Variation on the Electrical Properties of $BaTiO_3$-Based Ceramic. *Powder Technol.* **2016**, *292*, 84−93.
(160) Shamsi, J.; Urban, A. S.; Imran, M.; De Trizio, L.; Manna, L. Metal Halide Perovskite Nanocrystals: Synthesis, Post-Synthesis Modifications, and Their Optical Properties. *Chem. Rev.* **2019**, *119*, 3296−3348.
(161) Huang, H.; Bodnarchuk, M. I.; Kershaw, S. V.; Kovalenko, M. V.; Rogach, A. L. Lead Halide Perovskite Nanocrystals in the Research Spotlight: Stability and Defect Tolerance. *ACS Energy Lett.* **2017**, *2*, 2071−2083.
(162) Zhang, M. F.; Estournes, C.; Bietsch, W.; Müller, A. H. E. Superparamagnetic Hybrid Nanocylinders. *Adv. Funct. Mater.* **2004**, *14*, 871−882.
(163) Wang, Z.; Liu, J.; Chen, W. Plasmonic Ag/AgBr Nanohybrid: Synergistic Effect of SPR with Photographic Sensitivity for Enhanced Photocatalytic Activity and Stability. *Dalton Trans* **2012**, *41*, 4866−4870.
(164) Linic, S.; Christopher, P.; Ingram, D. B. Plasmonic-Metal Nanostructures for Efficient Conversion of Solar to Chemical Energy. *Nat. Mater.* **2011**, *10*, 911−921.
(165) Wang, M.; Sun, L.; Lin, Z.; Cai, J.; Xie, K.; Lin, C. *p-n* Heterojunction Photoelectrodes Composed of Cu_2O-loaded TiO_2 Nanotube Arrays with Enhanced Photoelectrochemical and Photoelectrocatalytic Activities. *Energy Environ. Sci.* **2013**, *6*, 1211−1220.
(166) Yao, X. K.; Mu, J.; Zeng, L. L.; Lin, J.; Nie, Z. H.; Jiang, X. Q.; Huang, P. Stimuli-Responsive Cyclodextrin-Based Nanoplatforms for Cancer Treatment and Theranostics. *Mater. Horiz.* **2019**, *6*, 846−870.
(167) Ge, Z. S.; Xu, J.; Hu, J. M.; Zhang, Y. F.; Liu, S. Y. Synthesis and Supramolecular Self-Assembly of Stimuli-Responsive Water-Soluble Janus-Type Heteroarm Star Copolymers. *Soft Matter* **2009**, *5*, 3932−3939.
(168) Pietrasik, J.; Budzałek, K.; Zhang, Y. M.; Hałagan, K.; Kozanecki, M. Macromolecular Templates for Synthesis of Inorganic Nanoparticles. In *Reversible Deactivation Radical Polymerization: Materials and Applications*; Matyjaszewski, K., Gao, H. F., Sumerlin, B. S., Tsarevsky, N. V., Eds.; American Chemical Society: Washington, DC, 2018; pp 169−200, ISBN13: 9780841233232.
(169) Xu, H.; Xu, Y.; Pang, X. C.; He, Y. J.; Jung, J.; Xia, H. P.; Lin, Z. Q. A General Route to Nanocrystal Kebabs Periodically Assembled on Stretched Flexible Polymer Shish. *Sci. Adv.* **2015**, *1*, e1500025−e1500035.
(170) Nie, Z.; Petukhova, A.; Kumacheva, E. Properties and Emerging Applications of Self-Assembled Structures Made from Inorganic Nanoparticles. *Nat. Nanotechnol.* **2010**, *5*, 15−25.
(171) Wang, L. B.; Xu, L. G.; Kuang, H.; Xu, C. L.; Kotov, N. A. Dynamic Nanoparticle Assemblies. *Acc. Chem. Res.* **2012**, *45*, 1916−1926.
(172) Förster, S.; Antonietti, M. Amphiphilic Block Copolymers in Structure-Controlled Nanomaterial Hybrids. *Adv. Mater.* **1998**, *10*, 195−217.
(173) Yi, C. L.; Yang, Y. Q.; Liu, B.; He, J.; Nie, Z. H. Polymer-Guided Assembly of Inorganic Nanoparticles. *Chem. Soc. Rev.* **2020**, *49*, 465−508.
(174) Jiang, W. Z.; Guo, J. W.; Wen, W. Q.; Jia, Y. G.; Liu, S. Nano-Carriers Based on pH-Sensitive Star-Shaped Copolymers for Drug-Controlled Release. *Materials* **2019**, *12*, 1610−1621.

https://dx.doi.org/10.1021/acsnano.0c06936
ACS Nano 2020, 14, 12491−12521